CALIFORNIA INSTITUTE OF TECHNOLOGY

CIT - ELECTRON TUBE & MICROWAVE LABORATORY REPORT

EXPERIMENTAL STUDY OF PLASMA WAVE RESONANCES IN A HOT NONUNIFORM PLASMA COLUMN

by

J. C. Nickel

Technical Report No. 22

Nonr 220(50)

May 1964

EXPERIMENTAL STUDY OF PLASMA WAVE RESONANCES IN A HOT NONUNIFORM PLASMA COLUMN

by

John C. Nickel

Technical Report No. 22

CALIFORNIA INSTITUTE OF TECHNOLOGY

Pasadena, California

A Technical Report to the Office of Naval Research

Contract Nonr 220(50)

May 1964

TABLE OF CONTENTS

ABSTRACT

I. INTRODUCTION 1

1.1 Description of the Problem 1

1.2 Separation of the Field Solutions Exterior to the Plasma Region from the Solutions within the Plasma Region 4

1.3 Early Plasma Models 9

1.4 Objectives of Our Experiments 17

II. THEORY OF A HOT NONUNIFORM PLASMA COLUMN 19

2.1 Introduction 19

2.2 Basic Equations 19

2.3 The Static Radial Density Profile 24

2.4 Properties and Solutions of the Plasma Wave Potential Equation 31

III. EXPERIMENTAL TECHNIQUES 36

3.1 Description and Construction of the Plasma Tubes 36

3.2 Low Frequency Observational Techniques 39

3.3 High Frequency Observational Techniques 44

3.4 Average Density Measurements 44

3.5 Methods of Taking Data 55

IV. EXPERIMENTAL RESULTS 63

4.1 Reduction of the Data 63

4.2 Experimental Results 64

4.3 Discussion of the Results 69

V. RESONANCES OF THE POSITIVE COLUMN IN AN AXIAL STATIC MAGNETIC FIELD 73

5.1 Introduction 73

5.2 Theory of a Hot, Nonuniform Magnetized Plasma Column 77

5.3 Experimental Results 80

VI. SUMMARY AND CONCLUSIONS 91

6.1 Comparison of Theory and Experiment 91

6.2 Plasma Wave Resonances as a Diagnostic Tool 93

6.3 Proposed Problems 96

APPENDIX A 98

A.1 Introduction 98

A.2 The Moment Equations 98

A.3 Example of the Adiabatic Approximation 102

APPENDIX B 105

APPENDIX C 112

C.1 Introduction 112

C.2 Determination of the Average Electron Density $\bar{n}$ in a Plasma Column Using the TM_{010} Mode of a Cylindrical Cavity 113

C.3 Determination of the Dielectric Constant of a Dielectric Rod Using the TM_{010} Mode of a Cylindrical Cavity 118

C.4 Determination of the Third Moment of the Electron Density Distribution $\int_0^{r_w} n(r)r^3dr$ Using the TM_{110} Mode of a Right Circular Cavity 119

APPENDIX D

D.1 Introduction 122

D.2 Admittance of the Split Cylinder Capacitor 122

D.3 Equivalent Circuits 126

ABSTRACT

The relative frequency spectrum $\omega^2/\overline{\omega_p^2}$ of plasma wave resonances in the positive column of a low pressure mercury discharge tube has been shown to depend upon the parameter $r_w^2/\overline{\lambda_D^2}$ where r_w is the radius of the column, $\overline{\lambda_D^2}$ is the Debye length defined in terms of the average electron density, and $\overline{\omega_p^2}$ is the square of the average plasma frequency. This paper presents observations of both dipole and quadrupole resonance spectra made on several discharge tubes with r_w ranging from 0.30 to 0.87 cm. For these measurements $r_w^2/\overline{\lambda_D^2}$ varies from about 10^2 to 10^5, and the best fit electron temperatures are found to be of the order of 3 ev. The average electron densities are directly measured using a cavity perturbation technique. The results of these observations are found to be in good agreement with the theory (1,2) based upon the first two moments of the correlationless Boltzmann equation in conjunction with Parker's electron density profile (3) for a low density positive column.

The results of a preliminary investigation of the effects of an axial, static magnetic field on the dipole resonance spectrum are also presented. These results indicate that in the presence of an axial magnetic field not only does the lowest resonance (approximately predicted by the cold plasma theory) split, but the next higher order resonance also splits. For the

lowest resonance, it is found that $\Delta\omega/\omega_g \approx .8 \pm .1$, while for the next higher order resonance $\Delta\omega/\omega_g \approx .5 \pm .2$, where ω_g is the cyclotron frequency. These preliminary results are in good accord with calculations made by Parker (1), again using the moment equation approach.

---

(1) J. V. Parker, PhD Thesis, California Institute of Technology, June 1964.

(2) J. C. Nickel, J. V. Parker, R. W. Gould, Phys. Rev. Letters 11, 183 (1963).

(3) J. V. Parker, Phys. Fluids 6, 1657 (1963).

I. INTRODUCTION

1.1 Description of the Problem

In 1951 Romell (1) published the results of a scattering experiment conducted on the positive column of a mercury discharge tube. In this experiment a discharge tube 3.2 cm in diameter and 80 cm long was bathed with 30 cm. radiation, and the scattered radiation was observed as a function of the discharge current in the plasma tube. His experimental arrangement was similar to that shown in Figure 1.1. Romell found that if the incident field was polarized with the electric vector perpendicular to the column, the scattering amplitude displayed a series of peaks or resonances as a function of discharge current, (Figure 1.2). However, if the incident field was polarized such that the electric vector was parallel to the plasma column, no such resonances were observed. In 1958 Boley (2), using apparatus similar to Romell's, investigated the angular dependence of the observed series of resonances and found that the three largest resonances observed in the free space scattering experiment were all dipolar in nature. In 1957 Dattner (3) performed a set of scattering experiments in a 6 cm. waveguide with the plasma column placed across the guide such that the electric field of the incident wave was perpendicular to the column axis. Again he found resonances in the scattering cross section similar to those found by Romell. Although the experiments of Romell, Boley, and Dattner graphically describe the problem, these men were not the first to observe the phenomenon. It was first observed in 1931 by Tonks (4), and has received

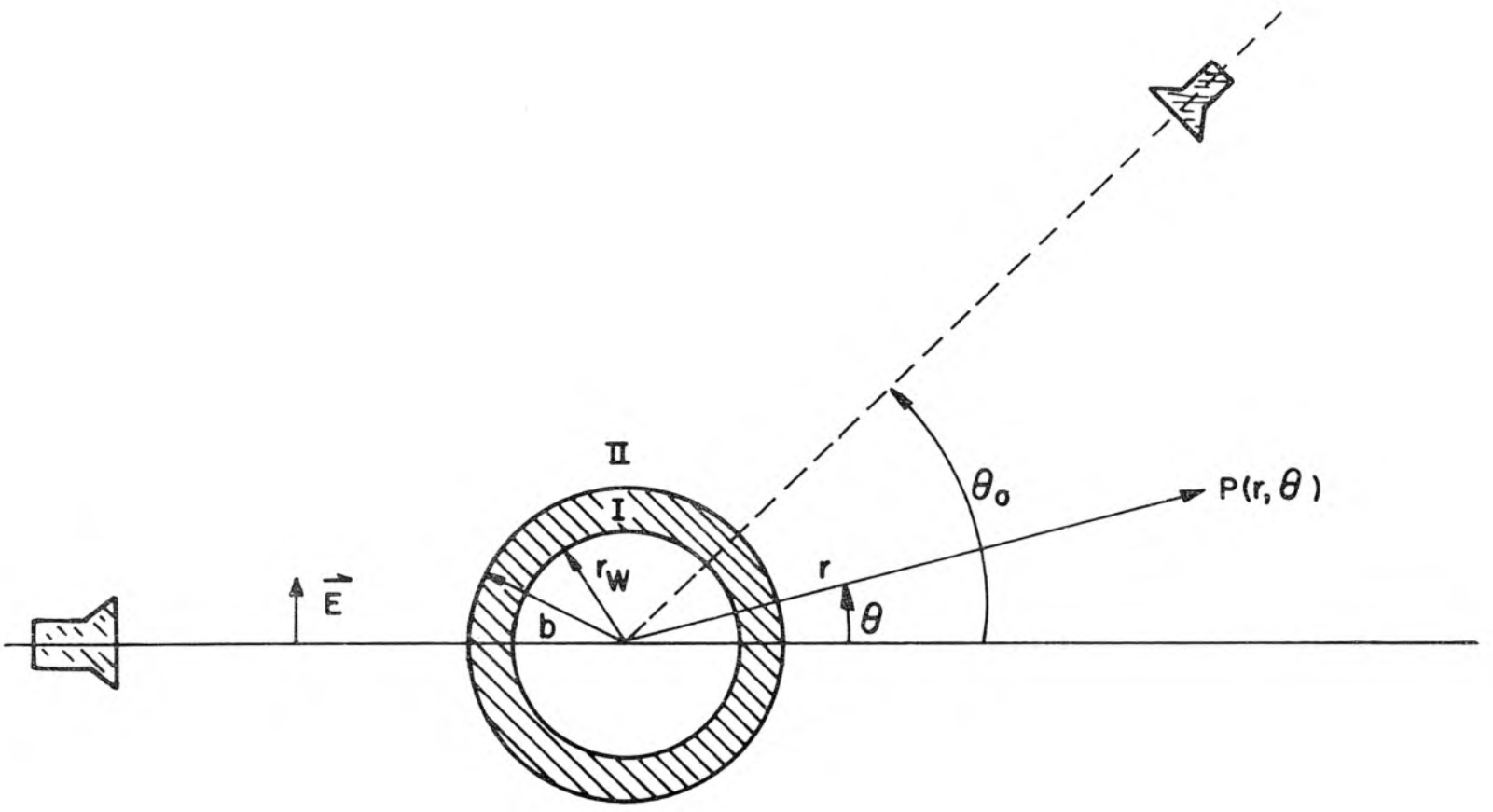

Figure 1.1 Experimental arrangement similar to that used by Romell

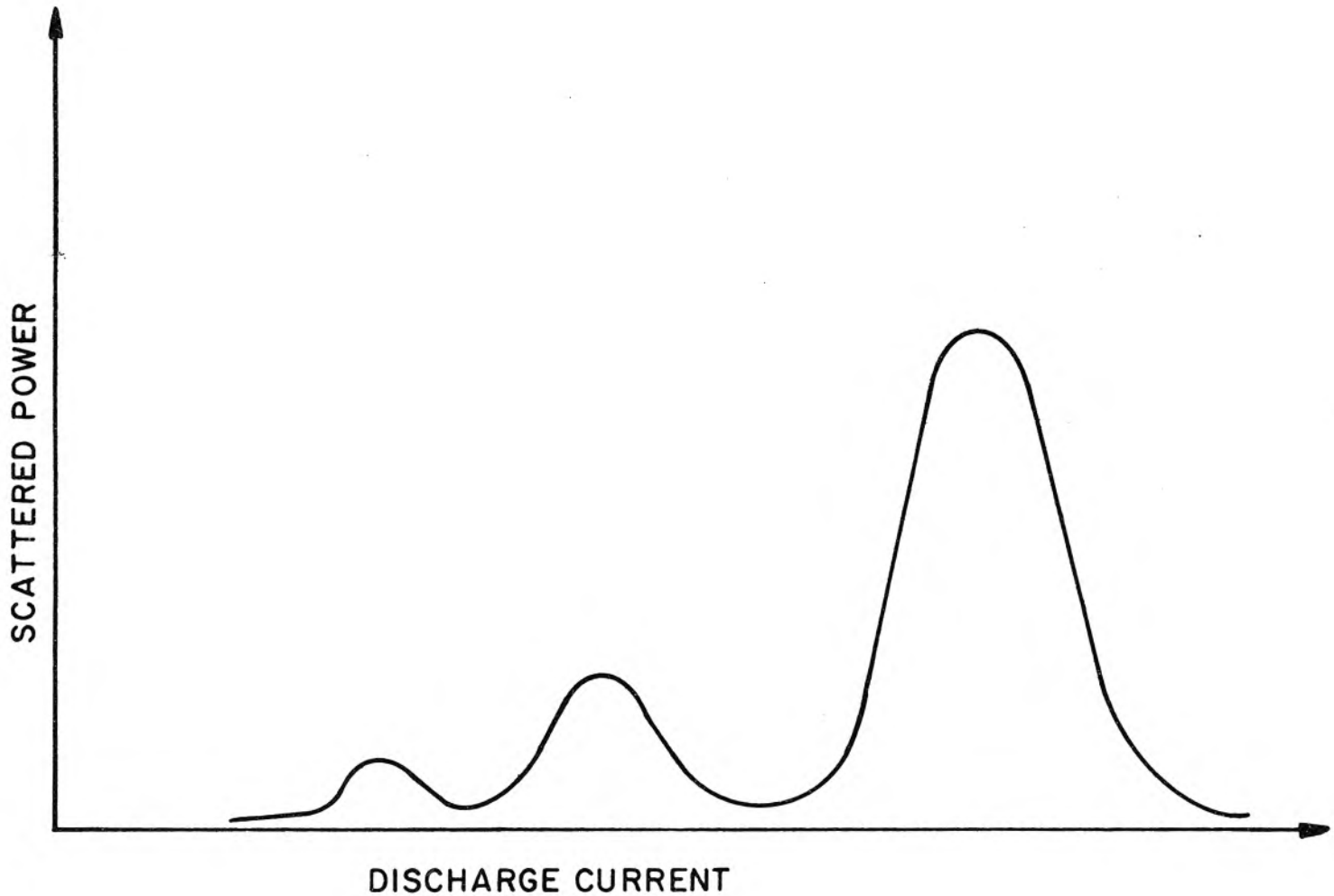

Figure 1.2 Resonance spectrum obtained by Romell

considerable attention since (5-15).

It has been the purpose of the present investigation to examine the properties of this series of resonances as a function of the exciting frequency and the plasma parameters. We have also investigated a similar series of resonances which are quadrupolar in nature, and finally we have made a preliminary investigation of the effect on the resonances of a static magnetic field parallel to the column axis.

1.2 Separation of the Field Solutions Exterior to the Plasma Region from the Solutions within the Plasma Region

The problem of analyzing the scattering experiments of Romell, Dattner, and others, as well as experiments performed in this investigation, resolves itself into two parts. In the region outside the plasma column the source-free Maxwell's equations hold (neglecting exciting elements). Inside of the column currents can flow and charges can build up so that in this region sources must be included in Maxwell's equations. It is possible at the outset to separate field solutions exterior to the plasma region from those within the plasma region. As an example, let us analyze Romell's experiment. Using the notation of Figure 1.1, we see that outside of the plasma all of the fields (E_r and E_θ) can be derived from B_z where B_z satisfies

$$(\nabla^2 + \beta^2)B_z = 0 \tag{1.1}$$

$$\beta^2 = \omega^2 \mu_o \epsilon \tag{1.2}$$

and where

$$E_r = \frac{i}{\omega \mu_o \epsilon} \frac{1}{r} \frac{\partial B_z}{\partial \theta} \tag{1.3}$$

$$E_\theta = \frac{-i}{\omega \mu_o \epsilon} \frac{\partial B_z}{\partial r} \quad . \tag{1.4}$$

In Region II $(r > b)$ we can write, assuming $e^{-i\omega t}$ time dependence

$$B_z^{II} = B_z^{inc} + B_z^{scat} = \sum_{n=0}^{\infty} (B_o \delta_n i^n) \left\{ J_n(\beta_2 r) + S_n H_n^{(1)}(\beta_2 r) \right\} \cos n\theta \tag{1.5}$$

where B_o is the magnitude of the incident magnetic field and

$$\delta_n = \begin{cases} 1 & n = 0 \\ 2 & n \neq 0 \end{cases} \quad .$$

Thus

$$E_r^{II} = \frac{-i}{\omega \mu_o \epsilon_o r} \sum_{n=0}^{\infty} (B_o \delta_n i^n) n \left\{ J_n(\beta_2 r) + S_n H_n^{(1)}(\beta_2 r) \right\} \sin n\theta \tag{1.6}$$

$$E_\theta^{II} = \frac{-i\beta_2}{\omega \mu_o \epsilon_o} \sum_{n=0}^{\infty} (B_o \delta_n i^n) \left\{ J_n'(\beta_2 r) + S_n H_n^{(1)'}(\beta_2 r) \right\} \cos n\theta \ . \tag{1.7}$$

Similarly, in Region I, $(r_w < r < b)$ we can write

$$E_r^I = \frac{-i}{\omega \mu_o \epsilon_1 r} \sum_{n=0}^{\infty} (B_o \delta_n i^n) n \left\{ A_n J_n(\beta_1 r) + B_n N_n(\beta_1 r) \right\} \sin n\theta \tag{1.8}$$

$$E_\theta^I = \frac{-i\beta_1}{\omega \mu_o \epsilon_1} \sum_{n=0}^{\infty} (B_o \delta_n i^n) \left\{ A_n J_n'(\beta_1 r) + B_n N_n'(\beta_1 r) \right\} \cos n\theta \ . \tag{1.9}$$

At $r = b$ and $r = r_w$ the tangential electric fields and the normal

electric displacements must be continuous. Let us assume that inside of the plasma we can write

$$E_r^p = \sum E_{rn}^p(r) \sin n\theta \tag{1.10}$$

$$E_\theta^p = \sum E_{\theta n}^p(r) \cos n\theta \tag{1.11}$$

where the functions $E_{rn}^p(r)$ and $E_{\theta n}^p(r)$ can depend upon the plasma parameters. If we define the quantity L_n as

$$L_n = \frac{n}{r_w} \frac{K_p E_{rn}^p}{E_{\theta n}^p} \tag{1.12}$$

where K_p is the relative dielectric constant of the plasma region, we can write the boundary conditions at $r = r_w$ and $r = b$ as

$$L_n = \frac{K_1 n^2}{r_w^2 \beta_1} \frac{A_n J_n(\beta_1 r_w) + B_n N_n(\beta_1 r_w)}{A_n J_n'(\beta_1 r_w) + B_n N_n'(\beta_1 r_w)} \tag{1.13}$$

$$A_n J_n(\beta_1 b) + B_n N_n(\beta_1 b) = J_n(\beta_2 b) + S_n H_n^{(1)}(\beta_2 b) \tag{1.14}$$

$$A_n J_n'(\beta_1 b) + B_n N_n'(\beta_1 b) = \frac{K_1 \beta_2}{\beta_1} \left\{ J_n'(\beta_2 b) + S_n H_n^{(1)'}(\beta_2 b) \right\} \tag{1.15}$$

where K_1 is the relative dielectric constant of Region I. These equations, 1.13, 1.14, 1.15, can be solved for the scattering amplitude S_n. In the experiments considered $\beta_1 r_w$, $\beta_1 b$, $\beta_2 b \ll 1$. If we make the small argument approximation in the various Bessel functions and look for the scattering amplitude S_n, we find

$$S_n = \frac{\pi\beta_2^{2n}}{i\,2^{n+1}\,n!(n-1)!} \times \frac{\frac{r_w}{n}\left[r_w^{2n}(K_1+1) - b^{2n}(K_1-1)\right] - \frac{r_w^2 L}{K_1 n^2}\left[r_w^{2n}(K_1+1) + b^{2n}(K_1-1)\right]}{\frac{r_w^2 L}{K_1 n^2}\left[\left(\frac{r_w}{b}\right)^{2n}(K_1-1) + (K_1+1)\right] + \frac{r_w}{n}\left[(K_1+1) - \left(\frac{r_w}{b}\right)^{2n}(K_1-1)\right]} \cdot \quad (1.16)$$

The scattering amplitude becomes large or a resonance occurs when the denominator of 1.16 vanishes or when

$$L_n = -\frac{n}{r_w} K_1 \frac{\left(\frac{b}{r_w}\right)^n (K_1+1) - \left(\frac{r_w}{b}\right)^n (K_1-1)}{\left(\frac{b}{r_w}\right)^n (K_1+1) + \left(\frac{r_w}{b}\right)^n (K_1-1)} \cdot \quad (1.17)$$

Defining the effective dielectric constant K_{eff} as

$$K_{eff} = K_1 \frac{\left(\frac{b}{r_w}\right)^n (K_1+1) - \left(\frac{r_w}{b}\right)^n (K_1-1)}{\left(\frac{b}{r_w}\right)^n (K_1+1) + \left(\frac{r_w}{b}\right)^n (K_1-1)} \quad (1.18)$$

we can write the resonance condition as

$$L_n = -\frac{n}{r_w} K_{eff} \cdot \quad (1.19)$$

We note that $1 \leq K_{eff} \leq K_1$ approaches the value K_1 when $b \gg r_w$ and has the value unity when $b = r_w$. The resonance condition would be the same if the plasma were surrounded by an infinite medium having the dielectric constant K_{eff}.

The left hand side of expression 1.19 depends only upon the field solutions in the plasma region, while the right hand side depends only upon the field solutions external to the plasma region. Thus in this sense the problem we are considering can be divided into two parts. We shall see (Chapter III and Appendix B) that for all of the experimental arrangements considered, the resonance condition can be written in the form given in equation 1.19 where K_{eff} depends on the apparatus surrounding the plasma column.

In all of the following analyses of the plasma region we shall use the quasi-static approximation. Since the wavelength of the exciting radiation is much longer than the diameter of the plasma column, we shall assume that $\underset{\sim}{E}$ is derivable from a scalar potential or that

$$\underset{\sim}{E} = - \nabla \phi \quad . \tag{1.20}$$

If we then assume that in the plasma region ϕ can be written as

$$\phi^p(r,\theta) = \sum_n \phi_n^p(r) \sin n\theta \tag{1.21}$$

where the functions $\phi_n^p(r)$ can depend upon the plasma parameters, we find that

$$L_n \equiv \frac{nK_p E_{rn}^p}{r_w E_{\theta n}^p} = \frac{K_p}{\phi_n^p(r_w)} \left. \frac{d\phi_n^p(r)}{dr} \right|_{r=r_w} \quad . \tag{1.22}$$

We shall refer to L_n simply as the logarithmic derivative.

1.3 Early Plasma Models

We can consider our plasma to be composed of electrons, ions and neutrals (the plasma is usually less than 1% ionized for experiments considered here). Since the ions are approximately 10^5 times as massive as the electrons, we shall assume that for high frequency disturbances considered here the ions remain at rest. Thus for our purposes we shall consider the plasma as consisting of an electron gas moving in a "stationary" background of ions. We shall, in general, describe the electron gas by the density $n(\underset{\sim}{r},t)$, the velocity $\underset{\sim}{v}(\underset{\sim}{r},t)$, the scalar pressure $p(\underset{\sim}{r},t)$ and the temperature T (assuming the gas to be Maxwellian). For our plasmas n is on the order of 10^9-10^{10} elec/cc and T is on the order of several electron volts. One of the fundamental problems is to describe the motion of this electron gas.

One of the first methods (1) of describing the motion of the electron gas was to use the hydrodynamic equations (Appendix A), neglecting the pressure term, coupled with Maxwell's equations. That is, we assume for the electron gas

$$\frac{\partial \underset{\sim}{v}}{\partial t} + (\underset{\sim}{v} \cdot \nabla)\underset{\sim}{v} = -\frac{e}{m}\underset{\sim}{E} \tag{1.23}$$

where we neglect the magnetic force. Linearizing this equation and assuming $e^{-i\omega t}$ time dependence, we find

$$\underset{\sim}{v} = -\frac{ie}{\omega m}\underset{\sim}{E} \tag{1.24}$$

from which we see that

$$\underset{\sim}{J} = - ne\underset{\sim}{v} = \frac{ine^2}{\omega m} \underset{\sim}{E} \quad . \tag{1.25}$$

Then from Maxwell's curl equation

$$\nabla \times \underset{\sim}{B} = \mu_o \underset{\sim}{J} - i\omega \mu_o \epsilon_o \underset{\sim}{E} \tag{1.26}$$

coupled with 1.25, we can write

$$\nabla \times \underset{\sim}{B} = - i\omega \mu_o \epsilon \underset{\sim}{E} \tag{1.27}$$

where

$$\epsilon = \epsilon_o \left(1 - \frac{\omega_p^2}{\omega^2}\right) \tag{1.28}$$

and

$$\omega_p^2 = \frac{ne^2}{m\epsilon_o} \tag{1.29}$$

is called the plasma frequency. Thus in this approximation the plasma can be described by a dielectric constant given by equation 1.28. If we now assume that our plasma column of radius r_w is described by a uniform dielectric constant ϵ and we write for the potential in the plasma region

$$\phi_1^p = \sum A_n r^n \sin n\theta \tag{1.30}$$

we find for the logarithmic derivative L_n

$$L_n = \frac{n}{r_w} \left(1 - \frac{\omega_p^2}{\omega^2}\right) \quad . \tag{1.31}$$

Substituting 1.31 into the resonance condition (equation 1.19), we find a single resonance occurs at

$$\omega^2 = \frac{\omega_p^2}{1 + K_{eff}} \tag{1.32}$$

There have been several attempts (16-19) to explain the resonance phenomenon in terms of a dielectric constant, but all predict only one resonance instead of the series observed. Kino and Crawford (9) have shown, using a variational technique, that if the dielectric constant is allowed to vary with r (corresponding to a radial electron density gradient), the dipole resonant frequency is given by

$$\omega^2 = \frac{\overline{\omega_p^2}}{1 + K_{eff}} \tag{1.33}$$

where

$$\overline{\omega_p^2} = \frac{\bar{n}e^2}{m\epsilon_o} \tag{1.34}$$

and $\bar{n}$ is the average electron density. It is found that at high electron densities (Chapter IV), equation 1.33 predicts the largest resonance of Figure 1.2 (at the highest current) with reasonable accuracy. It still predicts, however, only one resonance. During the rest of this paper we shall refer to the resonance predicted approximately by the dielectric model as the <u>main</u> resonance.

The description of the plasma in terms of a dielectric constant ignores several important features of the plasma. In this zero temperature approximation, longitudinal plasma waves of finite phase velocity and non-zero group velocity are not supported by the plasma. One might suspect that these plasma waves could play an important

role in our resonance problem. For example, one might imagine radially propagating plasma waves which are somehow reflected at the glass boundary $r = r_w$ giving rise to standing waves. The observed resonances might correspond to different half-wavelengths in the standing wave. In 1959 Gould (20) showed that if the thermal velocities were taken into account in a uniform plasma by a scalar pressure term in the hydrodynamic equations (Appendix A), a series of resonances could be obtained. These resonances do, in fact, correspond to radial standing plasma waves. Gould's analysis assumed the following set of equations

$$\frac{\partial n}{\partial t} + \nabla \cdot n\underset{\sim}{v} = 0 \tag{1.35}$$

$$\frac{\partial v}{\partial t} + \underset{\sim}{v} \cdot \nabla \underset{\sim}{v} = \frac{e}{m}\nabla\phi - \frac{1}{mn}\nabla p \tag{1.36}$$

$$\nabla^2\phi = -\frac{e}{\epsilon_o}[n_i(\underset{\sim}{r}) - n(\underset{\sim}{r})] \tag{1.37}$$

$$E = -\nabla\phi \tag{1.38}$$

where $n(r,\theta,t)$ is the electron density and $n_i(r,\theta,t)$ is the ion density. These equations were then linearized

$$n(r,\theta,t) = n_o + \tilde{n}(r,\theta)e^{-i\omega t} \tag{1.39}$$

$$n_i(r,\theta,t) = n_i(r,\theta) = n_i = \text{const.} \tag{1.40}$$

$$p(r,\theta,t) = p_o + \tilde{p}(r,\theta)e^{-i\omega t} \tag{1.41}$$

$$\phi(r,\theta,t) = \tilde{\phi}(r,\theta)e^{-i\omega t} \tag{1.42}$$

$$\underset{\sim}{v}(r,\theta,t) = \tilde{\underset{\sim}{v}}(r,\theta)e^{-i\omega t} \tag{1.43}$$

and the pressure related to the temperature (Appendix A) through

$$p_o = n_o kT \tag{1.44}$$

$$\tilde{p} = 3kT\tilde{n} \quad . \tag{1.45}$$

The above set of equations was combined into a single equation for the potential as

$$\nabla^2(\nabla^2 + k^2)\tilde{\phi}(r,\theta) = 0 \tag{1.46}$$

where

$$k^2 = \frac{\omega^2 - \omega_p^2}{w^2} = \frac{1}{3\lambda_D^2}\left[\frac{\omega^2}{\omega_p^2} - 1\right] \tag{1.47}$$

$$w^2 = \frac{3kT}{m} \tag{1.48}$$

$$\lambda_D^2 = \frac{\epsilon_o kT}{n_o e^2} \quad . \tag{1.49}$$

Solutions of equation 1.46 can be written in the form

$$\tilde{\phi}_n^p(r,\theta) = \left\{A_n\left(\frac{r}{r_w}\right)^n + B_n \frac{J_n(kr)}{J_n(kr_w)}\right\}\sin n\theta \quad . \tag{1.50}$$

Gould next specifies the boundary condition that at $r = r_w$ the normal component of the electron current $J_r = n_o e \tilde{v}_r$ must vanish.

This implies that

$$\frac{\partial \tilde{\phi}_n^p}{\partial r} - \frac{w^2}{\omega_p^2} \frac{\partial}{\partial r} (\nabla^2 \tilde{\phi}_n^p) = 0 \qquad (1.51)$$

and gives a relation between A_n and B_n. Using 1.51 the potential of equation 1.50 can be written as

$$\tilde{\phi}_n^p(r,\theta) = B_n \left\{ \frac{J_n(kr)}{J_n(kr_w)} - \frac{r_w k}{n}\left(1 + \frac{k^2 w^2}{\omega_p^2}\right) \frac{J_n'(kr_w)}{J_n(kr_w)} \left(\frac{r}{r_w}\right)^n \right\} \sin n\theta \; . \qquad (1.52)$$

The derivative of the potential may now be calculated and the logarithmic derivative L_n (equation 1.22) computed. It should be noted that K_p is set equal to one in equation 1.22 since in this analysis the effects of the electron motion are treated explicitly rather than through an equivalent dielectric constant. If this logarithmic derivative is inserted in the resonance condition of equation 1.19, one finds that the conditions for resonance are determined by the solution of

$$\frac{n}{kr_w} \frac{J_n(kr_w)}{J_n'(kr_w)} = \frac{\omega^2}{\omega_p^2} + \frac{1}{K_{eff}} \left(\frac{\omega^2}{\omega_p^2} - 1\right) \qquad (1.53)$$

where again

$$kr_w = \frac{1}{\sqrt{3}} \left[\frac{r_w}{\lambda_D} \frac{\omega^2}{\omega_p^2} - 1 \right]^{1/2} \; .$$

Solving equation 1.53 graphically using large values of r_w/λ_D which one expects, one finds a single resonance

$$\omega_o^2 \simeq \frac{\omega_p^2}{1 + K_{eff}} \qquad (1.54)$$

below the plasma frequency (corresponding to the main resonance discussed previously) and a series of resonances at the plasma frequency and above given by

$$\omega_n^2 = \omega_p^2\left(1 + \frac{3\lambda_D^2}{r_w^2} X_n^2\right) \tag{1.55}$$

where $X_1 \approx 5.3$, $X_2 \approx 8.5$, etc. Thus by considering radial plasma standing waves one can generate a series of resonances. It is found, however, that when the resonant frequencies predicted by equation 1.55 are compared with experiment, their relative spacing is much smaller than than experimentally observed. That is,

$$\omega_{n+1}^2 - \omega_n^2 = \omega_p^2 \frac{3\lambda_D^2}{r_w^2}\left(X_{n+1}^2 - X_n^2\right) \tag{1.56}$$

is smaller than that observed. Furthermore, it is experimentally observed that several of the resonances seen above the main resonance lie below the average plasma frequency $\overline{\omega_p^2}$. This is in contradiction to equation 1.55 which states that the plasma wave resonances lie above the plasma frequency. One can see from equation 1.56 that the frequency spacing could be increased if somehow r_w were smaller than we thought it was. That is, perhaps not all of the tube is active in supporting these plasma waves. One can conceive of this situation by assuming that the plasma column has a radial electron density profile. Consider the radial density profile shown in Figure 1.3. If the column is excited at a frequency

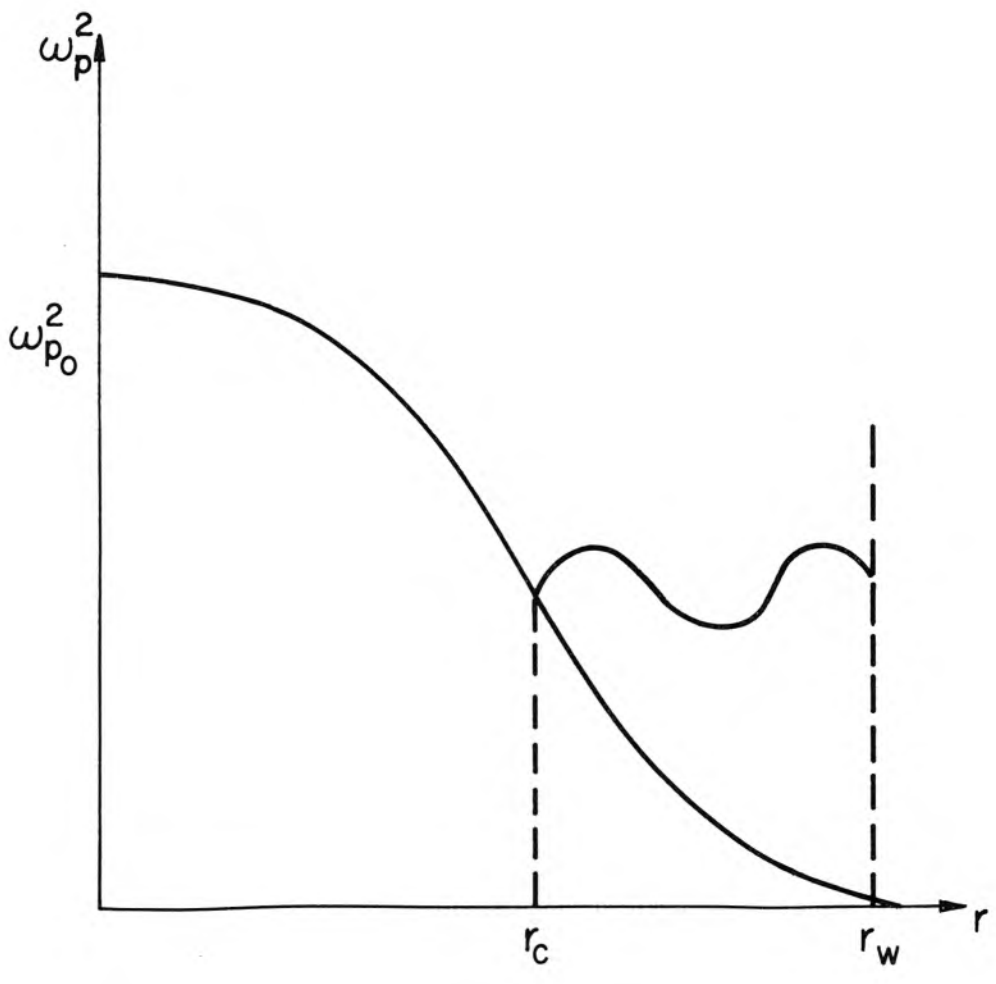

Figure 1.3

ω less than the center frequency, plasma waves can propagate only in the region $r > r_c$ where r_c is determined by $\omega_p(r_c) = \omega$. For $r < r_c$ we will have $\omega_p > \omega$ which implies an imaginary propagation constant k or evanescent waves (assuming a dispersion relation similar to equation 1.47 is valid with ω_p depending upon r). In this case we might imagine the standing waves to be set up between r_c and r_w.

In 1960 Gould (21) employed a WKB type method to determine the spectrum of plasma wave resonances assuming a radial density profile given by $n = n_o(1 - \alpha \frac{r^2}{r_w^2})$ where n_o is the density on the axis $r = 0$ and α is a parameter between 0 and 1. He found that indeed the relative resonant frequency spectrum could be made larger and, furthermore, it increased with increasing α. Thus it appears that to explain the observed resonance spectrum, at least several important properties of the plasma column must be considered. First, the thermal properties of the plasma must be included to allow propagating radial plasma waves (so that multiple resonances can be predicted at all). Second the radial plasma density profile must be considered.

1.4 Objectives of Our Experiments

In 1962 Parker calculated theoretical density profiles (22) for a mercury discharge similar to that used by us and others. These profiles are found to depend upon the parameter $r_w^2/\overline{\lambda_D^2}$ (Chapter II) where $\overline{\lambda_D^2} = \epsilon_o kT_e/\bar{n}e^2$ is the Debye length defined in terms of the average electron density $\bar{n}$. We shall refer to $\overline{\lambda_D^2}$ as the average Debye length in the remainder of this paper, but it should be noted that it is the Debye length defined in terms of the average electron density $\bar{n}$. The profiles obtained by Parker are shown in Figure 2.2. It is seen that the shape of the density profiles change only slightly in the range $10^4 \lesssim r_w^2/\overline{\lambda_D^2} < \infty$. It is just in this range that most of the previous investigators have concentrated their efforts. One might expect from what has been said in previous sections, that the relative frequency spectrum might not vary appreciably

in this region. We have concentrated our efforts on the range $2\times10^2 < r_w^2/\overline{\lambda_D^2} < 10^4$ in order to investigate the role of the density profile on the resonances.

It is also apparent from the discussion of Section 1.3 that not only should the $n = 1$ or dipole series of resonances exist, but the $n = 2,3,4 \cdots$ (quadrupole, sextupole, $\cdots$) series should also exist. We have therefore investigated the $n = 2$ or quadrupole resonance spectrum. Finally, we have made a preliminary investigation of the effects of a static axial magnetic field on the dipole resonance spectrum.

In Chapter II we shall discuss the theory of a hot nonuniform plasma column which is used in the interpretation of our data. Chapters III and IV will be devoted to a discussion of experimental techniques and results for the zero magnetic field case. Chapter V will discuss preliminary work on the finite magnetic field case and, finally, Chapter VI will be devoted to a summary and proposals for further work.

II. THEORY OF A HOT NONUNIFORM PLASMA COLUMN

2.1 Introduction

Let us consider an infinitely long plasma column of radius $r = r_w$. It is the purpose of this chapter to examine the simultaneous solution of the plasma dynamical equations and Maxwell's equations in order to determine the logarithmic derivative L_n (equation 1.22) at the surface of the plasma column ($r = r_w$). As in Section 1.3, we shall assume that the plasma consists of an electron gas moving in a "stationary" background of ions. We shall again describe the electron gas by its density $n(\underset{\sim}{r},t)$, its pressure $p(\underset{\sim}{r},t)$, its velocity $\underset{\sim}{v}(\underset{\sim}{r},t)$ and its temperature T (assuming the gas to have a Maxwellian velocity distribution.) In this chapter, however, we shall assume that the electron density has a radial density profile where, in the absence of any disturbances, $n = n_o f(r)$ (n_o is the density at $r = 0$). All dissipative effects will be ignored.

2.2 Basic Equations

We take for the dynamical equations describing the motion of the plasma, the first three moments of the Boltzmann equation (23), assuming a scalar pressure. The chain of moment equations has been terminated by neglecting the divergence of the heat flux tensor in the third moment. This assumption allows us to make an appropriate relation between the assumed scalar pressure $p(\underset{\sim}{r},t)$ and the density $n(\underset{\sim}{r},t)$ in the second moment, thus yielding a closed set of equations. The method of obtaining these equations from the Boltzmann equation is discussed in Appendix A. We have for the dynamical

equations:

$$\frac{\partial n}{\partial t} + \nabla \cdot n\underset{\sim}{v} = 0 \tag{2.1}$$

$$\frac{\partial \underset{\sim}{v}}{\partial t} + (\underset{\sim}{v} \cdot \nabla)\underset{\sim}{v} = -\frac{e}{m}(\underset{\sim}{E} + \underset{\sim}{v} \times B) - \frac{1}{mn}\nabla p \quad . \tag{2.2}$$

Equations 2.1 and 2.2 must be solved simultaneously with Maxwell's equations. Since in our experiments the wavelength of the exciting fields is so long (10 cm or greater) compared to the diameter of the plasma column (2 cm or less) we shall assume that $\underset{\sim}{E}$ is derivable from a scalar potential or that

$$\underset{\sim}{E} = -\nabla\phi \quad . \tag{2.3}$$

This quasi-static assumption reduces Maxwell's equations to the Poisson equation

$$\nabla^2\phi = -\frac{\rho}{\epsilon_o} = -\frac{e}{\epsilon_o}\left[n_1(\underset{\sim}{r},t) - n(\underset{\sim}{r},t)\right] \quad . \tag{2.4}$$

Equation 2.2 becomes

$$\frac{\partial \underset{\sim}{v}}{\partial t} + \underset{\sim}{v} \cdot \nabla\underset{\sim}{v} = \frac{e}{m}\left[\nabla\phi - \underset{\sim}{v} \times B\right] - \frac{1}{mn}\nabla p \quad . \tag{2.5}$$

Equations 2.1, 2.4 and 2.5 form a set of coupled nonlinear equations which is difficult to solve outright. Let us assume that the applied fields induce only small perturbations in the appropriate equilibrium quantities and write

$$n(\underset{\sim}{r},t) = n_o f(r) + \tilde{n}(\underset{\sim}{r})e^{-i\omega t} \tag{2.6}$$

$$n_i(\underset{\sim}{r},t) = n_i(r) \tag{2.7}$$

$$p(\underset{\sim}{r},t) = p_o(r) + \tilde{p}(\underset{\sim}{r})e^{-i\omega t} \tag{2.8}$$

$$\phi(\underset{\sim}{r},t) = \phi_o(r) + \tilde{\phi}(\underset{\sim}{r})e^{-i\omega t} \tag{2.9}$$

$$\underset{\sim}{v}(\underset{\sim}{r},t) = \tilde{\underset{\sim}{v}}(\underset{\sim}{r})e^{-i\omega t} \tag{2.10}$$

$$\underset{\sim}{B}(\underset{\sim}{r},t) = \tilde{\underset{\sim}{B}}(\underset{\sim}{r})e^{-i\omega t} \tag{2.11}$$

where it is assumed that $\tilde{n}(\underset{\sim}{r}) \ll n_o f(r)$, $\tilde{p}(\underset{\sim}{r}) \ll p_o(r)$, $\tilde{\phi}(\underset{\sim}{r}) \ll \phi_o(r)$. If equations 2.6 through 2.11 are substituted in equations 2.1, 2.4 and 2.5 and only terms linear in the perturbation quantities are retained, the following set of zero and first order equations are obtained:

Zero Order

$$\nabla p_o = e n_o f(r) \nabla \phi_o \tag{2.12}$$

$$\nabla^2 \phi_o = -\frac{e}{\epsilon_o}\left[n_i(r) - n_o f(r)\right] \tag{2.13}$$

First Order

$$-i\omega \tilde{n} + \nabla \cdot n_o f(r)\tilde{\underset{\sim}{v}} = 0 \tag{2.14}$$

$$i\omega m n_o f(r)\tilde{\underset{\sim}{v}} = -e n_o f(r) \nabla\tilde{\phi} + \nabla\tilde{p} - e\tilde{n}\nabla\phi_o \tag{2.15}$$

$$\nabla^2\tilde{\phi} = \frac{e}{\epsilon_o}\tilde{n} \quad . \tag{2.16}$$

The zero order equations 2.12 and 2.13 together with an appropriate

boundary condition at $r = r_w$ and an assumption concerning $n_i(r)$ will be employed in Section 2.4 to determine the static electron density profile $f(r)$. The first order equations 2.14, 2.15, and 2.16 govern the wave phenomena in the plasma. It is shown in Appendix A that if we assume the electron gas to have a Maxwellian velocity distribution, we can relate the pressure to the density as

$$p_o = n_o f(r) kT \tag{2.17}$$

$$\tilde{p} = \gamma kT \tilde{n} \tag{2.18}$$

where $\gamma = 3$. Equation 2.17 simply states that the electron gas follows the perfect gas law while equation 2.18 states that the perturbations obey the adiabatic law

$$\frac{p}{n^\gamma} = \frac{p_o}{n_o^\gamma} \quad . \tag{2.19}$$

Since we are going to be considering plasma waves traveling in the radial direction, the choice of $\gamma = 3$ which is appropriate to 1 degree of freedom is reasonable. Using equations 2.12, 2.17 and 2.18 the first order equations 2.14, 2.15 and 2.16 can be combined into a single fourth order partial differential equation for the potential perturbation $\tilde{\phi}$ (24) :

$$\nabla^4\tilde{\phi} + \frac{1}{r}\left(\frac{\nabla f}{f}\cdot\nabla\right)\nabla^2\tilde{\phi} + \left\{\frac{1}{r\lambda_{DO}^2}\left[\frac{\omega^2}{\omega_{po}^2} - f\right] - \frac{1}{r}\nabla\cdot\frac{\nabla f}{f}\right\}\nabla^2\tilde{\phi}$$

$$- \frac{1}{r\lambda_{DO}^2}\nabla\tilde{\phi}\cdot\nabla f = 0 \qquad (2.20)$$

where

$$\lambda_{DO}^2 = \frac{\epsilon_o kT}{n_o e^2} \qquad (2.21)$$

is the Debye length at the center of the discharge and

$$\omega_{po}^2 = \frac{n_o e^2}{m\epsilon_o} \qquad (2.22)$$

is the plasma frequency at the center of the discharge. In solving equation 2.20, we demand as a boundary condition that the normal component of the electron gas current density $\tilde{J}_r = n_o f(r) e\tilde{v}_r$ vanish at the wall $r = r_w$ (as in Section 1.3). Since $n_o f(r)$ does not vanish at $r = r_w$, we must have $\tilde{v}_r = 0$ at r_w. The vanishing of $\tilde{v}_r$ at $r = r_w$ demands that the potential satisfy

$$\frac{\partial}{\partial r}(\nabla^2\tilde{\phi}) - \frac{1}{r f}\frac{df}{dr}\nabla^2\tilde{\phi} - \frac{f(r)}{r\lambda_{DO}^2}\frac{d\tilde{\phi}}{dr} = 0 \quad \text{at} \quad r = r_w . \qquad (2.23)$$

Before equation 2.20 can be solved, a suitable expression for the static radial electron density profile $f(r)$ must be found. Such an expression has been found by Parker (22) using the complete plasma-sheath equations of Langmuir (33). The Langmuir formulation of the equations governing the static electron density profile and their

solutions will be discussed in the following section. We shall then return to discuss the solution of equation 2.20.

2.3 The Static Radial Density Profile

Consider the cross section of the cylindrical plasma column as shown on Figure 2.1. Langmuir assumes that equilibrium exists within the column with a potential distribution $\phi_o(r)$ through which the ions fall to the wall. We choose $\phi_o(r = 0) = 0$. Let the number of ions generated per unit volume per unit time be denoted by $S(r)$. Then if we consider a unit length of column, the number of ions generated per second in the volume between ρ and $\rho + d\rho$ is given by

$$\text{no. of ions per second per unit length generated between } \rho \text{ and } \rho + d\rho = S(\rho)2\pi\rho\, d\rho \quad . \tag{2.24}$$

The number of ions per second passing through the surface at r which originate in the volume between ρ and $\rho + d\rho$ will be

$$(dJ)A = dn_i(r)\, V_r(r,\rho)\rho\pi r \tag{2.25}$$

where $V_r(r,\rho)$ is the ion velocity at r . The ion density $n_i(r)$ at r can be thought of as arising from all volume elements with $\rho < r$. The contribution to the ion density $dn_i(r)$ due to the generation in the volume between ρ and $\rho + d\rho$ can be obtained by equating equations 2.24 and 2.25

$$S(\rho)\, 2\pi\rho\, d\rho = dn_i(r)\, V_r(r,\rho)2\pi r \tag{2.26}$$

or

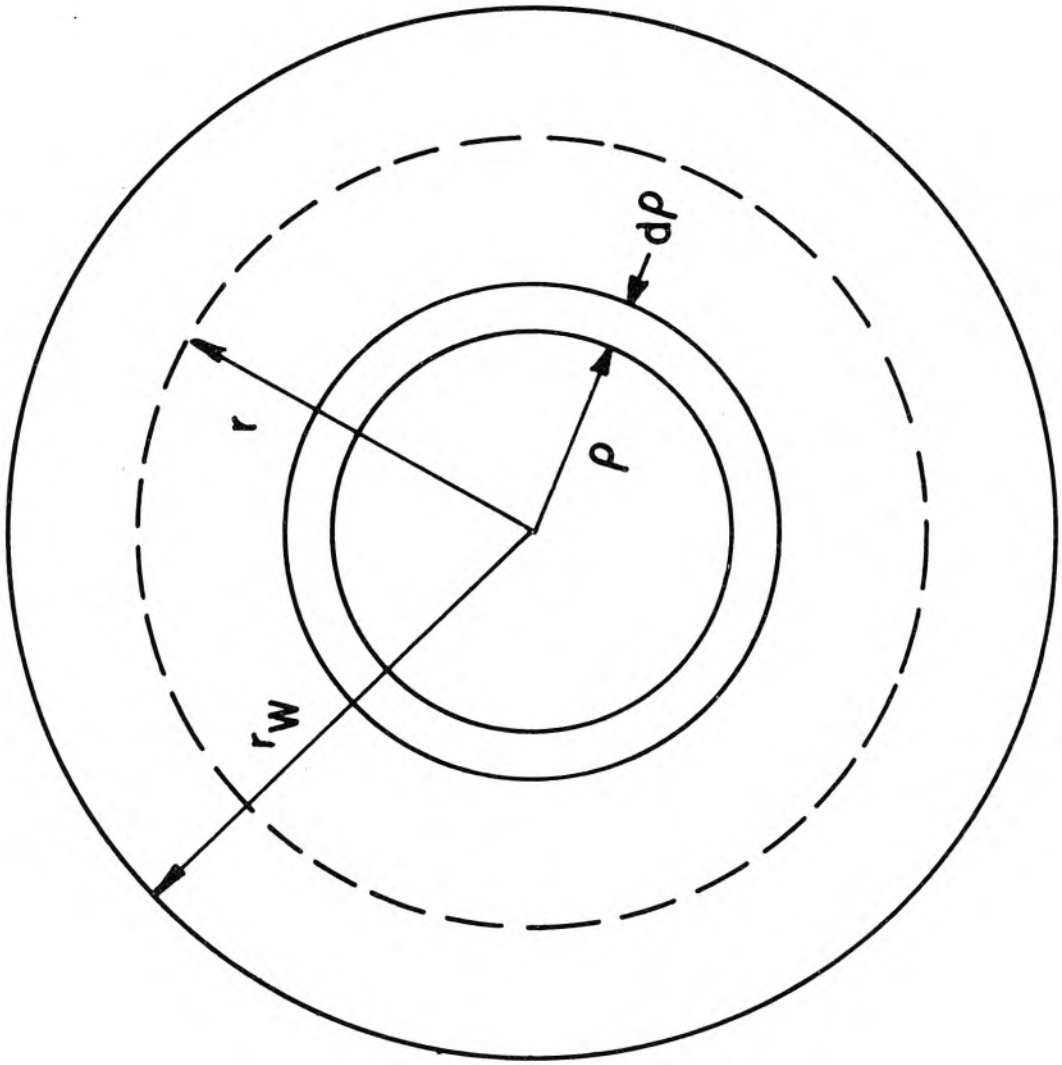

Figure 2.1 Geometry for density profile calculation

$$dn_i(r) = \frac{S(\rho)}{V_r(r,\rho)} \frac{\rho}{r} d\rho \quad . \tag{2.27}$$

Thus the ion density at r can be written as

$$n_i(r) = \int_0^r \frac{S(\rho)}{V_r(r,\rho)} \frac{\rho}{r} d\rho \quad . \tag{2.28}$$

Using equations 2.12 and 2.17 we can write for the electron density:

$$n(r) = n_o e^{\frac{e\phi_o(r)}{kT}} \quad . \tag{2.29}$$

From equation 2.13 Poisson's equation must also hold or

$$\nabla^2\phi_o = -\frac{e}{\epsilon_o} n_i(r) - n(r) \tag{2.30}$$

or

$$\nabla^2\phi_o(r) = \frac{e}{\epsilon_o} n_o e^{\frac{e\phi_o(r)}{kT}} - \frac{e}{\epsilon_o}\int_0^r \frac{S(\rho)}{V_r(r,\rho)} \frac{\rho}{r} d\rho \quad . \tag{2.31}$$

Equation 2.30 has been referred to as the complete plasma-sheath equation (33). We now make two assumptions concerning the ions in our plasma which allow us to relate $V_r(r,\rho)$ and $S(\rho)$ to the potential ϕ_o. These assumptions are:

A. The ions are formed at rest and fall to the wall through the potential without making any collisions.

B. The ions are generated at a rate proportional to the electron density or $S(r) = \alpha\, n(r)$.

From assumption A we can write

$$\frac{1}{2} m_i V_r^2(r,\rho) = e\left[\phi_o(\rho) - \phi_o(r)\right] \tag{2.32}$$

or

$$V_r(r,\rho) = \left(\frac{2e}{m_i}\right)^{1/2} \left[\phi_o(\rho) - \phi_o(r)\right]^{1/2} . \tag{2.33}$$

From assumption B we have

$$S(r) = \alpha n(r) = \alpha n_o e^{\frac{e\phi_o(r)}{kT}} . \tag{2.34}$$

With equations 2.32 and 2.33 the complete plasma-sheath equation becomes

$$\nabla^2\phi_o(r) = \frac{e}{\epsilon_o} n_o e^{\frac{e\phi_o(r)}{kT}} - \frac{\alpha n_o e}{\epsilon_o} \left(\frac{m_i}{2e}\right)^{1/2} \int_0^r \frac{e^{\frac{e\phi_o(\rho)}{kT}} \frac{\rho}{r}}{\left[\phi_o(\rho) - \phi_o(r)\right]^{1/2}} d\rho . \tag{2.35}$$

The properties of equation 2.34 can be made more apparent by introducing the dimensionless variables (33)

$$\eta = -\frac{e\phi_o}{kT} \tag{2.36}$$

$$s = \alpha\left(\frac{m_i}{2kT}\right)^{1/2} r . \tag{2.37}$$

If these variable changes are made in equation 2.34, the dimensionless complete plasma-sheath equation becomes

$$\frac{1}{\beta^2}\left\{ s\,\frac{d^2\eta}{ds^2} + \frac{d\eta}{ds} \right\} = \int_0^s \frac{e^{-\eta(\sigma)}\,\sigma\,d\sigma}{\left[\eta(s) - \eta(\sigma)\right]^{1/2}} - s\,e^{-\eta(s)} \qquad (2.38)$$

where

$$\beta^2 = \frac{2n_o e^2}{\alpha^2 m_i \epsilon_o} \quad . \qquad (2.39)$$

Thus the dimensionless potential distribution $\eta(s)$ is seen to depend upon the plasma parameters through the dimensionless parameter β^2. Given a value of β^2 equation 2.37 can be integrated to give $\eta(s)$ for $0 \leq s < \infty$.

The location of the wall or boundary of the plasma column will be determined by the boundary condition that the electron current equal the ion current at $r = r_w$. The ion current can be written as

$$J_i(r)\,A = 2\pi r\,J_i(r) = \int_0^r S(\rho)\,2\pi\rho\,d\rho \qquad (2.40)$$

or

$$J_i(r) = \int_0^r S(\rho)\,\frac{\rho}{r}\,d\rho \quad . \qquad (2.41)$$

The electron current density is taken to be the random current density of a Maxwellian gas of local density n_e or

$$J_e(r) = \frac{n(r)}{2\sqrt{\pi}}\left(\frac{2kT}{m_e}\right)^{1/2} \quad . \qquad (2.42)$$

Thus the boundary condition at $r = r_w$ becomes

$$\frac{n(r_w)}{2\sqrt{\pi}} \left(\frac{2kT}{m_e}\right)^{1/2} = \int_0^{r_w} S(\rho) \frac{\rho}{r} d\rho \tag{2.43}$$

or

$$e^{\frac{e\phi_o(r_w)}{kT}} \left(\frac{kT}{2\pi m_e}\right)^{1/2} = \alpha \int_0^{r_w} e^{\frac{e\phi_o(\rho)}{kT}} \frac{\rho}{r_w} d\rho \ . \tag{2.44}$$

In dimensionless form the wall condition 2.43 becomes

$$\left(\frac{m_i}{4\pi m_e}\right)^{1/2} = e^{\eta(s_w)} \int_0^{s_w} e^{-\eta(\sigma)} \frac{\sigma}{s_w} d\sigma \tag{2.45}$$

where again

$$s_w = \alpha \left(\frac{m_i}{2kT}\right)^{1/2} r_w \ . \tag{2.46}$$

The complete plasma-sheath equation together with the wall determination has been solved by Parker (22) for a number of values of β^2. The density profiles obtained in his calculation for a mercury plasma are shown in Figure 2.2, while Table 2.1 tabulates the important results for a mercury plasma which are pertinent to our experiments.

It is interesting and also important to note that for many considerations the ionization coefficient α does not need to be known. From equation 2.45 we can write

$$\alpha^2 = \left(\frac{2kT}{m_i}\right) \frac{s_w^2}{r_w^2} \ . \tag{2.47}$$

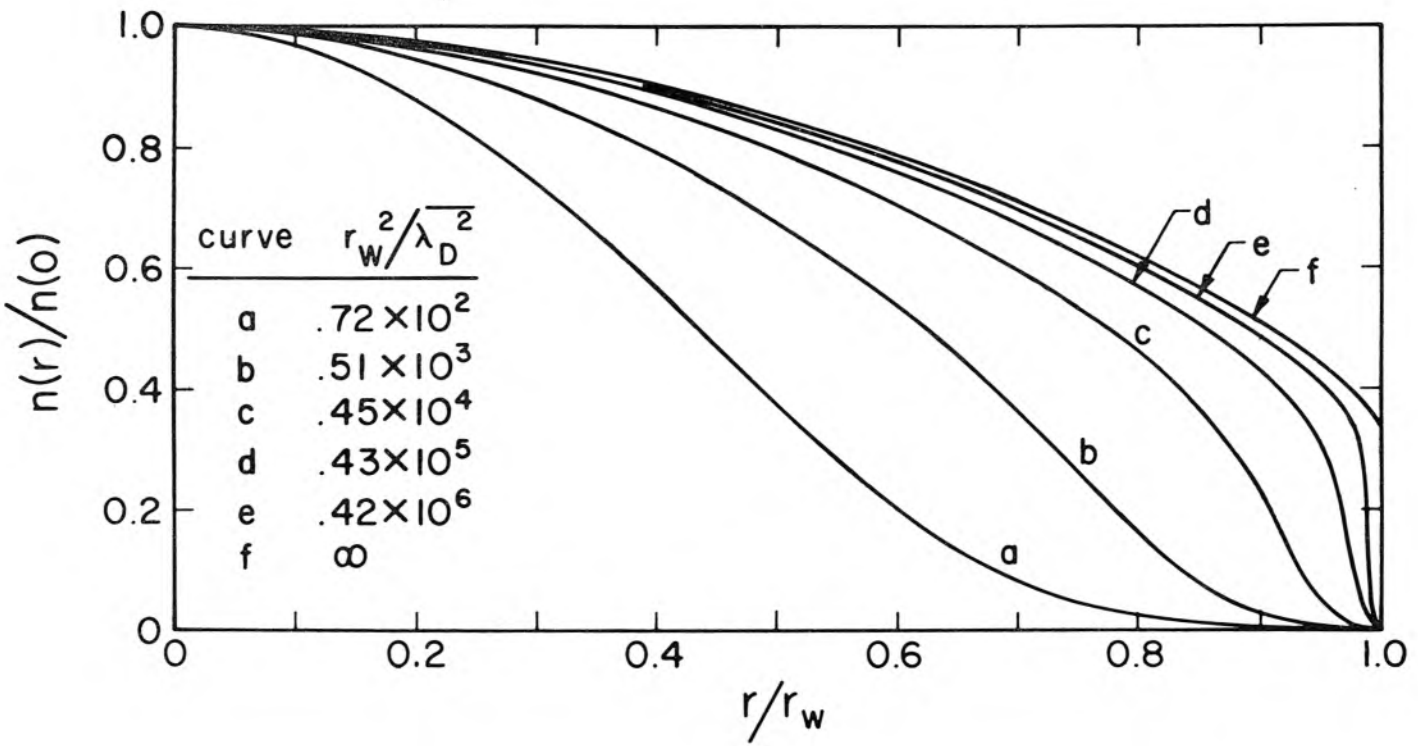

Figure 2.2 Density Profiles Calculated by Parker

Table 2.1

β^2	s_w	$\frac{<n>}{n_o}$	r_w^2/λ_{DO}^2	$r_w^2/\overline{\lambda_D^2}$
10^2	1.787	0.225	3.19×10^2	7.18×10
2×10^2	1.527	0.270	4.66×10^2	1.26×10^2
3.33×10^2	1.38	0.312	6.34×10^2	1.98×10^2
10^3	1.147	0.392	1.32×10^3	5.16×10^2
2×10^3	1.050	0.444	2.21×10^3	9.79×10^2
3.33×10^3	1.000	0.480	3.33×10^3	1.60×10^3
10^4	0.910	0.547	8.28×10^3	4.53×10^3
2×10^4	0.874	0.581	1.53×10^4	8.89×10^3
10^5	0.822	0.637	6.76×10^4	4.31×10^4
2×10^5	0.809	0.653	1.31×10^5	8.54×10^4
10^6	0.789	0.678	6.23×10^5	4.22×10^5
∞	0.772	0.698		

Then using equation 2.46 in equation 2.38 we have

$$\beta^2 = \frac{2n_o e^2}{m_1 \epsilon_o} \frac{m_i}{2kT} \frac{r_w^2}{s_w^2} = \frac{1}{s_w^2} \frac{r_w^2}{\lambda_{DO}^2} = \left(\frac{n_o}{\overline{n}}\right) \frac{1}{s_w^2} \frac{r_w^2}{\overline{\lambda_D^2}} \quad . \tag{2.48}$$

Since $n_o/\overline{n}$ and s_w are calculated for each value of β^2, we see from equation 2.47 that the density profile curves can also be labeled by their values of r_w^2/λ_{DO}^2 or $r_w^2/\overline{\lambda_D^2}$ as well as by β^2.

2.4 Properties and Solutions of the Plasma Wave Potential Equation

From Parker's density profile calculation comes the radial density profile function $f(r) = \frac{n(r)}{n_o}$ needed for the solution of the plasma wave potential equation 2.20. To shed more light on equation

2.20, let us introduce the dimensionless variable

$$\xi = \frac{r}{r_w} \quad . \tag{2.49}$$

We can then write

$$\nabla = \frac{\partial}{\partial r}\underset{\sim}{I}_r + \frac{1}{r}\frac{\partial}{\partial \theta} = \frac{1}{r_w}\frac{\partial}{\partial \xi}\underset{\sim}{I}_r + \frac{1}{r_w \xi}\frac{\partial}{\partial \theta}\underset{\sim}{I}_r = \frac{1}{r_w}\nabla_\xi \tag{2.50}$$

where we define

$$\nabla_\xi = \frac{\partial}{\partial \xi}\underset{\sim}{I}_r + \frac{1}{\xi}\frac{\partial}{\partial \theta}\underset{\sim}{I}_\theta \quad . \tag{2.51}$$

We can then rewrite the potential equation 2.20 as

$$\nabla_\xi^4 \tilde{\phi} + \frac{1}{\gamma}\left(\frac{\nabla_\xi f}{f} \cdot \nabla_\xi\right)\nabla_\xi^2 \tilde{\phi} + \left\{\frac{1}{\gamma}\frac{r_w^2}{\lambda_{DO}^2}\left[\frac{\omega^2}{\omega_{po}^2} - f\right] - \frac{1}{\gamma}\nabla_\xi \cdot \frac{\nabla_\xi f}{f}\right\}\nabla_\xi^2 \tilde{\phi} - \frac{1}{\gamma}\frac{r_w^2}{\lambda_{DO}^2}\nabla_\xi \tilde{\phi} \cdot \nabla_\xi f = 0 \quad . \tag{2.52}$$

The boundary condition, equation 2.23, can be written as

$$\frac{\partial}{\partial \xi}\left(\nabla_\xi^2 \tilde{\phi}\right) - \frac{1}{\gamma f}\frac{df}{d\xi}\nabla_\xi^2 \tilde{\phi} - \frac{f}{\gamma}\frac{r_w^2}{\lambda_{DO}^2}\frac{d\tilde{\phi}}{d\xi} = 0 \qquad \text{at} \quad \xi = 1 \quad . \tag{2.53}$$

Thus we see that the equations governing the behavior of the plasma depend upon the dimensionless parameters r_w^2/λ_{DO}^2 and ω^2/ω_{po}^2 as well as the electron density profile function f . As we have seen

in the previous section, the density profile function f depends upon β^2 or equivalently r_w^2/λ_{DO}^2. Also from Section 2.4 we see that we can use the parameters $r_w^2/\overline{\lambda_D^2}$ and $\omega^2/\overline{\omega_p^2}$ instead of r_w^2/λ_{DO}^2 and ω^2/ω_{po}^2 respectively (since for each r_w^2/λ_{DO}^2 we can calculate $n_o/\overline{n}$). Expressing the results in terms of $r_w^2/\overline{\lambda_D^2}$ and $\omega^2/\overline{\omega_p^2}$ is more convenient for comparison with experiment. Parker (24) has solved equations 2.52 and 2.53 for a mercury plasma column to obtain the ratio

$$\frac{d\Phi_n}{d\xi}\Big/\Phi_n(\xi) \equiv \Phi_n'(\xi)/\Phi_n(\xi)$$

as a function of $\omega^2/\overline{\omega_p^2}$ for a number of values of the parameter $r_w^2/\overline{\lambda_D^2}$ where he has assumed that

$$\tilde{\phi}(\xi,\theta) = \Phi(\xi)e^{in\theta} \quad . \tag{2.54}$$

From equations 2.52, 2.53 and 2.54 we see that the solutions depend upon the integer n. Thus different solutions are obtained depending upon whether we are considering the dipole, quadrupole, sextupole, $\cdots$ $(n = 1,2,3,\cdots)$ modes.

We note that the resonance condition (equations 1.19 and 1.22 with $K_p = 1$) can be written as

$$L_n = \frac{1}{\tilde{\phi}_n(r)}\frac{d\tilde{\phi}_n(r)}{dr} = \frac{1}{r_w\tilde{\phi}_n(\xi)}\frac{d\tilde{\phi}_n}{d\xi}$$

$$= \frac{1}{r_w}\frac{\Phi'(\xi)}{\Phi(\xi)} = -\frac{n}{r_w}K_{eff} \tag{2.55}$$

or

$$\frac{\Phi'(\xi)}{\Phi(\xi)} = - n K_{eff} \quad . \tag{2.56}$$

The theoretical curves of Φ'/Φ as a function of $\omega^2/\overline{\omega_p^2}$ for a number of values of $r_w^2/\overline{\lambda_D^2}$ for both the dipole and quadrupole (n = 1 and 2) cases are given in Parker's thesis (24). As an example of the results he obtains, Figure 2.3 shows Φ'/Φ as a function of $\omega^2/\overline{\omega_p^2}$ for $r_w^2/\overline{\lambda_D^2} = 1580$ and n = 1 (for mercury). Also plotted on this figure is the curve (dashed line) $\Phi'/\Phi = -n K_{eff} = -2.1$ (n = 1 in this case and hence $K_{eff} = 2.1$). The intersections of this curve with the Φ'/Φ curves give the solutions to the resonance condition, equation 2.56. The intersection at the lowest value of $\omega^2/\overline{\omega_p^2}$ corresponds to the main resonance, the intersection at the next to lowest value of $\omega^2/\overline{\omega_p^2}$ corresponds to the first resonance, etc. By considering other values of $r_w^2/\overline{\lambda_D^2}$, the resonance spectrum $\omega^2/\overline{\omega_p^2}$ as a function of $r_w^2/\overline{\lambda_D^2}$ can be synthesized.

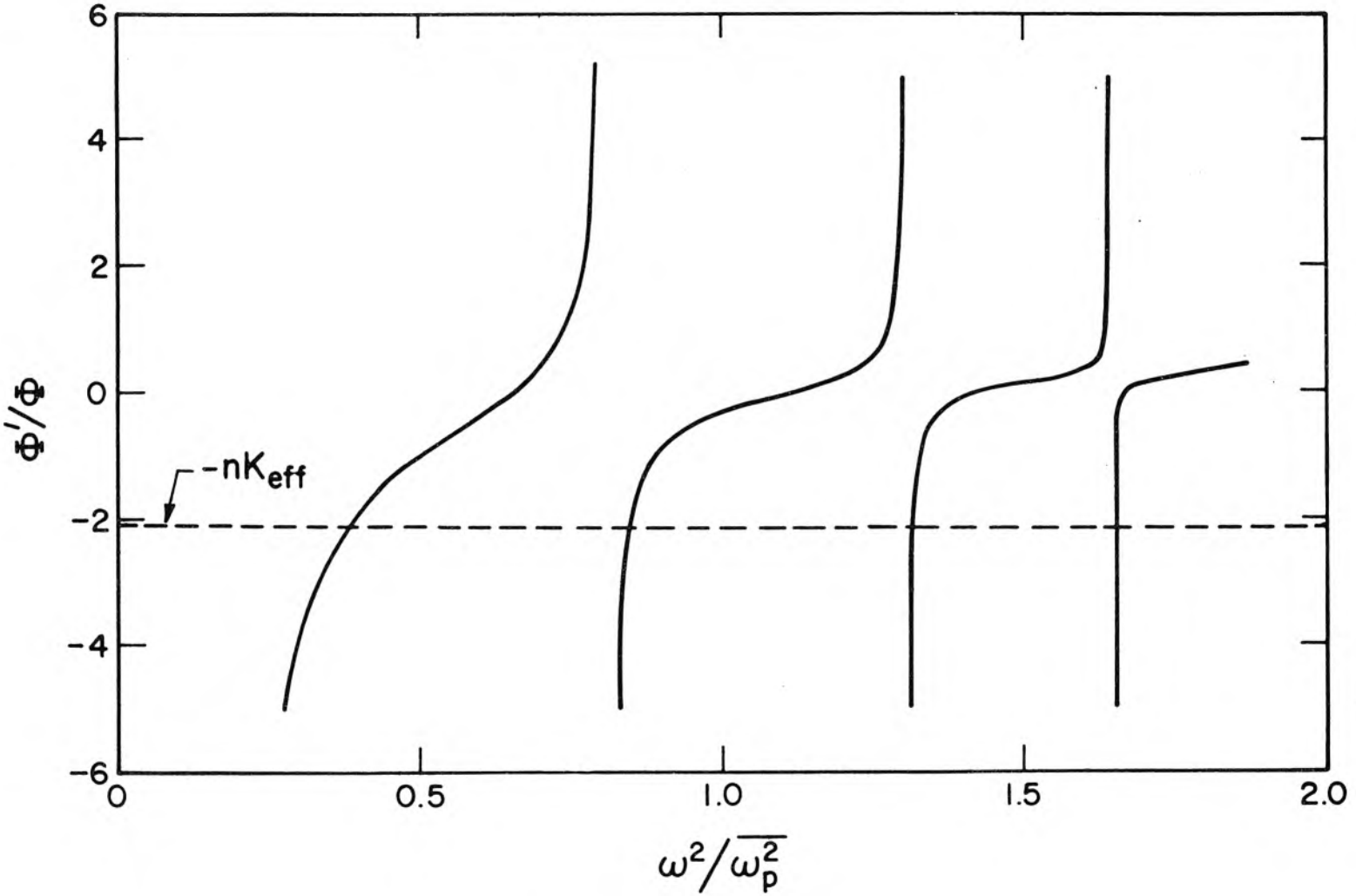

Figure 2.3 Theoretical curves obtained by Parker of Φ'/Φ as a function of $\omega^2/\overline{\omega_p^2}$ for $r_w^2/\overline{\lambda_D^2} = 1580$

III. EXPERIMENTAL TECHNIQUES

3.1 Description and Construction of the Plasma Tubes

The experiments described in the following sections were performed on a series of mercury filled discharge tubes constructed as the one shown in Fig. 3.1. The cathodes used were of the oxide-coated variety and are the same type used by General Electric in their 6011-710 thyratrons. The anodes were kovar cups sealed on the end of the barrel. The processing of the tubes followed standard procedures. The tube envelope and anode were constructed and chemically cleaned. The cathode was attached and the entire tube was pumped and baked ($350^{\circ}C$) to an ultimate pressure of about 10^{-7} mm Hg. The oxide cathode was then activated, and the tube was rebaked and pumped. Finally the mercury was added. This was accomplished either by breaking a mercury capsule after the tube had been sealed off or by distilling mercury into the tube from an external vessel and then sealing it off. After the tube was processed, there was about 1/4" of mercury in the mercury well (Fig. 3.1). The vapor pressure of the mercury vapor in the well could be controlled by controlling the temperature of the well. In our experiments the mercury well was placed in a dewar of water which assumed the room temperature of about $21^{\circ}C$ which corresponds to a well vapor pressure of about 1.3μ Hg. The neutral gas density n_w in the well is given by

$$n_w = \frac{p_w}{kT_w} \tag{3.1}$$

where p_w is the mercury vapor pressure in the well, T_w is the

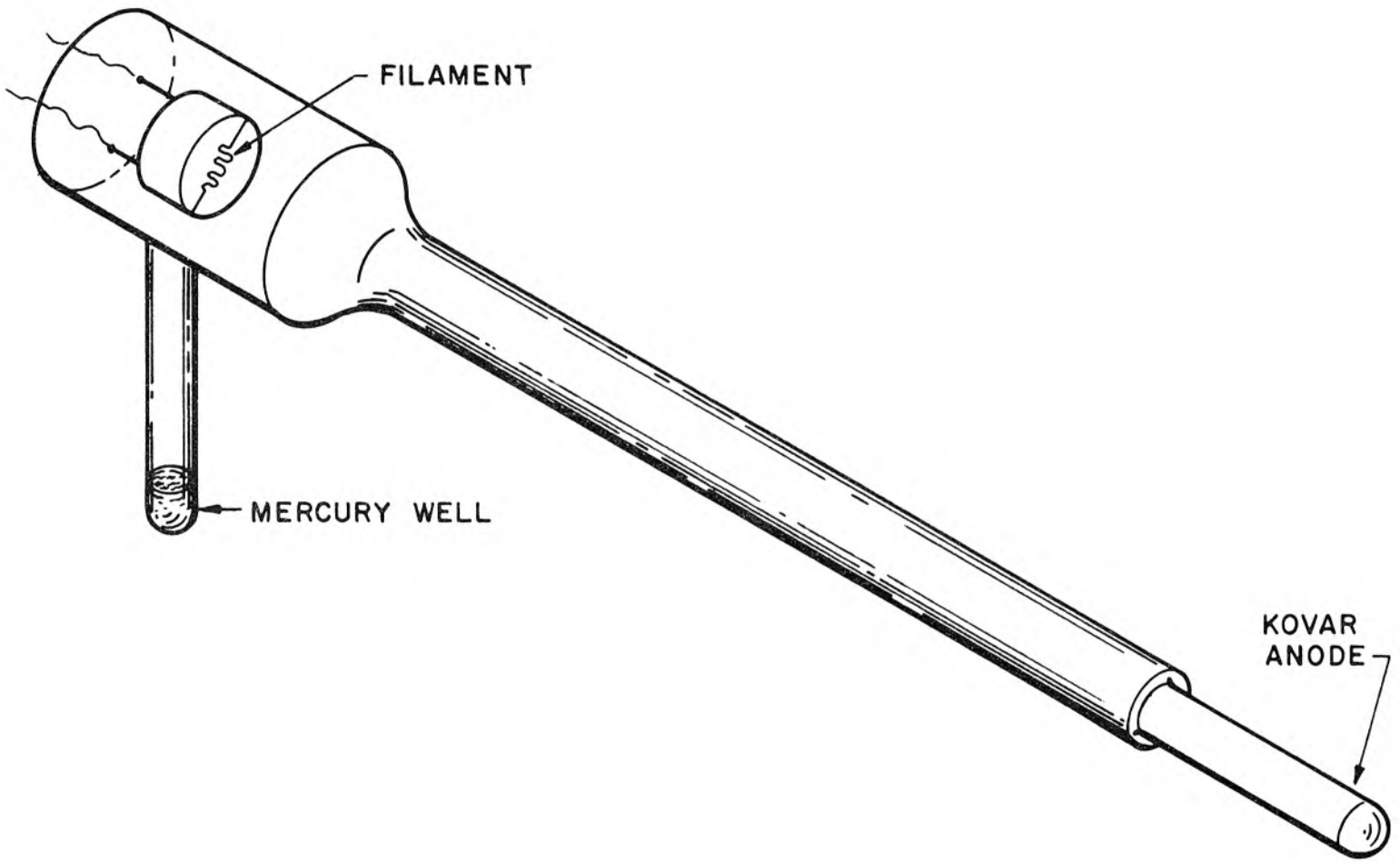

Figure 3.1 Mercury Discharge Tube

temperature of the well, and k is the Boltzmann constant. For our operating conditions $n_w \approx 4.3 \times 10^{13}$ atoms/cm^3. If there are temperature gradients between the barrel and the well, the number density in the barrel n_b will not be equal to that in the well. Dushman (34) (page 65) shows that if the barrel is at a temperature T_g, then the barrel number density is given by

$$n_b = n_w \left(\frac{T_w}{T_b}\right)^{1/2} \quad . \tag{3.2}$$

For our discharges $T_w \approx T_b$ so that $n_b \approx n_w$.

One of the useful properties of these plasma tubes is that the average electron density $\bar{n}$ is approximately proportional to the current flowing through the discharge. Since the current density $\underset{\sim}{J}$ is given by $\underset{\sim}{J} = \bar{n}e\underset{\sim}{v}$ where $\underset{\sim}{v}$ is the drift velocity along the axis of the tube, we have for the total current I, $I = JA = \bar{n}evA$ where A is the cross sectional area of the column. In these plasma tubes the voltage drop across the tube remains practically constant over a wide current range. Thus the electric field and hence the drift velocity v remain practically constant and $I \propto \bar{n}$. Therefore we can adjust the average current density in the column merely by adjusting the discharge current. In our experiments the average density in the column varies from about 10^9 electrons/cc to about 5×10^{11} electrons/cc. Thus the percentage of ionization ranges from about 1% to less than .01%.

In performing experiments on these tubes it was found that they showed a negative resistance characteristic of low currents. Below certain currents they resonated with the external circuitry and broke

into oscillation, and these oscillations seriously interfered with the primary measurements. It was found that a 500 ohm resistor placed directly at the anode eliminated the oscillation problem quite satisfactorily.

3.2 Low Frequency Observational Techniques

In the low frequency region, from about 200 mc to 1500 mc, the plasma wave resonances were observed using the split-cylinder and wire multipole devices shown in Figure 3.2. The radii of these devices is kept much smaller than the wavelength of the exciting radiation so that the quasi-static approximation is appropriate in their analysis. If the opposite electrodes in the dipole devices are fed 180° out of phase, then the fields produced by them near the axis are proportional to $r^n e^{in\theta}$ where $n = 1,3,5,\cdots$. Thus such a device is capable of exciting the $n = 1,3,5,\cdots$ radial plasma modes. It is found experimentally, however, that if the radius of the device is kept about three times larger than the radius of the column, only the $n = 1$ plasma mode will be appreciably excited. Thus, in practice, the dipole device can be used to investigate the $n = 1$ or dipole plasma mode. It is also found that if the adjacent electrodes of the quadrupole devices are fed 180° out of phase, the fields near the axis are proportional to $r^n e^{in\theta}$ where $n = 2,6,10,\cdots$. It is also experimentally verified that if the radius of the device is greater than approximately $2r_w$, only the $n = 2$ or quadrupole plasma mode is excited. Therefore the quadrupole devices can be used to investigate quadrupole plasma modes. To insure the electrode

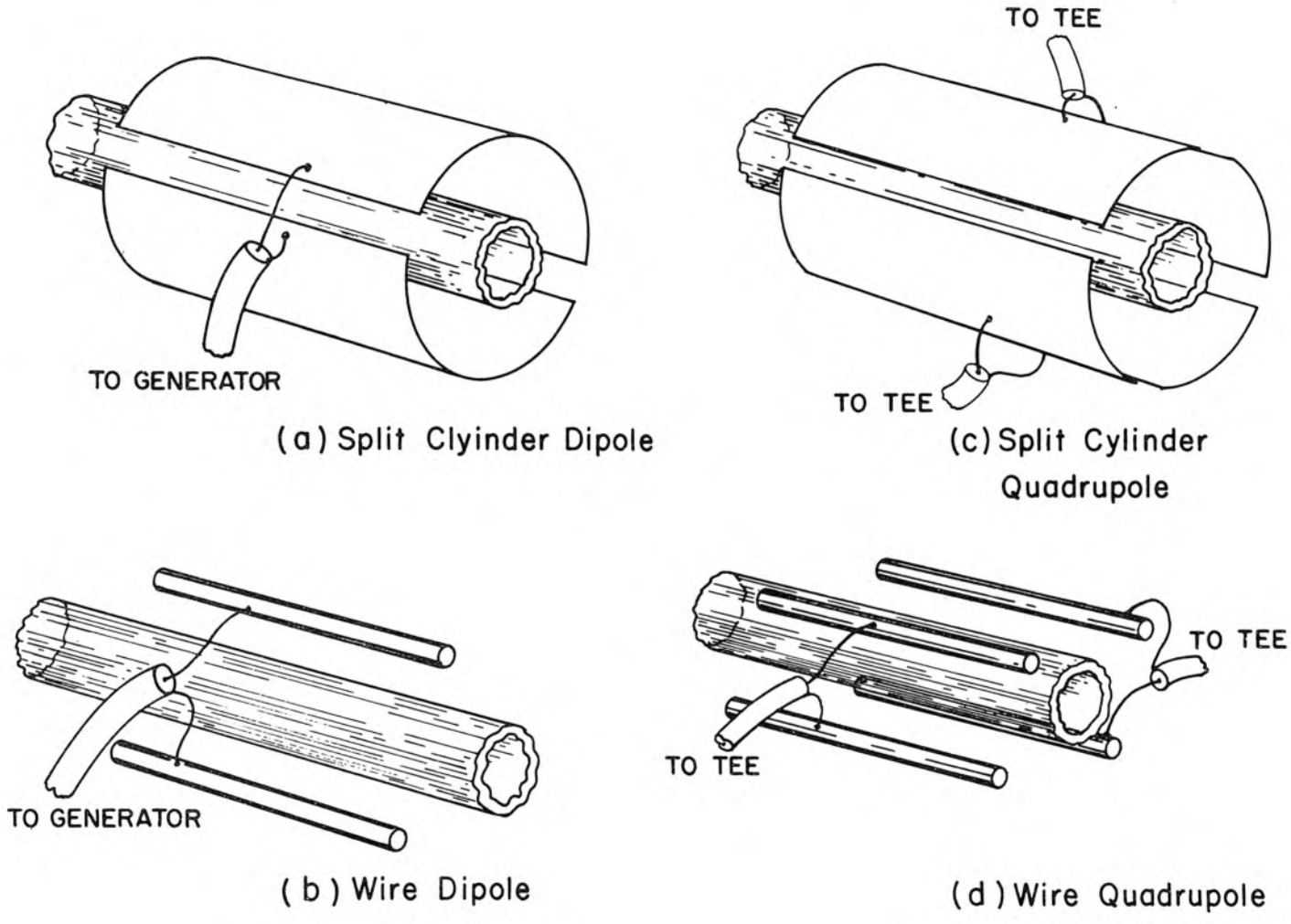

Figure 3.2 Multipole Devices

phase conditions in the quadrupole devices, adjacent pairs of electrodes were fed from two equal length sections of coaxial cable. The two sections of coaxial cable were then joined at a tee and fed from a common generator. It was found that if the proper phase relations were upset by making the sections of coaxial cable unequal in length, the dipole mode was observed in addition to the quadrupole mode.

The experimental arrangement incorporating these multipole devices is shown in Figure 3.3b. The multipole devices were fed through a directional coupler and the reflected signal was monitored. The resonance detection method is based upon the fact that at resonance the fields in the column become large and the tube absorbs a more than average amount of power due to dissipative phenomena (not discussed in Chapter 2). The power in the reflected signal will be that of the incident signal minus any power dissipated in the column, radiated from the multipole device, or dissipated in the lines. In the off resonance condition the column will absorb relatively little energy. However, when the electron density in the column is adjusted (by adjusting the discharge current) to give a resonance condition, the plasma column will absorb more energy and a decrease will be noted in the reflected signal. Thus by monitoring the reflected signal, we can obtain an absorption spectrum of the positive column.

It is shown in Appendix B that the resonance condition for a plasma column in the split cylinder geometry (Figure 3.2a,c) may be written as:

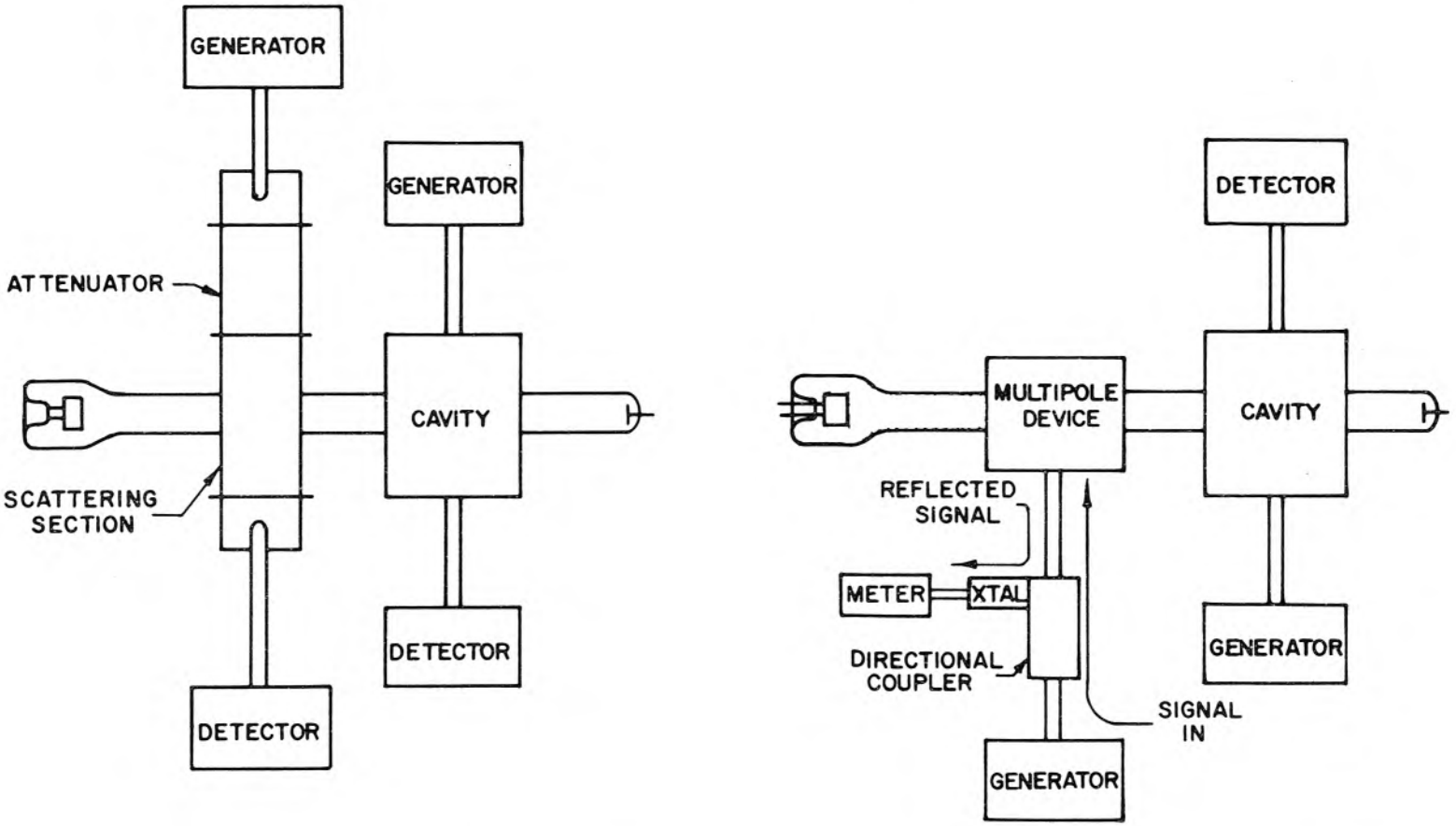

(a) Waveguide Arrangement

(b) Multipole Arrangement

Figure 3.3 Experimental Arrangements

$$L_n = -\frac{n}{r_w} K \frac{(\frac{b}{r_w})^n (K+g) - (\frac{r_w}{b})^n (K-g)}{(\frac{b}{r_w})^n (K+g) + (\frac{r_w}{b})^n (K-g)} = -\frac{n}{r_w} K_{eff}(K, r_w, b, c) \tag{3.3}$$

where L_n is the logarithmic derivative defined in Chapter I, K is the relative dielectric constant of the surrounding glass and

$$g = \frac{1 + (\frac{b}{c})^{2n}}{1 - (\frac{b}{c})^{2n}} \tag{3.4}$$

measures the influence of the metal cylinder ($g \to 1$ when the cylinder is removed). r_w, b, and c are the inner and outer radii of the glass tube and the radius of the device respectively, and the integer n in the above expressions denotes the angular dependence ($e^{in\theta}$). As in Chapter I, the left hand side of the resonance condition is dependent only on the solution of the equations for the plasma and the electromagnetic field in the plasma region, while the right hand side is dependent only on the electromagnetic field solution exterior to the plasma.

In a similar manner, the resonance condition for the ideal wire multipoles may be written as (Appendix B):

$$L_n = -\frac{n}{r_w} \frac{(\frac{b}{r_w})^n (K+1) - (\frac{r_w}{b})^n (K-1)}{(\frac{b}{r_w})^n (K+1) + (\frac{r_w}{b})^n (K-1)} = -\frac{n}{r_w} K_{eff}(K, r_w, b, c=\infty). \tag{3.5}$$

It is seen from equation 3.5 that the resonance condition for the ideal

wire multipoles should be independent of the wire position c. Experimentally it is found that the resonance condition is somewhat dependent on c, especially for the main resonance. This may be due to the finite size of the wires, an effect which would be difficult to include in the calculation.

3.3 High Frequency Observational Techniques.

In the high frequency region between 2300 mc and 4000 mc the resonances were observed using a waveguide arrangement similar to that used by Dattner (3). A schematic of the apparatus used is shown in Figure 3.3a. The plasma tube is placed across a section of S-band waveguide operating in the dominant TE_{01} mode such that the electric field is perpendicular to the column. When the electron density is adjusted to resonance (using a pulse technique described in Section 3.5), radiation is scattered out of the forward direction and a decrease is noted in the transmitted signal. To isolate the scattering section from the generator and to reduce spurious resonances, an attenuator was placed between the scattering section and the exciting waveguide to coax adapter.

3.4 Average Electron Density Measurements

As stated in Chapter II, we must measure the frequency spectrum $\omega^2/\overline{\omega_p^2}$ as a function of the parameter $r_w^2/\overline{\lambda_D^2}$. In both the multipole device and waveguide arrangements, the incident frequency is held constant and the average electron density in the column is adjusted to resonance. Thus at each resonance we must measure $\omega^2/\overline{\omega_p^2}$ and

$r_w^2/\overline{\lambda_D^2}$. The radius r_w and the frequency ω can be measured in a straightforward manner, but to determine the quantities $\overline{\omega_p^2}$ and $\overline{\lambda_D^2}$ we must know the average electron density $\bar{n}$ and the electron temperature T_e . As will be discussed in Chapter IV, the electron temperature will be determined by a best fit technique. The average density $\bar{n}$, however, is directly measured using a cavity perturbation technique. We use a right circular transmission cavity oscillating in the TM_{010} mode. If a plasma column is placed along the axis of such a cavity, the resonant frequency of the cavity will be shifted, and this frequency shift can be related to the average density in the plasma. The exact mechanics of relating the frequency shifts to the average electron density in the column is given in Appendix C, but for convenience, some of the main features are repeated here.

Consider an empty cavity having a resonant frequency ω_{oo} and field distributions given by $\underset{\sim}{E}_o(\underset{\sim}{r})$ and $\underset{\sim}{B}_o(\underset{\sim}{r})$. If we now introduce a piece of dielectric (of dielectric constant ϵ) into the cavity, the frequency will be shifted to a new value ω and the field configurations will be given by $\underset{\sim}{E}(\underset{\sim}{r})$ and $\underset{\sim}{B}(\underset{\sim}{r})$. It can be shown (31) that the exact frequency shift of the cavity is given by

$$\frac{\omega - \omega_{oo}}{\omega} = \frac{\int_{v_o} \Delta\epsilon \, \underset{\sim}{E}_o^* \cdot \underset{\sim}{E} \, dv}{\int_{v_o} \left[\epsilon_o \, \underset{\sim}{E}_o^* \cdot \underset{\sim}{E} + \frac{B_o^* \cdot B}{\mu_o} \right] dv} \tag{3.6}$$

where $\Delta\epsilon = \epsilon - \epsilon_o$ and v_o is the volume of the cavity. In general, $\underset{\sim}{E}(\underset{\sim}{r})$ and $\underset{\sim}{B}(\underset{\sim}{r})$ are difficult to determine exactly. In equation 3.6

let us write $\lambda\Delta\epsilon$ instead of $\Delta\epsilon$ where $0 \leq \lambda \leq 1$. Let us then expand the perturbed quantities ω, $\underset{\sim}{E}(\underset{\sim}{r})$ and $\underset{\sim}{B}(\underset{\sim}{r})$ in power series in λ :

$$\underset{\sim}{E}(\underset{\sim}{r}) = \underset{\sim}{E}_o(\underset{\sim}{r}) + \lambda\underset{\sim}{E}_1(\underset{\sim}{r}) + \lambda^2\underset{\sim}{E}_2(\underset{\sim}{r}) + \cdots \tag{3.7}$$

$$\underset{\sim}{B}(\underset{\sim}{r}) = \underset{\sim}{B}_o(\underset{\sim}{r}) + \lambda\underset{\sim}{B}_1(\underset{\sim}{r}) + \lambda^2\underset{\sim}{B}_2(\underset{\sim}{r}) + \cdots \tag{3.8}$$

$$\omega = \omega_{oo} + \lambda\,\omega_1 + \lambda^2\omega_2 + \cdots \quad . \tag{3.9}$$

If equations 3.7, 3.8 and 3.9 are substituted in equation 3.6, one obtains to first order (neglecting all terms of $O(\lambda^2)$):

$$\frac{\omega - \omega_{oo}}{\omega_{oo}} = -\frac{\int_{V_o} \Delta\epsilon\,\underset{\sim}{E}_o^* \cdot \underset{\sim}{E}_o \, dv}{\int_{V_o}\left[\epsilon_o \underset{\sim}{E}_o^* \cdot \underset{\sim}{E}_o + \frac{\underset{\sim}{B}_o^* \cdot \underset{\sim}{B}_o}{\mu_o}\right] dv} = -\frac{\int_{V_o} \Delta\epsilon\,\underset{\sim}{E}_o^* \cdot \underset{\sim}{E}_o \, dv}{8\overline{w}_e} \tag{3.10}$$

where

$$\overline{w}_e = \frac{1}{4}\epsilon_o \int_{V_o} \underset{\sim}{E}_o^* \cdot \underset{\sim}{E}_o dv = \overline{w}_e = \frac{1}{4\mu_o}\int_{V_o} \underset{\sim}{B}_o^* \cdot \underset{\sim}{B}_o \, dv \tag{3.11}$$

is the average stored electric field energy in the empty cavity ($\overline{w}_e = \overline{w}_B$ at resonance).

The specific experimental arrangement which we have used for making average electron density measurements (utilizing a right circular transmission cavity operating in the TM_{010} mode) is shown in Figure 3.4. The plasma column ($r \leq r_w$) is characterized by the effective dielectric constant

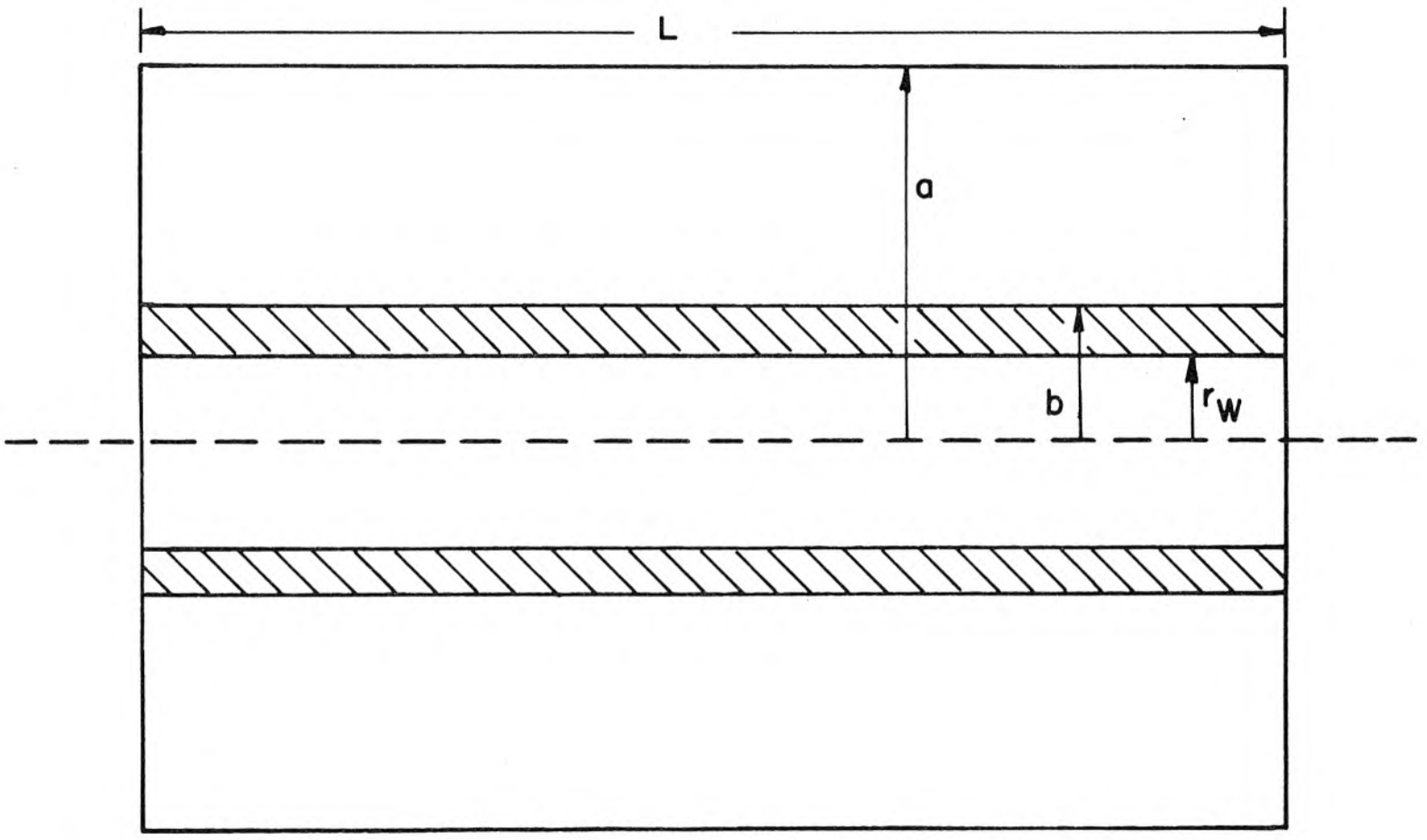

Figure 3.4 Cavity Geometry

$$\epsilon(r) = \epsilon_o\left[1 - \frac{\omega_p^2(r)}{\omega^2}\right] = \epsilon_o\left[1 - \frac{e^2}{m\epsilon_o\omega^2}\, n(r)\right] . \qquad (3.12)$$

Thus for the plasma region

$$(\Delta\epsilon)_p = \epsilon - \epsilon_o = -\frac{\epsilon_o e^2}{m\epsilon_o\omega^2}\, n(r) \quad . \qquad (3.13)$$

The glass tube surrounding the plasma column is characterized by the relative dielectric constant K . Thus for the glass region ($r_w \leq r \leq b$)

$$(\Delta\epsilon)_g = \epsilon - \epsilon_o = \epsilon_o(K - 1) . \qquad (3.14)$$

Now the TM_{010} cavity mode is characterized by having only an axial (z) component of the electric field (neglecting the effects of the end holes where the column enters and exits) which is given by

$$E_z(r) = A\, J_o\left(\frac{\beta_{01} r}{a}\right) \qquad (3.15)$$

where β_{01} is the first zero of $J_o(x)$. By employing equations 3.13, 3.14 and 3.15 in equation 3.10 we can calculate the expected frequency shift produced by the glass and plasma. If, in calculating the integral in the numerator of equation 3.10, we use the small argument approximation of $J_o(\beta_{01} r/a)$ for $r \leq b$ (that is, $E_z \approx A$ for $r \leq b$ or approximately uniform), we can write (see Appendix C) :

$$\frac{\omega - \omega_{oo}}{\omega_{oo}} \approx \frac{1}{2J_1^2(\beta_{01})} \left\{ \frac{1}{\omega^2} \left(\frac{e^2}{m_o}\right) \frac{r_w^2}{a^2} \bar{n} - (K-1) \frac{b^2 - r_w^2}{a^2} \right\} . \qquad (3.16)$$

Let the resonant frequency with the plasma off ($\bar{n} = 0$) be ω_o . Then

$$\frac{\omega_o - \omega_{oo}}{\omega_{oo}} \approx - \frac{1}{2J_1^2(\beta_{01})} (K-1) \frac{b^2 - r_w^2}{a^2} . \qquad (3.17)$$

If equation 3.17 is now subtracted from equation 3.16 we have

$$\frac{\omega - \omega_o}{\omega_{oo}} = \frac{1}{2J_1^2(\beta_{01})} \left\{ \frac{1}{\omega^2} \left(\frac{e^2}{m_o}\right) \frac{r_w^2}{a^2} \bar{n} \right\} . \qquad (3.18)$$

It is shown in Appendix C that to the same order retained in this perturbation calculation

$$\frac{\omega - \omega_o}{\omega_{oo}} = \frac{\omega - \omega_o}{\omega_o} . \qquad (3.19)$$

In our arrangement ω_{oo} and ω_o typically differ by about 150 mc out of 3000 mc which might lead to an indeterminacy of about 5% in the density measurements employing equation 3.18. In order to shed some light on this problem we performed a series of experiments measuring the dielectric constant of a lucite rod both with and without a surrounding glass tube (the lucite rod simulating the plasma, except that we could remove the glass envelope.)

It is shown in Appendix C that the frequency shift produced by a dielectric rod (no surrounding glass tube) is given by

$$\frac{\omega' - \omega_{oo}}{\omega_{oo}} \approx \frac{-1}{2J_1^2(\beta_{01})} (K_L - 1) \frac{r_w^2}{a^2} \tag{3.20}$$

where ω' is the resonant frequency of the cavity with the dielectric rod, ω_{oo} is the resonant frequency of the empty cavity, K_L is the relative dielectric constant of the rod, and r_w is the radius of the rod. It is also shown in Appendix C that the frequency shift produced by a dielectric rod of radius r_w surrounded by a glass tube of inner radius r_w and outer radius b is given by

$$\frac{\omega - \omega_{oo}}{\omega_{oo}} \approx \frac{1}{2J_1^2(\beta_{01})} \left\{ - (K_L - 1) \frac{r_w^2}{a^2} - (K - 1) \frac{b^2 - r_w^2}{a^2} \right\} \tag{3.21}$$

where again K_L is the dielectric constant of the rod and K is the dielectric constant of the glass tube. If we now remove the dielectric rod from the glass tube (equivalent to extinguishing the plasma) and call the resultant resonant frequency ω_o, we have

$$\frac{\omega_o - \omega_{oo}}{\omega_{oo}} \approx - \frac{1}{2J_1^2(\beta_{01})} (K - 1) \frac{b^2 - r_w^2}{a^2} \quad . \tag{3.22}$$

If we subtract equation 3.22 from equation 3.21 we have

$$\frac{\omega - \omega_o}{\omega_{oo}} = - \frac{1}{2J_1^2(\beta_{01})} (K_L - 1) \frac{r_w^2}{a^2} \tag{3.23}$$

which brings us back to the same problem encountered in equations 3.18 and 3.19. Again, to the order retained in the calculation

$$\frac{\omega - \omega_o}{\omega_{oo}} = \frac{\omega - \omega_o}{\omega_o} \quad . \tag{3.24}$$

which is more appropriate to use in the denominator of equation 3.24 ω_{oo} or ω_o . In one experiment we used just a lucite rod and a cavity. We measured ω', ω_{oo}, r_w and a and determined the dielectric constant K_L of the rod using equation 3.20. This we called the standard K_L . In another experiment we employed the same lucite rod in conjunction with a closely fitted glass tube. We first measured the resonant frequency of the cavity ω with both the glass and the lucite present. We then measured the resonant frequency ω_o with only the glass tube present. K_L was then calculated using 3.23 and 3.24 for the two possible values of ω in the denominator of equation 3.24, ω_{oo} and ω_o , and the results were compared to the standard K_L determined by the first experiment. We found ω_o to be the more appropriate value to use, giving an agreement with the standard K_L to well within 1% . If ω_{oo} were used in the denominator of 3.24, the two values of K_L would differ by about 4% . The value of K_L for lucite determined in this manner was 2.47. The accepted handbook value is 2.58 (37).

In view of the results of the experiments with the lucite rod, we chose to use ω_o in the denominator of equation 3.19. Thus equation 3.18 could be written as

$$\frac{\omega - \omega_o}{\omega_o} \approx \frac{1}{2J_1^2(\beta_{01})} \left\{ \frac{1}{\omega_o^2} \left(\frac{e^2}{m\epsilon_o}\right) \frac{r_w^2}{a^2} \bar{n} \right\} \tag{3.25}$$

or

$$\bar{n} \cong \frac{8\pi^2 m\epsilon_o J_1^2(2.405)}{e^2} \frac{a^2}{r_w^2} f_o \Delta f \qquad (3.26)$$

where f_o is the resonant frequency of the cavity with the glass but no plasma and $\Delta f = f - f_o$ where f is the resonant frequency with the plasma. Equation 3.26 was used in all of our experiments to relate the cavity frequency shifts to the average electron densities.

For our experimental arrangement one would expect the perturbation treatment to converge rapidly. Since the plasma column and glass tube are parallel to E_z and since at the interfaces of these media E_z must remain continuous, the fields should not be drastically disturbed by the column.

In deriving equation 3.26 it was assumed that in the TM_{010} mode the only component of the electric field is along the axis of the cavity. Since the plasma column must pass through the cavity, there will be some perturbation in the field configuration near the holes in the end plates. To minimize this effect, the cavities were constructed as long as possible, consistent with good mode separation. The cavities used were about three inches in diameter, 3.5 inches long, and resonated at about 3000 mc. The holes in the end plates were just sufficient to allow the tubes to pass through.

As shown in Figure 3.3a,b, a cavity was placed adjacent to the resonance detecting device so that the average density $\bar{n}$ and the resonant frequency ω could be measured simultaneously. It was determined experimentally that the longitudinal variations (along the

column) of the average electron density were negligible for the larger tubes. Thus in these cases the electron density measured at the site of the cavity could be equated to the density at the site of the resonance detecting device. For the smaller tubes some longitudinal variations were found and the cavity was actually moved over the site of the resonance detecting device in measuring the density.

For the range of densities investigated, the frequency shifts Δf varied from about 0.5 mc to 30 mc. To measure these small shifts, a Hewlett-Packard model 524D electronic counter and Model 540B transfer oscillator were employed. The cavity was set to resonance by observing maximum transmission through the cavity with a Hewlett-Packard Model 425A microvoltmeter. The resonant frequency was then determined directly with the counter arrangement. It was found that the resonant frequency of the cavity could be determined to within 0.1 mc. Thus the frequency shifts could be determined to within about 0.2 mc.

Another series of experiments was carried out in an effort to measure the third moment of the electron density profile I_3

$$I_3 = \int_0^{r_w} n(r)\, r^3 dr \qquad (3.27)$$

but due to a lack of experimental resolution, the results were negative. The motivation behind such experiments was to make a direct experimental determination of $r_w^2 / \overline{\lambda_D^2}$. In his work on the electron density profiles, Parker defines a quantity $M(r_w^2 / \overline{\lambda_D^2}), (0 \leq M \leq 0.5)$ as

$$M = \frac{\int_0^{r_w} n(r) r^3 dr}{r_w^2 \int_0^{r_w} n(r) r dr} = \frac{2I_3}{r_w^4 \bar{n}} \quad . \tag{3.28}$$

If we assume these profiles to be correct, then each profile corresponding to a given value of $r_w^2/\overline{\lambda_D^2}$ (Chapter II) can be equally well labeled by its value of M. Thus if we can measure the value of M for our column, we can determine $r_w^2/\overline{\lambda_D^2}$ and hence the density profile by means of Parker's calculations. It is seen from equation 3.28 that we can measure M by simultaneously measuring I_3 and the average density $\bar{n}$. The method of measuring $\bar{n}$ has been discussed in the preceding paragraphs. I_3 can be measured in a similar fashion by observing the frequency shifts produced by the plasma in a right circular cavity operating in the TM_{110} mode. It is shown in Appendix C that I_3 can be related to the frequency shift in the TM_{110} mode by

$$I_3 = \frac{16\pi^2 m\epsilon_o}{\beta_{11}^2 e^2} J_2^2(\beta_{11})\, a^4 f_o \Delta f \tag{3.29}$$

where β_{11} is the first root of $J_1(x)$, f_o is the resonant frequency of the cavity without the glass, and $\Delta f = f - f_o$ where f is the resonant frequency with the plasma present. The frequency shifts observed were on the order of only 0.2 mc (which is to be expected from equation 3.29 if reasonable values are substituted for

I_3, a, and f_o) which makes the measurement impractical in light of the experimental uncertainty (about 0.2 mc) present in the cavity shifts.

3.5 Methods of Taking Data

It was found that the best method of taking data was to keep the incident frequency constant and vary the average electron density $\bar{n}$ by varying the current to obtain the resonances. If the electron density was kept constant and the frequency varied, it was found that frequency variations in the radiation resistance of the multipole devices, and impedance mismatches in the waveguide system, made interpretation of the data very difficult.

In the low frequency region (using multipole devices), the current required for observing the resonances varied from a few milliamps to about 200 milliamps and in this range the tubes could be operated continuously without excessive anode heating. The current was controlled by a current controller shown in Figure 3.5 which has two modes of operation. The first mode, which was used in obtaining all of the zero magnetic field data, allowed the current to be adjusted manually by changing R_1. Thus the electron density in the tube could be adjusted for resonance by varying R_1 and its average value could be measured simultaneously. In the second mode of operation the current could be swept between fixed values by applying a sweep voltage from a generator on terminals A and adjusting R_1 and R_2. A voltage proportional to the current in the plasma column is available across R_3 and can be used to drive one axis of an X-Y

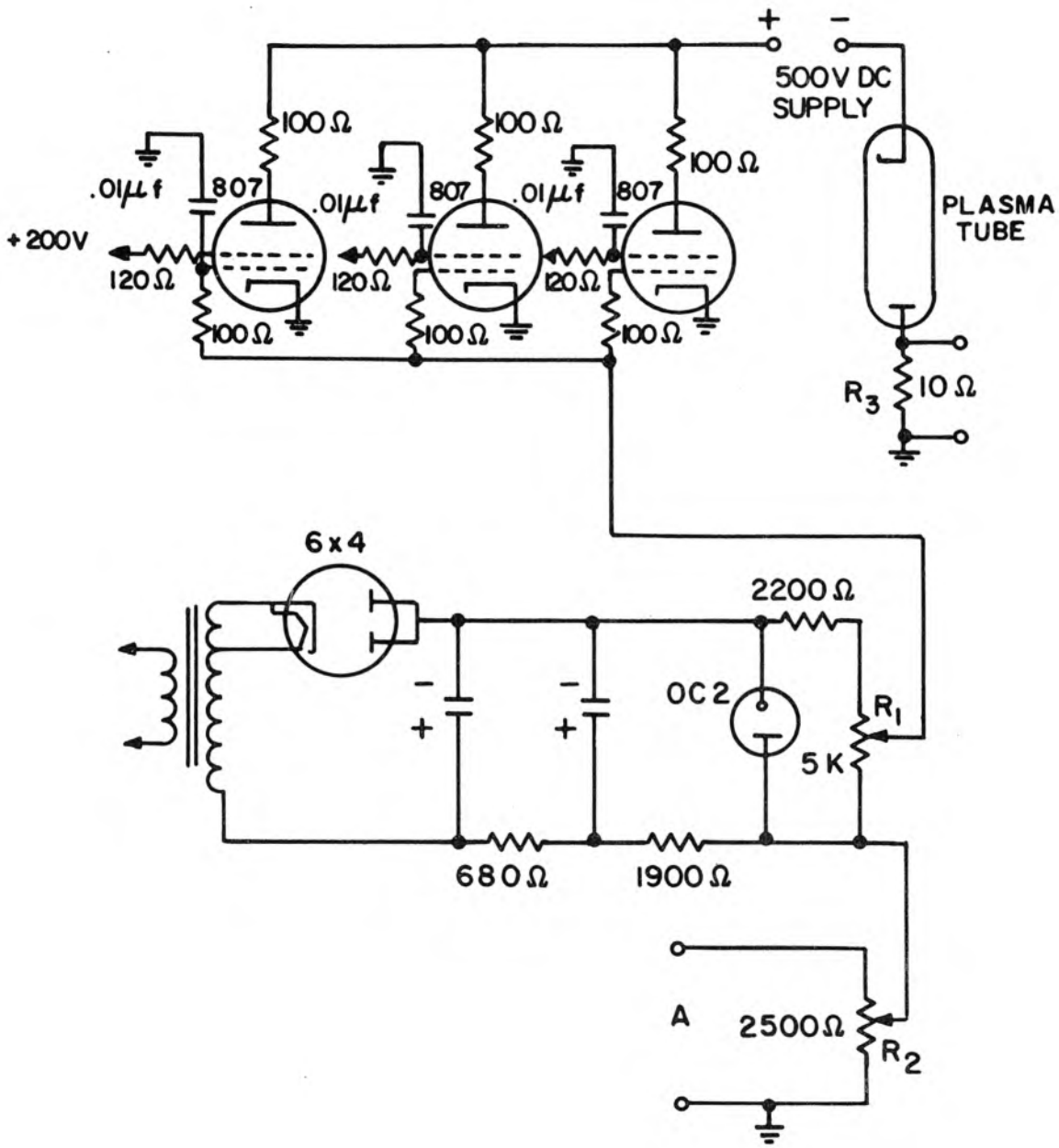

Figure 3.5 Current Controller

recorder. In using the swept mode with the multipole devices, the reflected signal can be fed into the x axis input while the y axis is driven by the voltage developed across R_3. Thus an absorption spectrum is traced out by the X-Y recorder. If several spectra are obtained at different incident frequencies, we obtain the positions of the resonances a s a function of current. Figure 3.6 shows the dipole absorption spectra for tube No. 1 at three different frequencies taken with a split cylinder capacitor. The current is swept along the horizontal x axis and goes from 0 to 200 ma. The vertical y axis measures the power absorption with the dotted line indicating total absorption. Figure 3.7 gives an amplified absorption spectrum taken with the same tube and the same arrangement. The average density as a function of current $\bar{n}(I)$ can be obtained by now feeding the output of the cavity into the x axis keeping the current sweeping as in the resonance measurements. By changing the frequency of the cavity input signal and tracing the cavity response as a function of current (maximum transmission corresponding to resonance of the cavity at that frequency), we can obtain $\bar{n}(I)$ using equation 3.26. Hence we can obtain the resonance positions as a function of $\bar{n}$.

In the high frequency measurements ($\sim$ 3000 mc), the current needed for suitable electron densities was on the order of one Ampere. Since at these currents the tubes could not be operated continuously due to excessive anode heating, they were pulsed. Figure 3.8 shows a schematic of the thyratron controlled RC pulser employed. In the

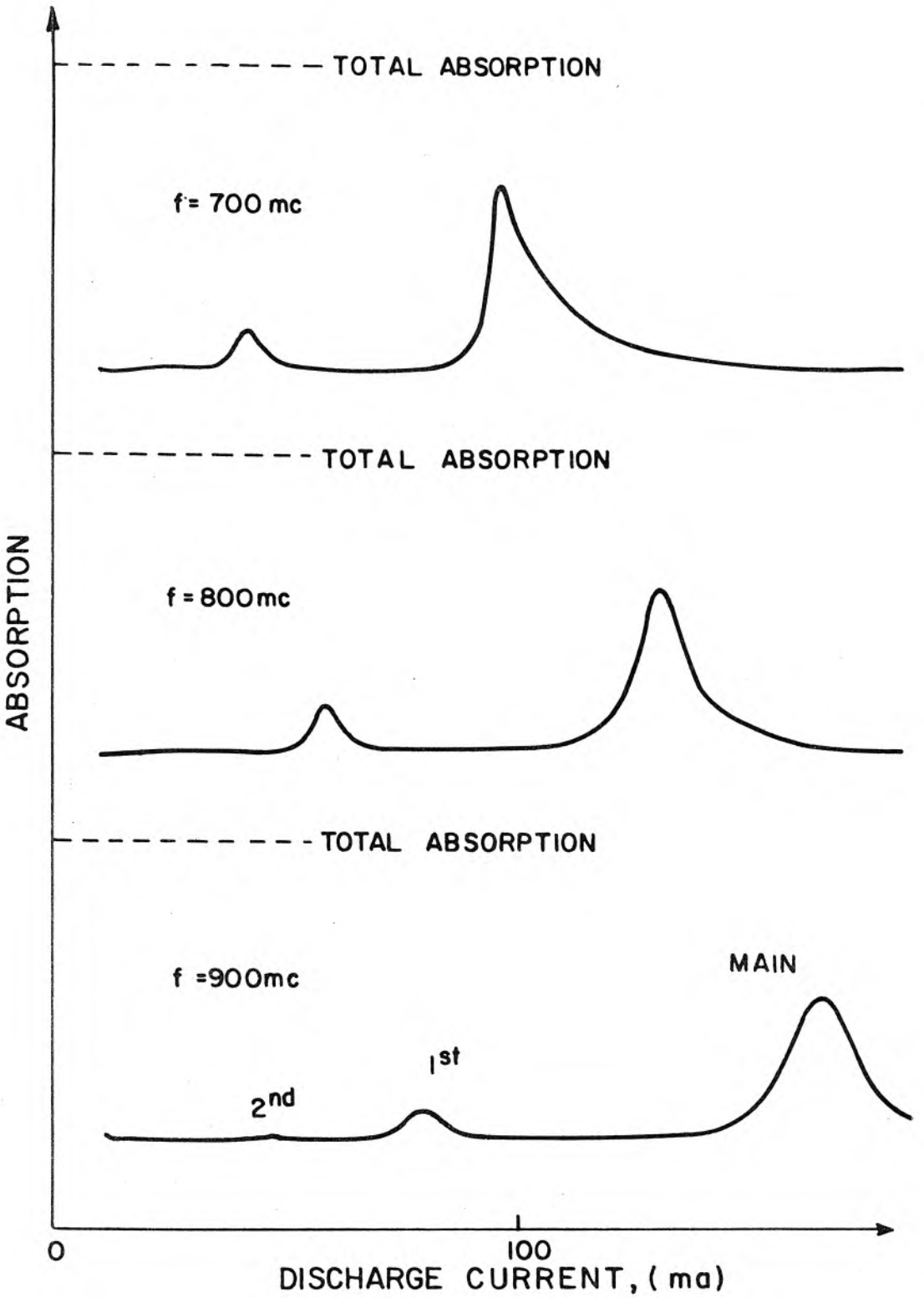

Figure 3.6 Dipole Absorption Spectra for Tube No. 1

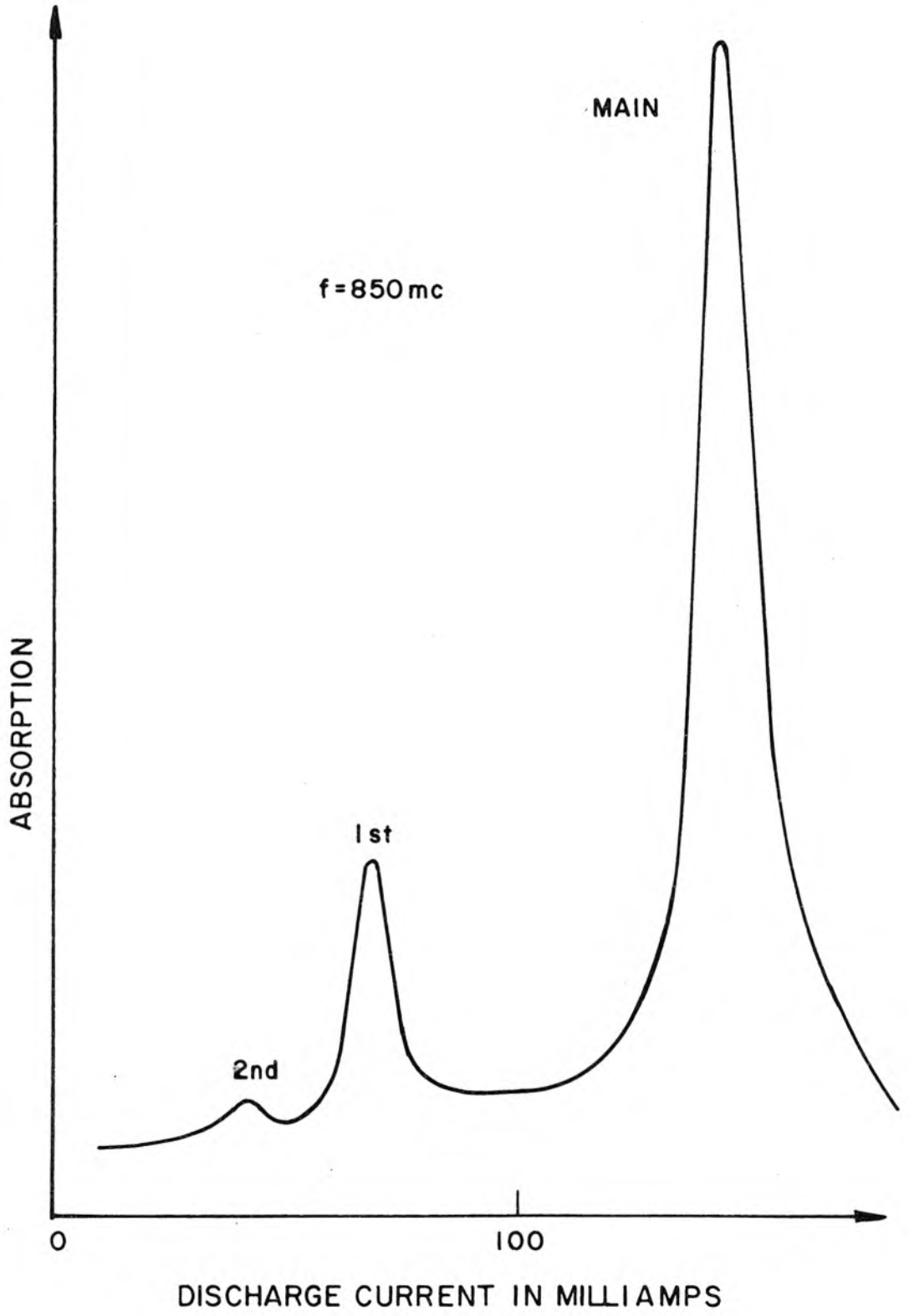

Figure 3.7 Amplified Dipole Absorption Spectrum

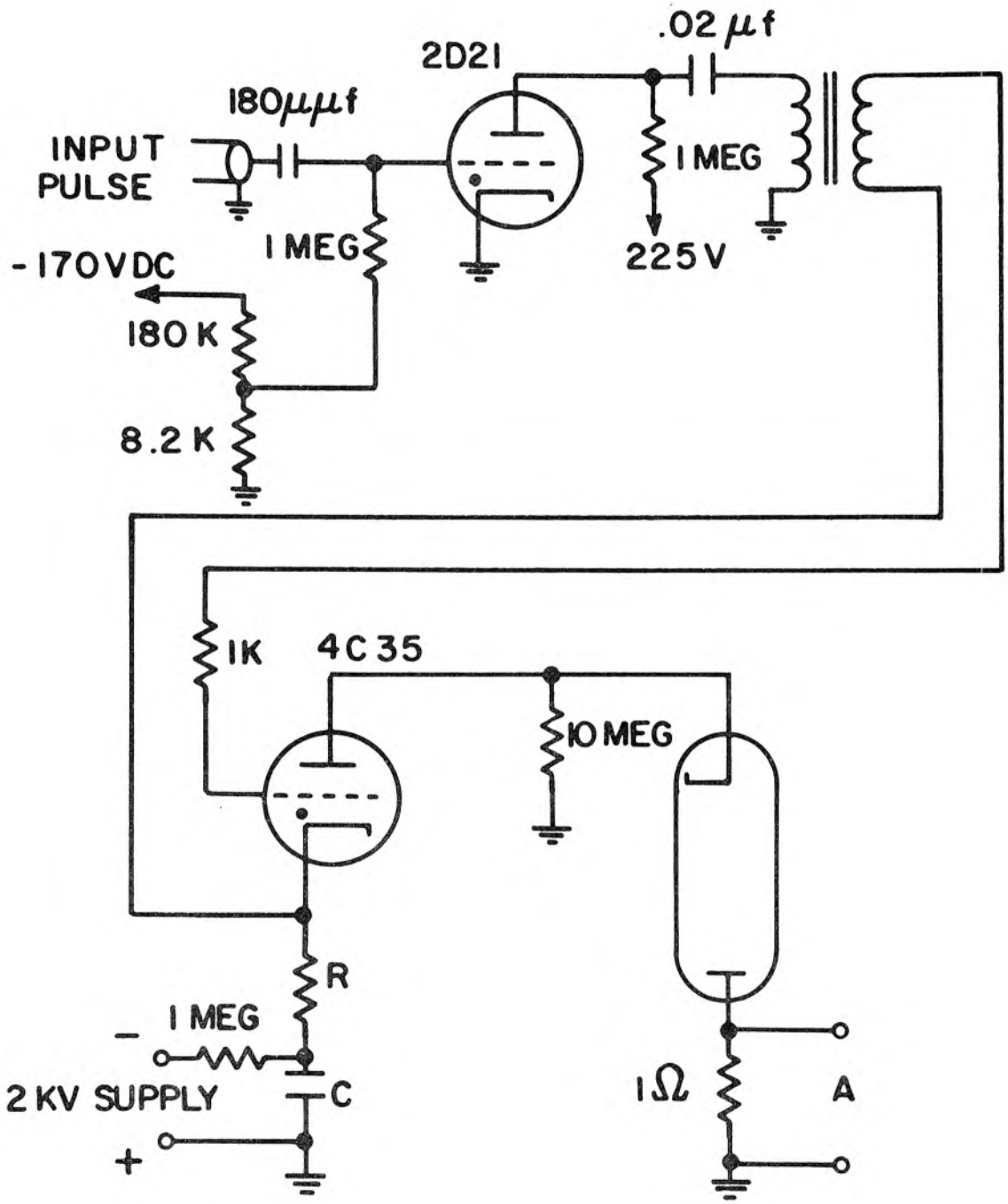

FIGURE 3.8 Thyratron Controlled Pulser

experiments reported here the RC time constant was 1.65×10^{-4} seconds. This time constant is long compared to the 4 μsec electron density decay time constant (38), so that steady state conditions are approximated. The pulse method of obtaining data is much the same as the continuous sweep method. The x axis of a dual trace oscilloscope is triggered as the pulse is initiated. The waveguide output is fed into one y axis and a voltage proportional to the tube current (from terminals A in Figure 3.8) is fed into the other y axis, and both traces are photographed. Figure 3.9a gives an example of two such absorption spectra taken on tube No. 1. The top spectrum was taken at 2923 mc while the bottom spectrum was taken at 2720 mc. The exponentially decaying curves are signals proportional to the current. Thus we obtain scattering spectra as a function of the tube current. Once again we calibrate the tube current as a function of the average electron density by observing the cavity response as a function of current. Here the cavity output (transmission cavity) is fed into the y axis previously fed by the waveguide output. The cavity resonance and hence the average electron density (employing equation 3.26) can now be determined as a function of current. Figure 3.9b gives an example of the cavity transmission measurement. In the upper trace the incident cavity frequency was 2945.6 mc while in the lower trace it was 2941.5 mc. Again the exponentially decaying curves are signals proportional to the tube current.

The shot to shot errors (reproducibility) were less than those introduced in reducing the data.

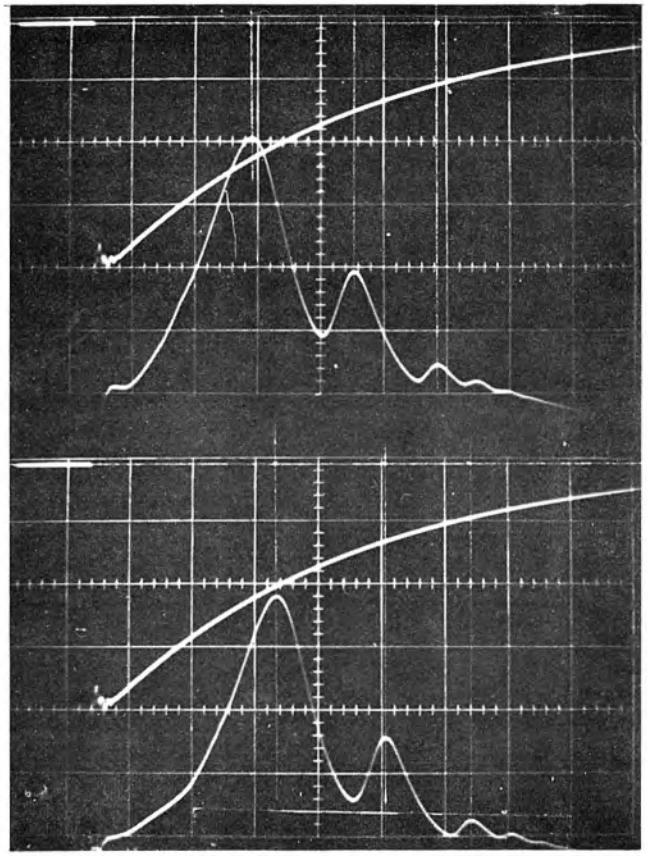

a) Absorption Spectra

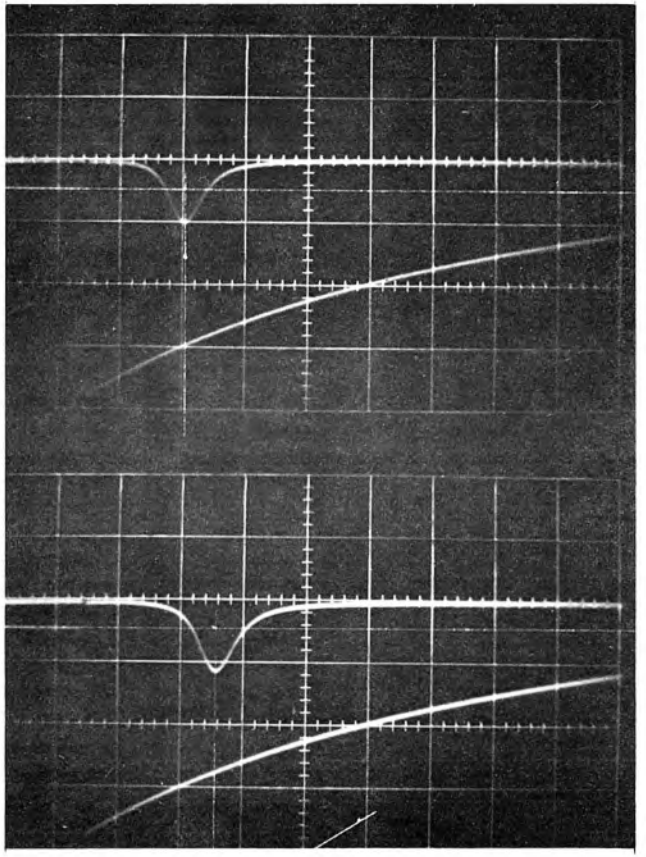

b) Cavity Transmission Response

Figure 3.9 Pulse Technique for Obtaining Data

IV. EXPERIMENTAL RESULTS

4.1 Reduction of the Data

It was shown in Chapter II that if a value of K_{eff} is given for an experimental arrangement, Parker's calculations (24) predict theoretically $\omega^2/\overline{\omega_p^2}$ as a function of $r_w^2/\overline{\lambda_D^2}$. In observing the resonances we have an experimental measure of the resonant frequencies, the average electron densities $\bar{n}$, the radius of the column r_w, and K_{eff}. We do not, however, have an experimental measurement of the electron temperature T_e and thus we cannot determine $\overline{\lambda_D^2}$ by direct measurement. It is well known, however, that for our type of mercury discharge the electron temperature T_e is approximately 3 ev. (29) Since we have not measured the electron temperature in our experiments we could either

(a) assume T_e = 3ev and see how well the measurements agree with the theoretical predictions

or

(b) take the assumed temperature as a parameter to be adjusted to secure the best fit between experiment and theoretical predictions.

We have chosen the latter approach, although it is not clear that the small deviations from T_e = 3 ev are really significant in view of the other limitations of the theory and experiment.

In plotting the data we plot $r_w^2/\overline{\lambda_D^2}$ on a logarithmic scale (Figures 4.1, 4.2, 4.3 and 4.4). This has the advantage that since

$$\log \frac{r_w^2}{\overline{\lambda_D^2}} = \log \frac{\bar{n} e^2 r_w^2}{\epsilon_o K} - \log T_e \qquad (4.1)$$

adjusting the temperature simply moves all of the experimental points linearly parallel to the $r_w^2/\overline{\lambda_D^2}$ axis. Thus for a given K_{eff} we can determine a set of theoretical curves (solid lines in Figures 4.1, 4.2, 4.3 and 4.4). We can then assume a reasonable value for T_e (say 3 ev) and reduce the experimental data. Then by simply moving the entire body of experimental points to the left or to the right, obtaining best agreement with the theoretical curves, we can determine the best fit electron temperature T_e.

4.2 Experimental Results

Figure 4.1 shows the dipole spectrum of tube No. 1 which has the radius $r_w = 0.5$ cm. The solid lines are theoretical curves, while the circles are experimental points. The data for $r_w^2/\overline{\lambda_D^2} > 10^4$ was taken in a waveguide apparatus (Figure 3.3a), while that for $r_w^2/\overline{\lambda_D^2} < 10^4$ was taken with the multipole devices. For $r_w^2/\overline{\lambda_D^2} < 10^4$ the main resonance was measured with a split cylinder device (as were all of the main resonances in this range since a well defined K_{eff} could be calculated. From Figure 2.3 we see that the main resonance is particularly sensitive to K_{eff}.) The first and second plasma wave resonances were measured with both split cylinder and wire multipole devices. The best fit electron temperature of 3 ev was determined by considering both the dipole spectrum and the quadrupole spectrum of the same tube. The

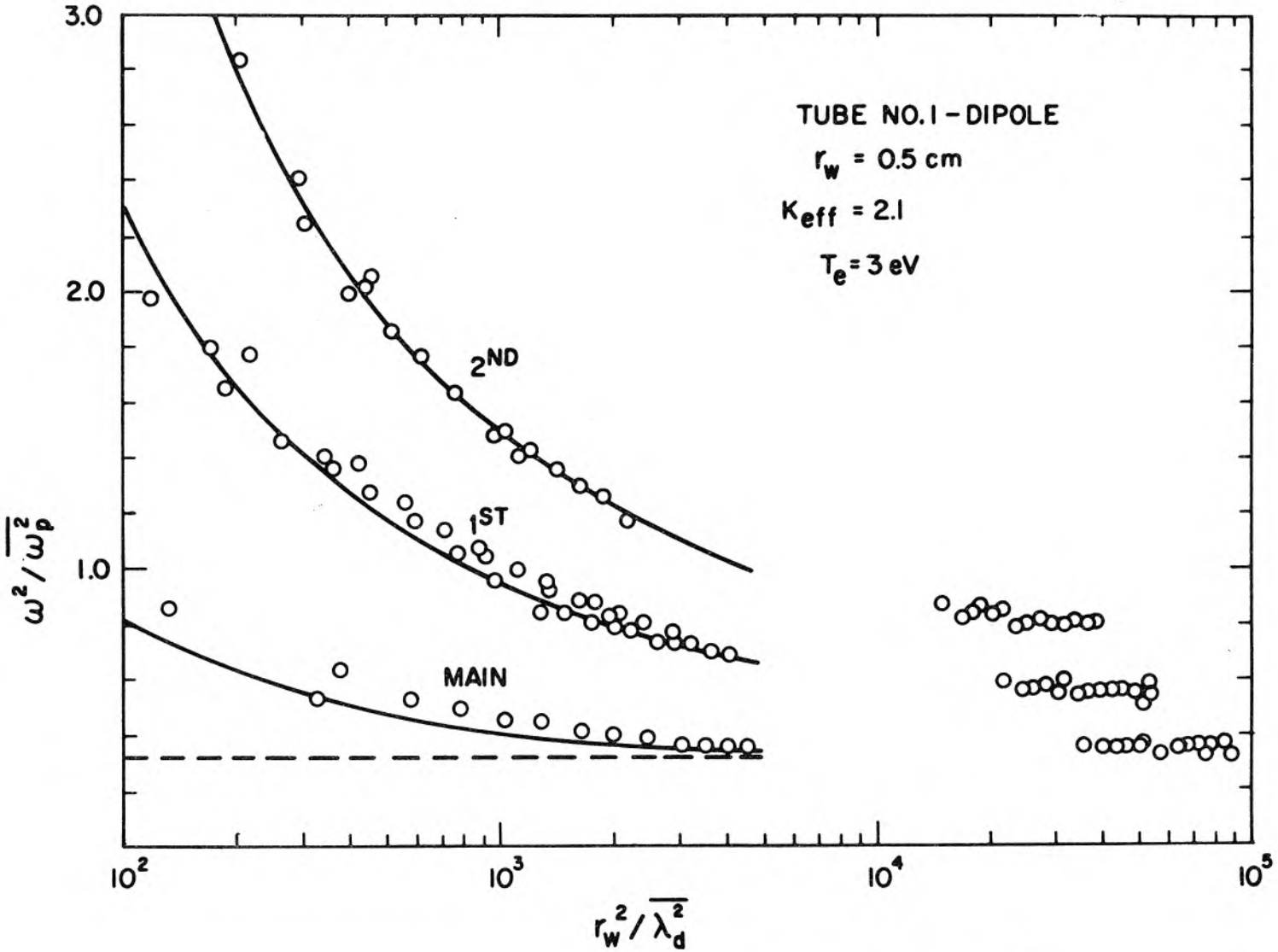

Figure 4.1 Dipole Spectrum of Tube No. 1

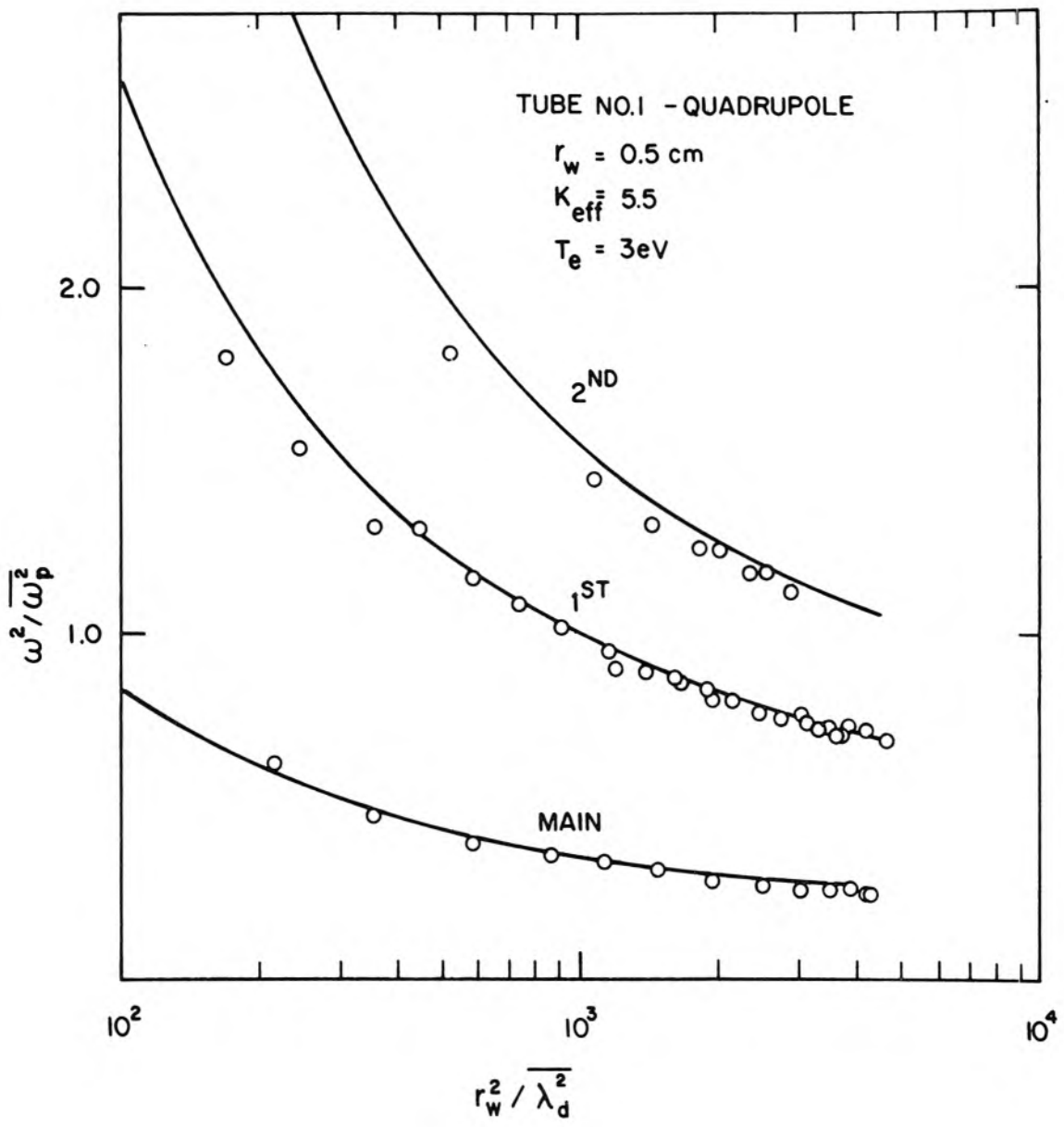

Figure 4.2 Quadrupole Spectrum of Tube No. 1

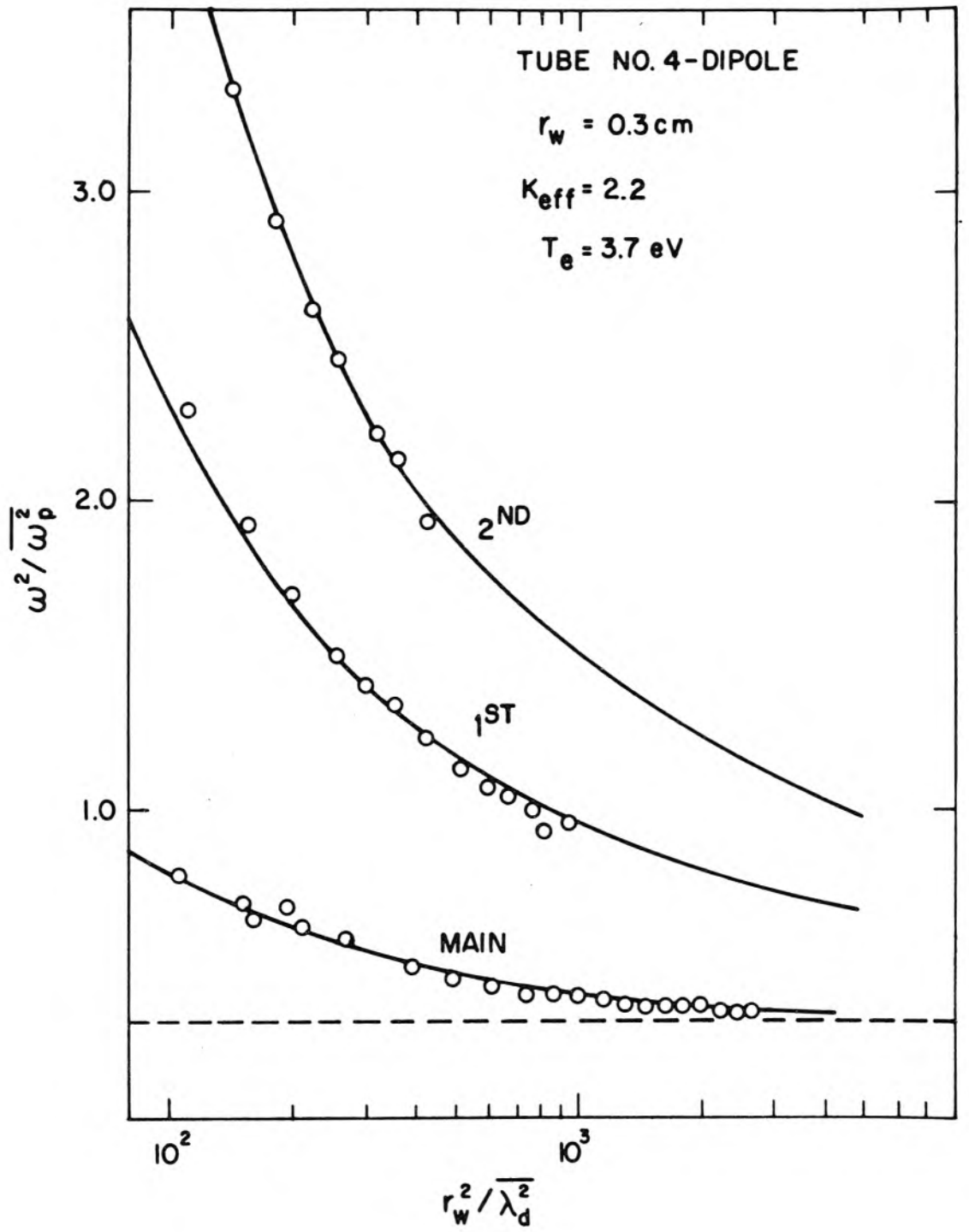

Figure 4.3 Dipole Spectrum of Tube No. 4

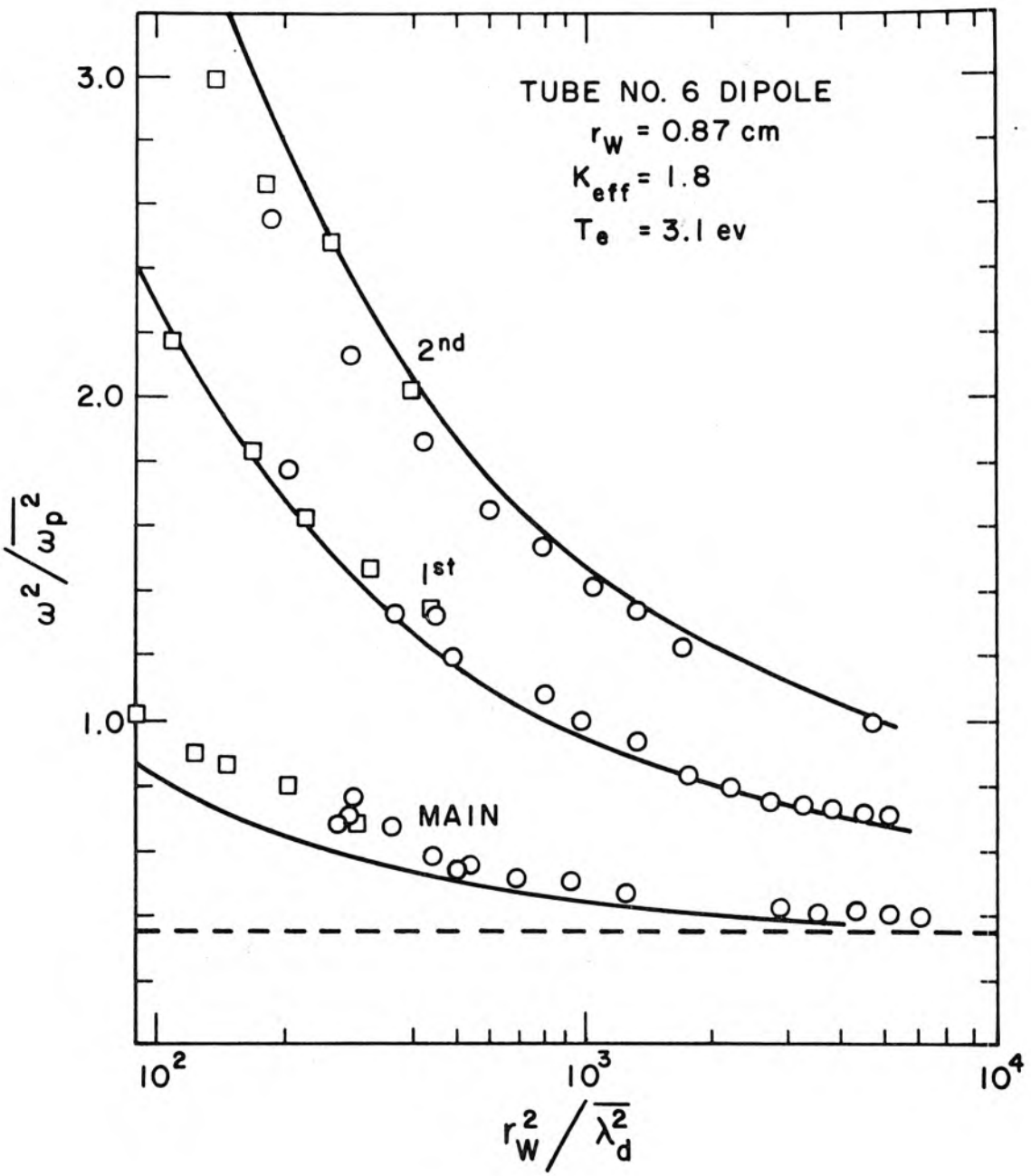

Figure 4.4 Dipole Spectrum of Tube No. 6

quadrupole spectrum is shown in Figure 4.2. The dashed line in Figure 4.1 is the theoretical prediction of the cold plasma theory for the main resonance:

$$\omega^2 / \overline{\omega_p^2} = \frac{1}{1 + K_{eff}} \quad . \tag{4.2}$$

Figure 4.3 gives the dipole spectrum of tube No. 4 which has a smaller radius (r_w = 0.3 cm). Here the best fit electron temperature is slightly larger or 3.7 ev. Once again the dashed line is the cold theory prediction of the main resonance. Finally, Figure 4.4 gives the dipole spectrum of tube No. 6 which has a larger radius (r_w = 0.87 cm). The circles in Figure 4.4 are data points taken in the manner discussed in Section 3.5. The average electron density is adjusted for resonance and the average density is simultaneously measured by the cavity method. The squares are data points taken by an extrapolation method. It is assumed for low currents that the average electron density $\bar{n}$ is directly proportional to the current I or that $\bar{n} = CI$ where C is a constant. The constant C is determined at reasonably high currents, where the cavity method can be employed with some precision. The densities at lower currents can then be obtained as a function of I using the above relation. Here the best fit electron temperature is 3.1 ev.

4.3 Discussion of the Results

There are several aspects of these results which deserve special attention. The generally good agreement between theory and

experiment over such large ranges of $r_w^2/\overline{\lambda_D^2}$ is indicative of the validity of both the electron density profiles and the moment equation approach used by Parker (24) and discussed in Chapter II. Thus the resonance phenomena seem to definitely arise from standing radial plasma waves associated with the hot plasma model.

One of the first features that one observes in examining the results shown in Figures 4.1, 4.2, 4.3, and 4.4 is that for any given resonance (main, first, second), the ratio $\omega^2/\overline{\omega_p^2}$ increases for decreasing $r_w^2/\overline{\lambda_D^2}$. Furthermore the relative spacing between the resonances (main and first, first and second) increases for decreasing $r_w^2/\overline{\lambda_D^2}$. The fact that for a given resonance $\omega^2/\overline{\omega_p^2}$ increases for decreasing $r_w^2/\overline{\lambda_D^2}$ is partially due to the fact that the ratio $\overline{n}/n_o$ (Table 2.1) decreases for decreasing $r_w^2/\overline{\lambda_D^2}$. We can remove the effect of changing $\overline{n}/n_o$ by assuming the validity of the theoretical density profiles and plotting ω^2/ω_{po}^2 instead of $\omega^2/\overline{\omega_p^2}$. Figure 4.5 gives the theoretical dipole spectrum for tube No. 1 where ω^2/ω_{po}^2 has been plotted as a function of r_w^2/λ_{DO}^2. It is seen, although to a lesser degree, that for a given resonance ω^2/ω_{po}^2 still increases for decreasing r_w^2/λ_{DO}^2 (especially for the first and second plasma wave resonances). It is also seen that the relative spacing between the resonances increases for decreasing r_w^2/λ_{DO}^2.

We have seen in equations 2.52 and 2.53 that the resonance spectrum ω^2/ω_{po}^2 depends both on the parameter r_w^2/λ_{DO}^2 and the density profile $f(r) = n(r)/n_o$. Furthermore, we have seen that

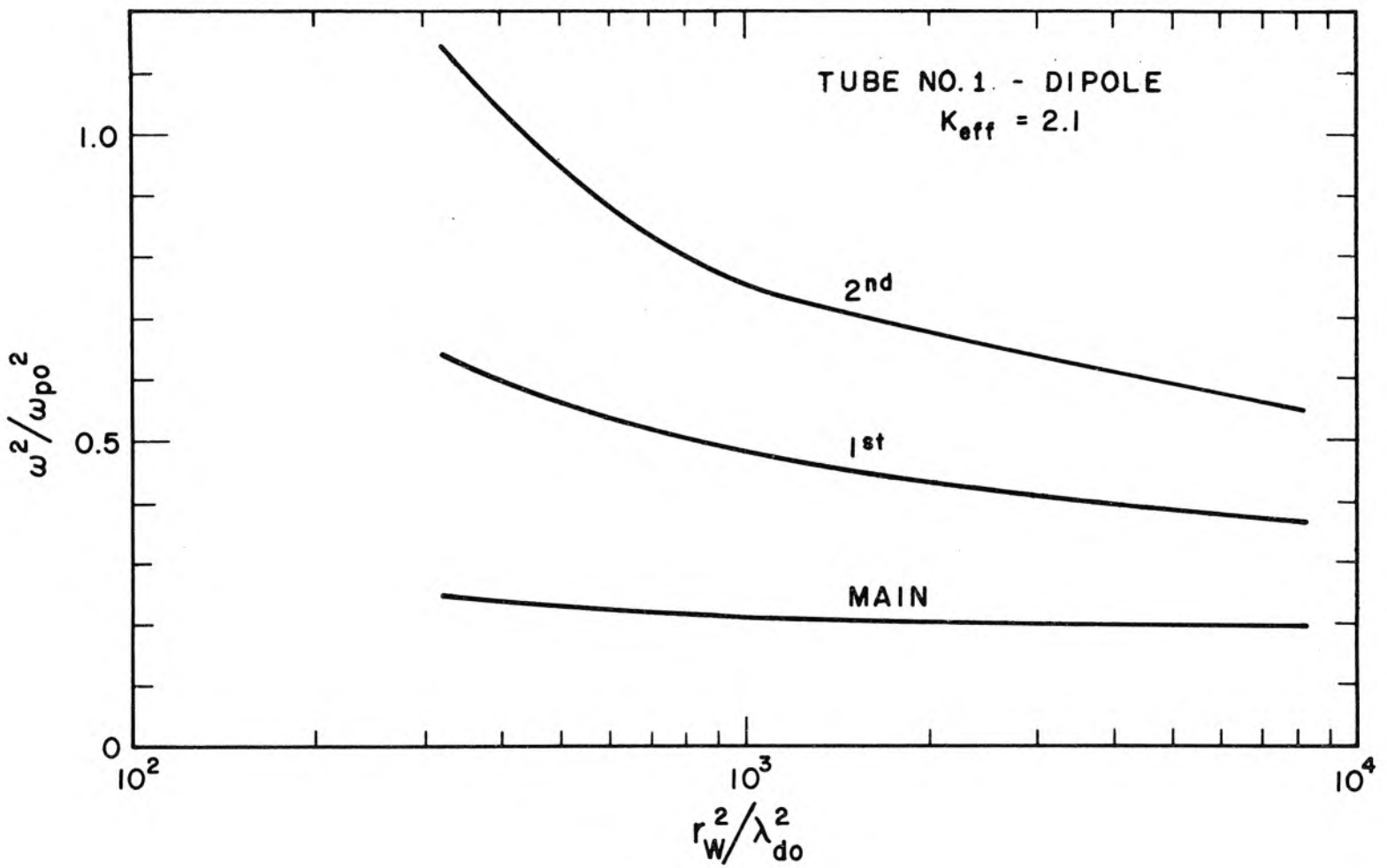

Figure 4.5 Theoretical Dipole Spectrum of Tube No. 1.

the density profile $f(r)$ also depends upon r_w^2/λ_{DO}^2. To take into account the effects of r_w^2/λ_{DO}^2 and $f(r)$ on the resonance spectrum ω^2/ω_{po}^2 and to rigorously describe the salient features of Figure 4.5, as well as Figures 4.1 through 4.4, we must resort to the actual solutions of Parker's equations discussed in Chapter II.

We note also in the dipole spectra, Figures 4.1, 4.3, and 4.4, that the divergence between the experimental data and the cold plasma prediction (dashed line) of the main resonance becomes smaller as $r_w^2/\overline{\lambda_D^2}$ increases.

V. RESONANCES OF THE POSITIVE COLUMN IN AN AXIAL STATIC MAGNETIC FIELD

5.1 Introduction

The effect of a static magnetic field on the plasma wave resonances has been studied off and on for a period of about thirty years (4,25,26,27). The major effort, both experimentally and theoretically, has gone into a study of the main resonance. It has been shown (25) that the main resonance splits into two distinct resonances with the application of a relatively weak ($\sim$20 Gauss in our case) axial magnetic field. It is the purpose of this chapter to present some preliminary data indicating that not only the main resonance, but the first plasma wave resonance as well, splits in the presence of an axial magnetic field.

Until quite recently the theoretical approach has been to describe the plasma by a dielectric tensor (28)

$$\underline{\underline{\epsilon}} = \begin{pmatrix} \epsilon_1 & \epsilon_2 & 0 \\ -\epsilon_2 & \epsilon_1 & 0 \\ 0 & 0 & \epsilon_3 \end{pmatrix} \tag{5.1}$$

where

$$\epsilon_1 = \epsilon_o \left[1 - \frac{\omega_p^2}{\omega^2 - \omega_g^2} \right] \tag{5.2}$$

$$\epsilon_2 = i\epsilon_o \frac{\omega_g \omega_p^2}{\omega(\omega^2 - \omega_g^2)} \tag{5.3}$$

$$\epsilon_3 = \epsilon_o \left[1 - \frac{\omega_p^2}{\omega^2} \right] \tag{5.4}$$

$$\omega_g = \frac{eB_o}{m} \quad . \tag{5.5}$$

In the above description it is assumed that the plasma has a uniform electron density n and that there is a uniform magnetic field B directed along the axis of the column in the +z direction. This description in terms of an effective dielectric tensor is equivalent to the zero temperature model discussed in Section 1.3. Thus we would only expect to obtain the approximate behavior of the main resonance from this model. The higher order plasma wave resonances are excluded.

Inside of the plasma the electric fields must satisfy

$$\nabla \cdot \underset{\sim}{D} = \nabla \cdot (\underline{\underline{\epsilon}} \cdot \underset{\sim}{E}) = 0 \quad . \tag{5.6}$$

If we once again invoke the quasi-static approximation and write $\underset{\sim}{E} = -\nabla\phi$, equation 5.6 becomes

$$\epsilon_1 \nabla^2\phi = 0 \quad . \tag{5.7}$$

Thus if $\epsilon_1 \neq 0$, the potential in the plasma region must satisfy Laplace's equation

$$\nabla^2\phi = 0 \quad . \tag{5.8}$$

Let us write for the potential in the plasma region ($r < r_w$)

$$\phi_n^p(r,\theta) = A_n r^n e^{\pm i n\theta} \quad . \tag{5.9}$$

Then

$$D_{nr}^p = \epsilon_1 E_{nr}^p + \epsilon_2 E_{n\theta}^p = -n A_n r^{n-1} e^{\pm in\theta} (\epsilon_1 \pm i\epsilon_2) . \tag{5.10}$$

Now the resonance condition, equation 1.22, written in terms of the normal displacement becomes

$$L_n \equiv - \left. \frac{D_{nr}^p}{\epsilon_o \phi_n^o} \right|_{r=r_w} = - \frac{n}{r_w} K_{eff} \quad . \tag{5.11}$$

Thus the resonance condition for a magnetized plasma column becomes

$$\frac{\epsilon_1 \pm i\epsilon_2}{\epsilon_o} = - K_{eff} \tag{5.12}$$

or

$$1 - \frac{\omega_p^2}{\omega^2 - \omega_g^2} \mp \frac{\omega_g \omega_p^2}{\omega(\omega^2 - \omega_g^2)} = - K_{eff} \quad . \tag{5.13}$$

Taking the (+) sign, we have

$$\omega_+(\omega_+ - \omega_g) = \frac{\omega_p^2}{1 + K_{eff}} = \omega_o^2 \tag{5.14}$$

or

$$\omega_+ = \frac{\omega_g}{2} + \frac{1}{2}(\omega_g^2 + 4\omega_o^2)^{1/2} \tag{5.15}$$

where ω_o is the resonant frequency in the absence of a magnetic field. Taking the (-) sign, we have

$$\omega_-(\omega_- + \omega_g) = \frac{\omega_p^2}{1 + K_{eff}} = \omega_o^2 \tag{5.16}$$

or

$$\omega_- = -\frac{\omega_g}{2} + \frac{1}{2}(\omega_g^2 + 4\omega_o^2)^{1/2} \quad . \tag{5.17}$$

Thus the cold plasma model predicts that the main resonance is split into two resonances ω_+ and ω_- depending upon the sign of the assumed $e^{\pm in\theta}$ angular dependence. The introduction of the static magnetic field has given a preferred direction to the plasma which causes the left and right handed polarizations to couple differently. Crawford (25) has applied the above equations to the main resonance of the nonuniform case by using $\overline{\omega_p^2}$ for ω_p^2 in equations 5.14 and 5.16. It is clear from the results of Chapter IV that such an approach will be invalid for low values of $r_w^2/\overline{\lambda_D^2}$ since $\omega_o^2 = \overline{\omega_p^2}/1 + K_{eff}$ does not adequately describe the main resonance in the absence of the magnetic field. We shall show in Section 6.3 that the above theory describes the main resonance reasonably well if we take ω_o^2 to be the zero magnetic field resonant frequency predicted by the hot plasma model rather than $\omega_o^2 = \overline{\omega_p^2}/(1 + K_{eff})$.

If the hot plasma model is employed, not only do the difficulties with the main resonance disappear, but the higher order resonances are satisfactorily taken into account. Parker has made calculations based upon the hot plasma model discussed in Chapter II which agree

quite well with the experimental results. In these calculations he includes a $\underset{\sim}{v} \times \underset{\sim}{B}_o$ term in the momentum transfer equation to account for the static magnetic field $B_o \underset{\sim}{I}_z$.

5.2 Theory of a Hot, Nonuniform, Magnetized Plasma Column

We assume the magnetic field to be given by $\underset{\sim}{B} = B_o \underset{\sim}{I}_z$. Since we use the same model discussed in Chapter II, equations 2.14, 2.15 and 2.16 hold, except that we must add a Lorentz force $en_o f(r) B_o \underset{\sim}{v} \times \underset{\sim}{I}_z$ to the force equation 2.15. These equations are:

$$-i\omega \tilde{n} + \nabla \cdot n_o f(r) \tilde{\underset{\sim}{v}} = 0 \tag{5.18}$$

$$i\omega m n_o f(r) \tilde{\underset{\sim}{v}} = -en_o f(r) \nabla \tilde{\phi} + en_o f(r) B_o \underset{\sim}{v} \times \underset{\sim}{I}_z + \gamma kT \nabla \tilde{n} - kT \frac{\nabla f}{f} \tilde{n} \tag{5.19}$$

$$\nabla^2 \tilde{\phi} = \frac{e}{\epsilon_o} \tilde{n} \tag{5.20}$$

where all of the above quantities are defined in Chapter II. If we cross equation 5.19 with $\underset{\sim}{I}_z$ and observe that $(\underset{\sim}{v} \times \underset{\sim}{I}_z) \times \underset{\sim}{I}_z = -\underset{\sim}{v}$, we obtain

$$n_o f \underset{\sim}{v} \times \underset{\sim}{I}_z = -\frac{en_o f}{i\omega m} (\nabla \tilde{\phi} \times \underset{\sim}{I}_z) - \frac{en_o f B_o}{i\omega m} \underset{\sim}{v} + \frac{\gamma kT}{i\omega m} (\nabla \tilde{n} \times \underset{\sim}{I}_z) - \frac{kT\tilde{n}}{i\omega m f} (\nabla f \times \underset{\sim}{I}_z) \quad . \tag{5.21}$$

Equation 5.21 can now be substituted into equation 5.19 to obtain an

equation for $n_o f\tilde{\underset{\sim}{v}}$:

$$n_o f\tilde{\underset{\sim}{v}} = \frac{1}{(1-\omega_g^2/\omega^2)}\left\{\frac{-en_o f}{i\omega m}\nabla\tilde{\phi} + \frac{\gamma kT}{i\omega m}\nabla\tilde{n} - \frac{kT}{i\omega m}\frac{\nabla f}{f}\tilde{n}\right\}$$

$$+ \frac{\omega_g/\omega}{(1-\omega_g^2/\omega^2)}\left\{\frac{-en_o f}{i\omega m}\nabla\tilde{\phi} + \frac{\gamma kT}{i\omega m}\nabla\tilde{n} - \frac{kT\tilde{n}}{i\omega m}\frac{\nabla f}{f}\right\} \times \underset{\sim}{I}_z \quad . \qquad (5.22)$$

If equations 5.20 and 5.22 are now substituted into equation 5.18, we obtain a single equation for the potential:

$$\nabla^2\tilde{\phi} + \frac{1}{(1-\omega_g^2/\omega^2)}\nabla\cdot\underset{\sim}{A} + \frac{\omega_g/\omega}{i(1-\omega_g^2/\omega^2)}(\nabla\times\underset{\sim}{A})\cdot\underset{\sim}{I}_z = 0 \qquad (5.23)$$

where

$$\underset{\sim}{A} = \frac{\omega_{po}^2}{\omega^2}\left[-f\nabla\tilde{\phi} + \gamma\lambda_{DO}^2\nabla(\nabla^2\tilde{\phi}) - \lambda_{DO}^2\nabla^2\tilde{\phi}\frac{\nabla f}{f}\right] \quad . \qquad (5.24)$$

If we now assume that

$$\tilde{\phi}(r,\theta) = \tilde{\phi}(r)e^{\pm in\theta} \qquad (5.25)$$

and introduce the dimensionless parameter

$$\xi = r/r_w \qquad (5.26)$$

so that

$$\nabla_r^2 \equiv \left(\frac{1}{r}\frac{d}{dr}\left(r\frac{d}{dr}\right) - \frac{n^2}{r^2}\right) = \frac{1}{r_w^2}\left(\frac{1}{\xi}\frac{d}{d\xi}\left(\xi\frac{d}{d\xi}\right) - \frac{n^2}{\xi^2}\right) \equiv \frac{1}{r_w^2}\nabla_\xi^2 \tag{5.27}$$

we can write equation 5.23 as

$$\nabla_\xi^2\tilde{\phi} + \frac{\omega_{po}^2/\omega^2}{1-\omega_g^2/\omega^2}\left[-\left\{f + \frac{\lambda_{DO}^2}{r_w^2}\frac{1}{\xi}\frac{d}{d\xi}\left(\frac{\xi}{f}\frac{df}{d\xi}\right)\right\}\nabla_\xi^2\tilde{\phi} - \frac{df}{d\xi}\frac{d\tilde{\phi}}{d\xi}\right. \tag{5.28}$$

$$\left. + \frac{3\lambda_{DO}^2}{r_w^2}\nabla_\xi^2\nabla_\xi^2\tilde{\phi} - \frac{\lambda_{DO}^2}{r_w^2}\frac{1}{f}\frac{df}{d\xi}\frac{d}{d\xi}\left(\nabla_\xi^2\tilde{\phi}\right)\right]$$

$$\pm \frac{(\omega_g/\omega)(\omega_{po}^2/\omega^2)}{(1-\omega_g^2/\omega^2)}\left[\frac{\lambda_{DO}^2}{r_w^2}\frac{1}{\xi f}\frac{df}{d\xi}\nabla_\xi^2\tilde{\phi} - \frac{1}{\xi}\frac{df}{d\xi}\tilde{\phi}\right] = 0 \quad .$$

An inspection of equation 5.28 yields several interesting facts. The potential $\phi(\xi)$ depends not only upon the density profile $f(\xi)$ and the dimensionless parameters r_w^2/λ_{DO}^2 and ω^2/ω_{po}^2 (as in Chapter II), but also upon the dimensionless parameter ω/ω_g. Furthermore, it depends (as in Section 5.1) upon the sign chosen in the assumed $e^{\pm in\theta}$ angular dependence. It should be noted that equation 5.28 reduces to equation 2.52 in the limit that $B \to 0$. One can now assume values of r_w^2/λ_{DO}^2, ω^2/ω_{po}^2, ω/ω_g and f, and proceed to determine ϕ, subject to the boundary condition that the normal electron current must vanish. One can then compute the logarithmic derivative L_n and determine the resonance spectrum from the resonance condition of equation 1.19.

Parker (24) has solved equation 5.28 for various values of the plasma parameters, and some of these results will be discussed in the

next section. In these calculations one important assumption has been made which limits the validity of the solutions to weak magnetic fields. For the radial density profiles $f(\xi)$ Parker uses the profiles obtained in the zero magnetic field case (Section 2.4). One might rightfully argue that the application of a static magnetic field would change the density profiles from their zero magnetic field values, especially when the electron cyclotron radius approaches the tube radius. In our experiments the electron cyclotron radius of an electron having the velocity $v = v_{rms}$ varied from about 2 to 4 mm, while r_w was 5 mm. Thus we are probably pushing the limit of validity of the density profiles.

5.3 Experimental Results

A series of magnetic field experiments were carried out on tube No. 1 ($r_w = 0.5$ cm, $T_e = 3$ ev) with the two values of magnetic field 20 and 40 Gauss. The magnetic field was obtained from a solenoid 10 inches long and 2.75 inches in diameter (inside diameter), and was measured by a Radio Frequency Laboratories Model 1890 Gaussmeter. In these experiments the plasma column was first aligned along the axis of the solenoid. Then a split cylinder capacitor (for the main resonance) or a wire dipole (for the first plasma wave resonance) was placed around the tube and positioned so as to lie in the middle, lengthwise, of the solenoid. The wire dipole was used for observing the first plasma wave resonance because a closer device-column coupling could be obtained conveniently. Again the split cylinder capacitor was employed for observing the main resonance because a well

defined value of K_{eff} could be computed. It will be recalled (Chapter II) that the theoretical predictions of the main resonance are relatively sensitive to the value of K_{eff} while the first plasma wave resonance is relatively insensitive to this value.

The current in the tube was swept in time in a manner described in Section 3.5, and the data was taken in the following way. With the tube and resonance detecting device in place in the solenoid, a set of resonance curves was taken with zero magnetic field. This process consisted of repeatedly changing the input frequency, allowing the current to sweep through the resonances, and displaying the absorption spectrum on an X-Y recorder (Section 3.5). The same process was then repeated for $B = 20$ and 40 Gauss and was done separately for the main and first resonances (since a split cylinder device was used for the main resonance and a wire device for the first resonance). Figure 5.1 illustrates a typical absorption spectrum for an incident frequency of 500 mc and an axial magnetic field of 20 Gauss. Note the small resonance occurring at about 23 ma. (between the main and first resonances). This small resonance, barely perceptible with zero magnetic field, seemed to be enhanced with increasing magnetic field. This resonance remains unexplained. Figure 5.2 illustrates the absorption spectrum for three values of axial magnetic field B_o (B_o = 0, 20, and 40 Gauss). Here the incident frequency is 550 mc. Note again the anomalous resonance (and its enhancement for increasing B_o) at about 30 ma.

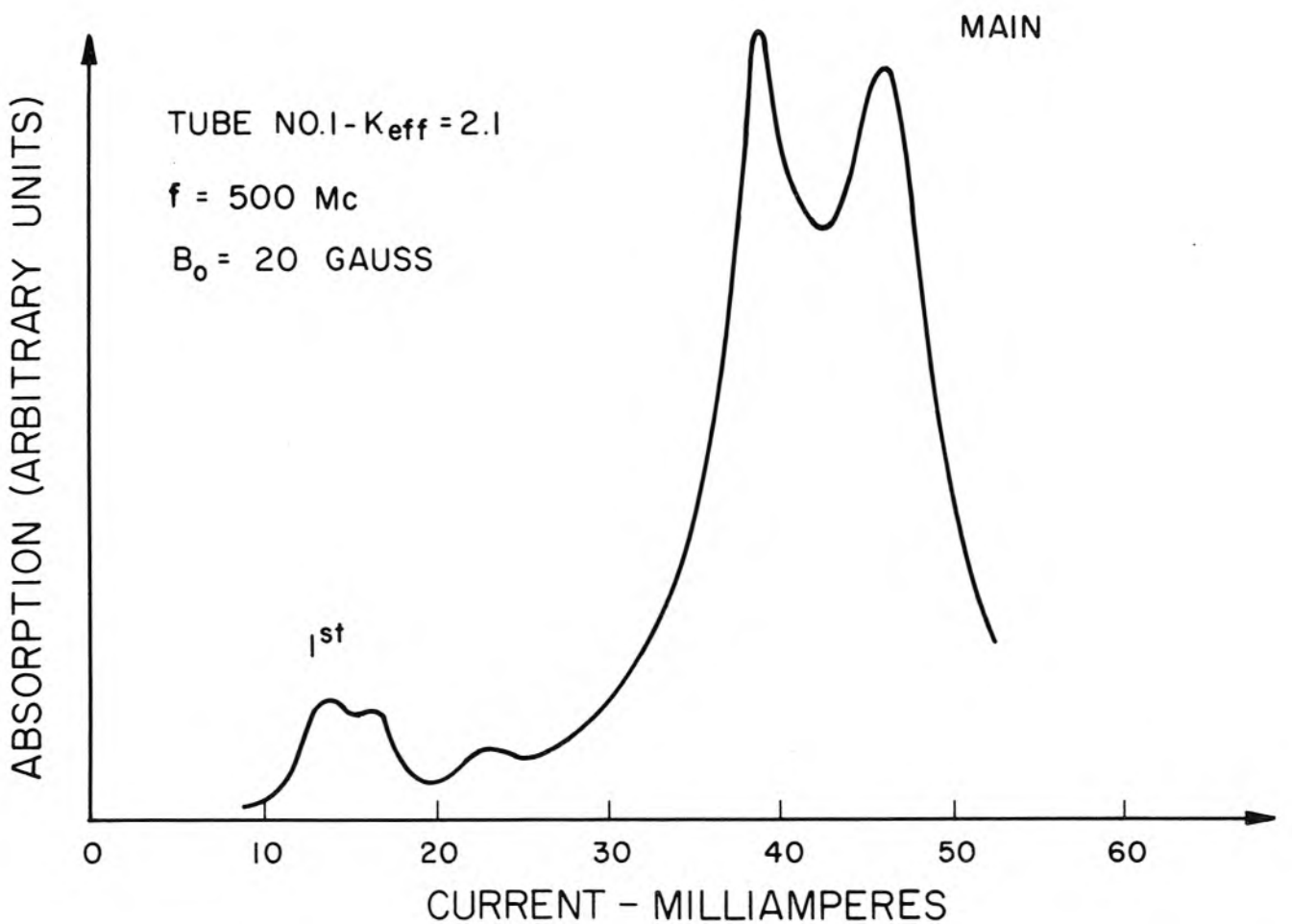

Figure 5.1 Dipole Absorption Spectrum of Tube No. 1 for B_o = 20 Gauss

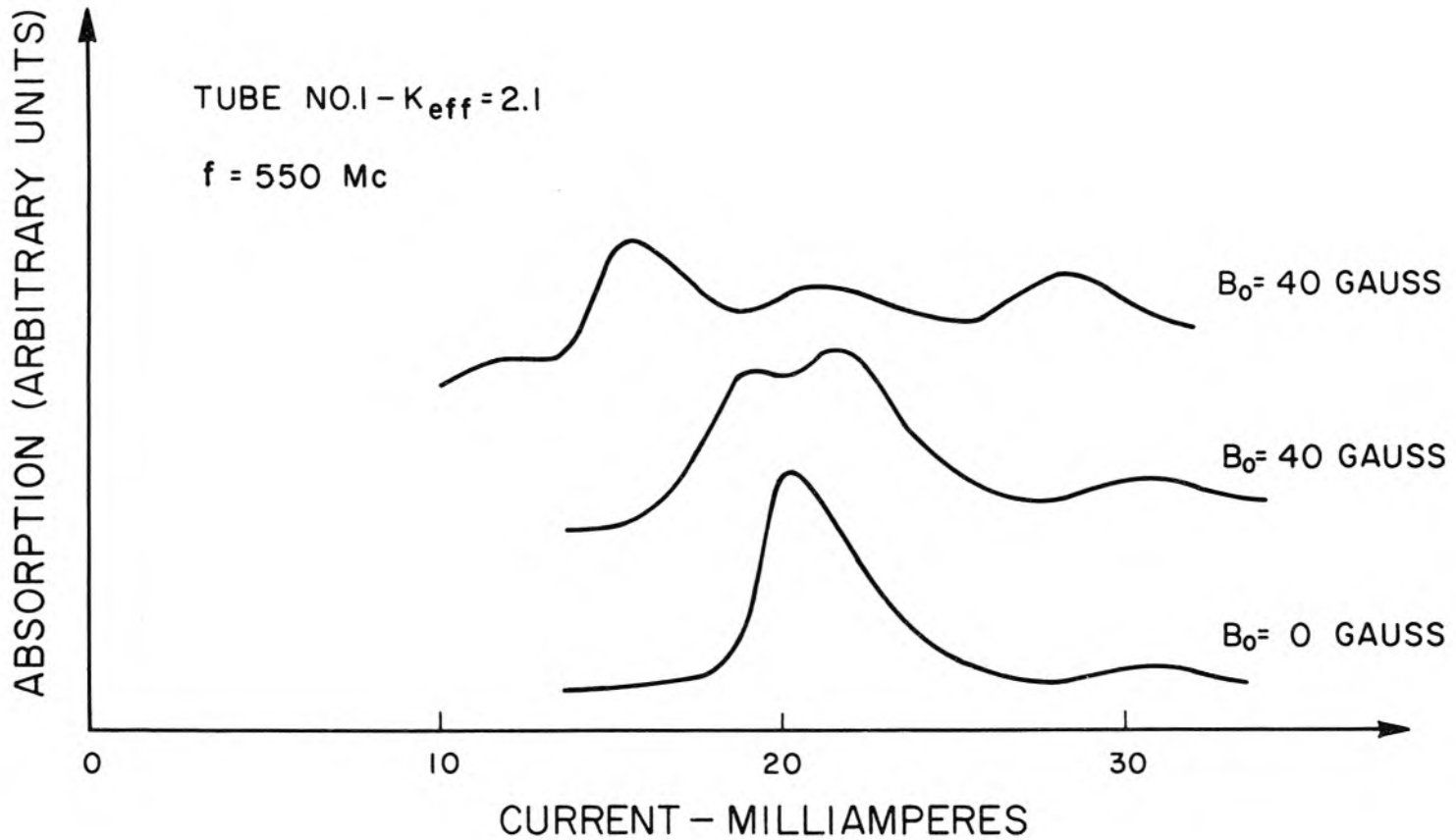

Figure 5.2 Dipole Absorption Spectra for B_o = 0, 20, and 40 Gauss

Figure 5.3 Dipole Resonance Spectrum for B = 20 Gauss

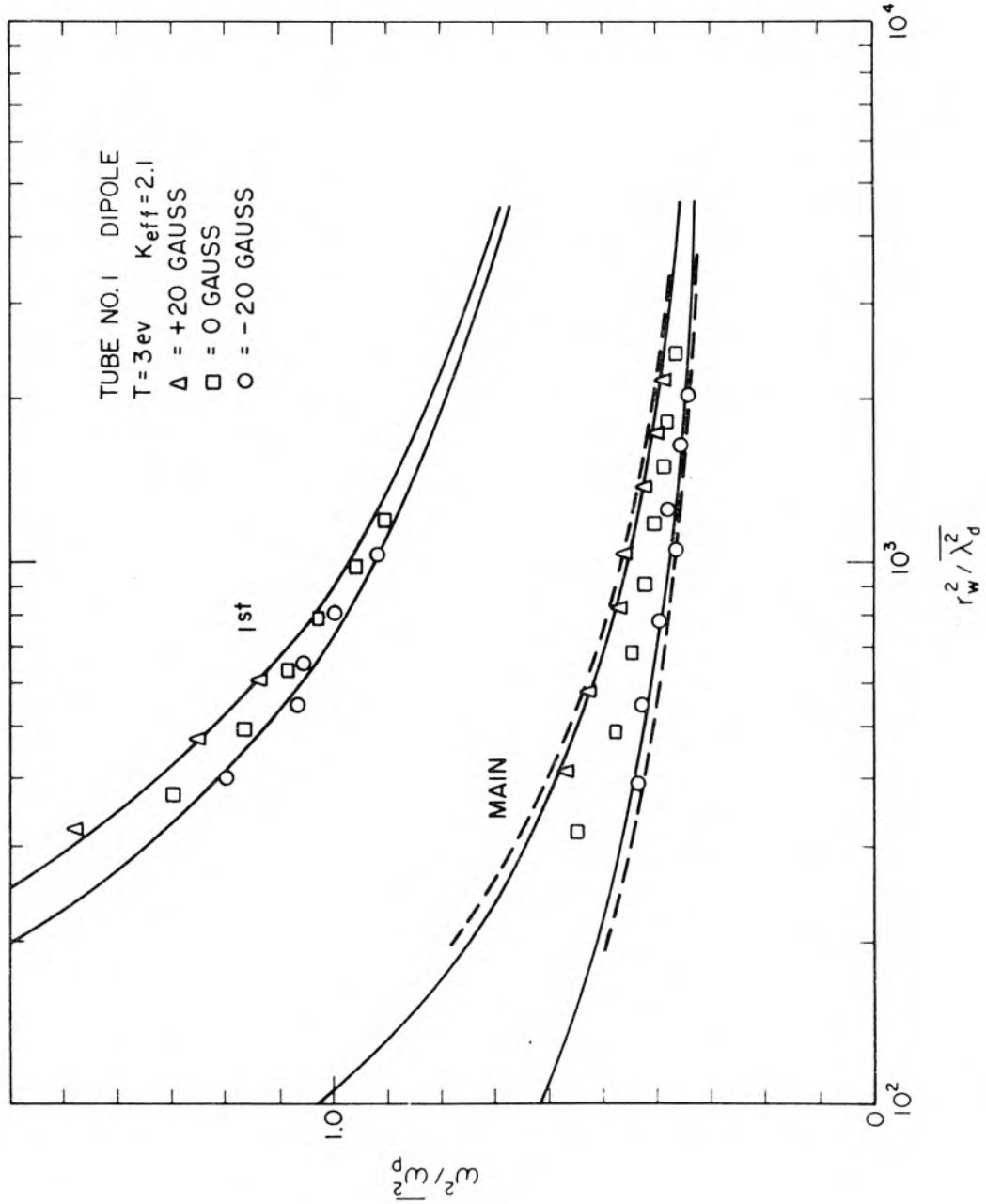

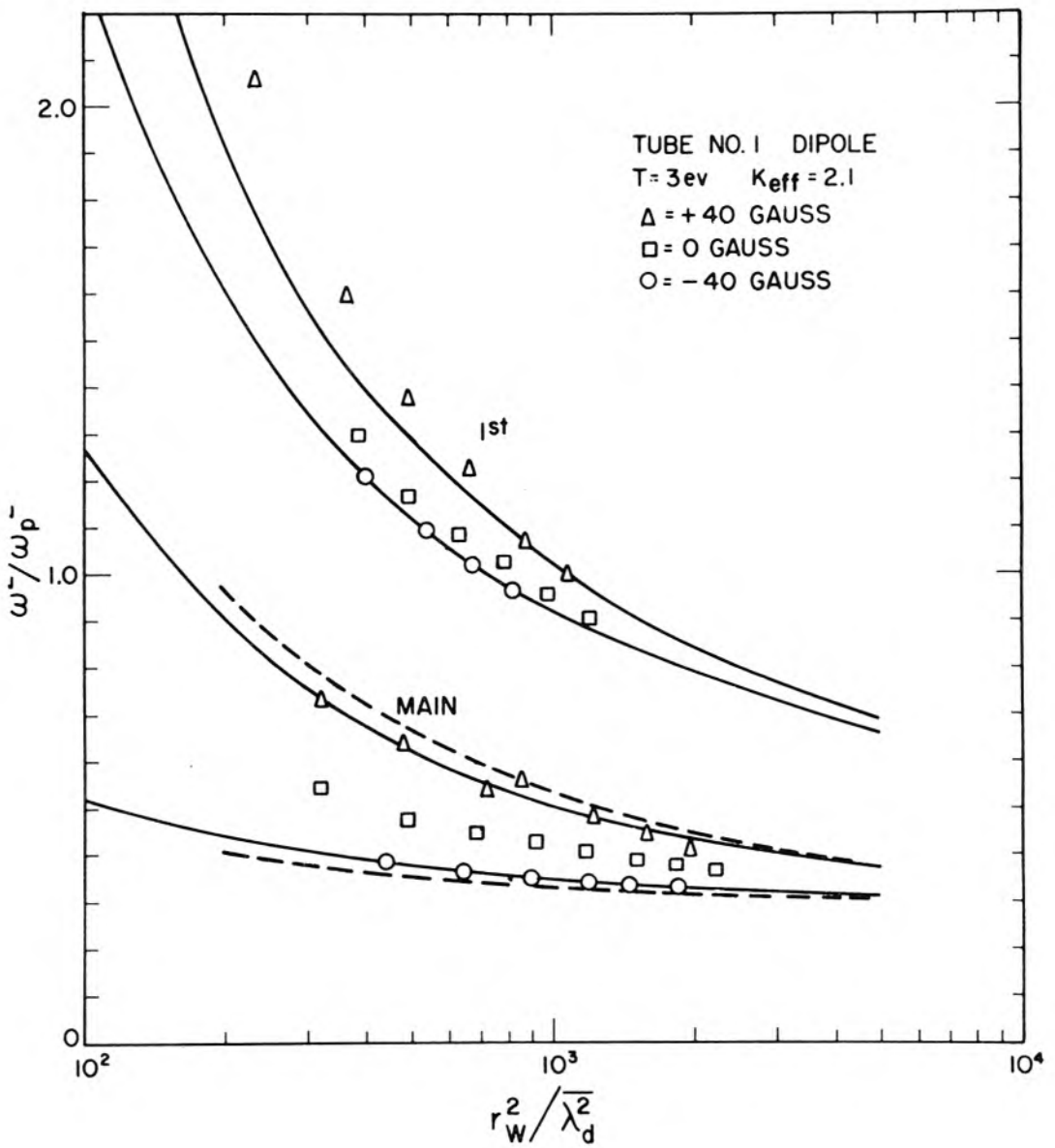

Figure 5.4 Dipole Resonance Spectrum for B = 40 Gauss

By comparing the zero magnetic field spectra with the zero magnetic field theoretical results, one can calibrate the sweeping current in terms of the average electron density. It was found in a separate experiment using a set of Helmholtz coils, a cavity, and tube No. 1, that the average electron density in the column did not change detectably as the magnetic field was changed from 0 to 40 Gauss. This is not to say that the density profile did not change, but at least the average density $\bar{n}$ remained invariant. Thus it makes sense to use the zero magnetic field density versus current curves in the non-zero magnetic field cases also. This is precisely what was done, and the results for B = 20 and 40 Gauss are shown in Figures 5.3 and 5.4. Once again the parameter $\omega^2/\overline{\omega_p^2}$ is plotted versus $r_w^2/\overline{\lambda_D^2}$. We have again chosen T_e = 3 ev as the electron temperature. In contrast to the zero magnetic field case we see that each resonance is now split into two resonances. We have labeled the branches of these split resonances by means of (+) or (-) B (for example, +20 Gauss and -20 Gauss). We see from equation 5.28 that choosing +B is equivalent to choosing the (+) sign in the assumed $e^{\mp in\theta}$ angular dependence; similarly for the (-) sign. The points are experimental results while the solid lines are theoretical results appropriate to this particular tube, calculated by Parker (24). No theoretical curves are drawn through the zero magnetic field experimental points since in the process of determining the average density $\bar{n}$, those points have been chosen so they fall exactly on the theoretical curves. The dashed curves indicate the theoretical results based on the cold plasma theory

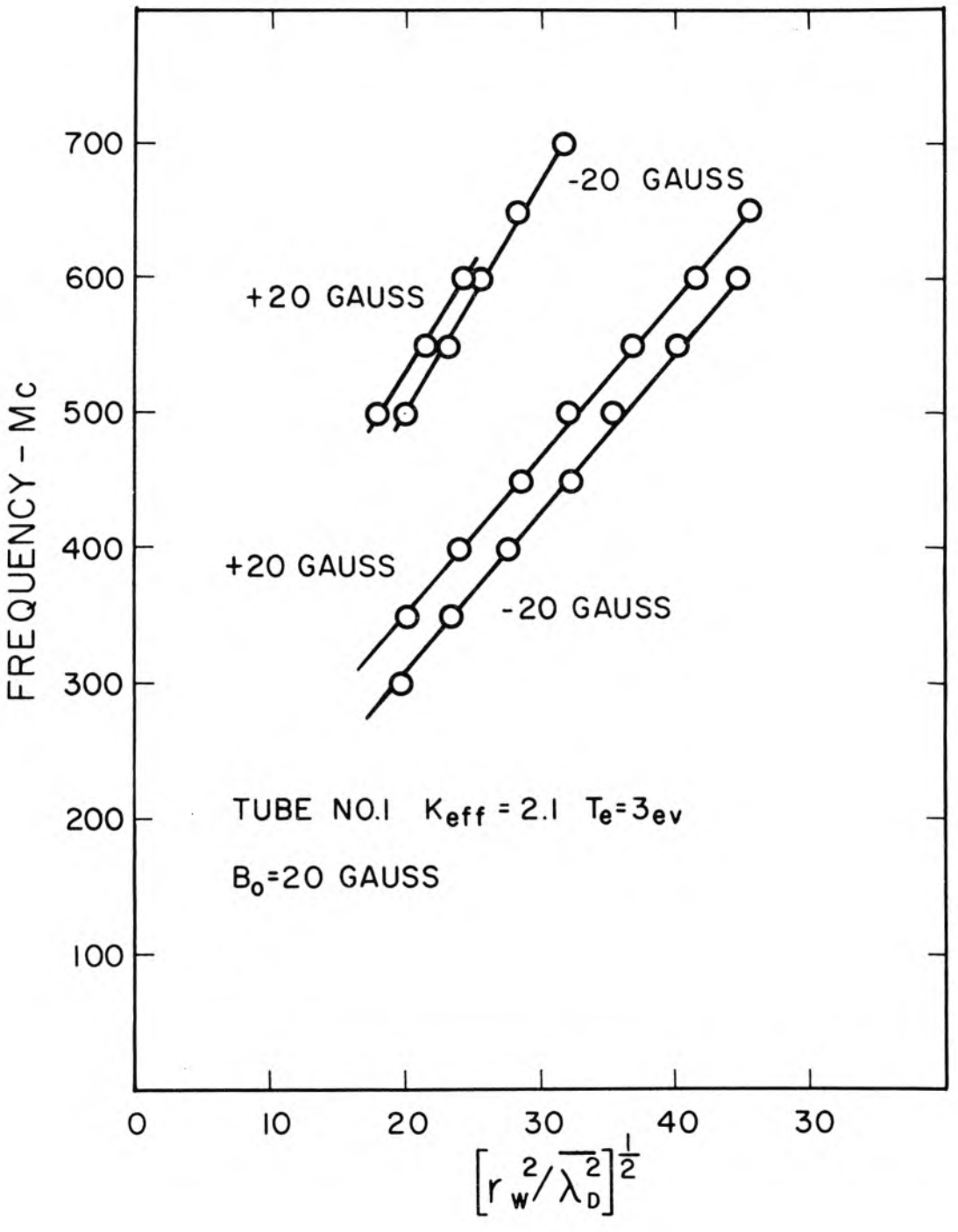

Figure 5.5 Dipole Resonance Spectrum for B_o = 20 Gauss

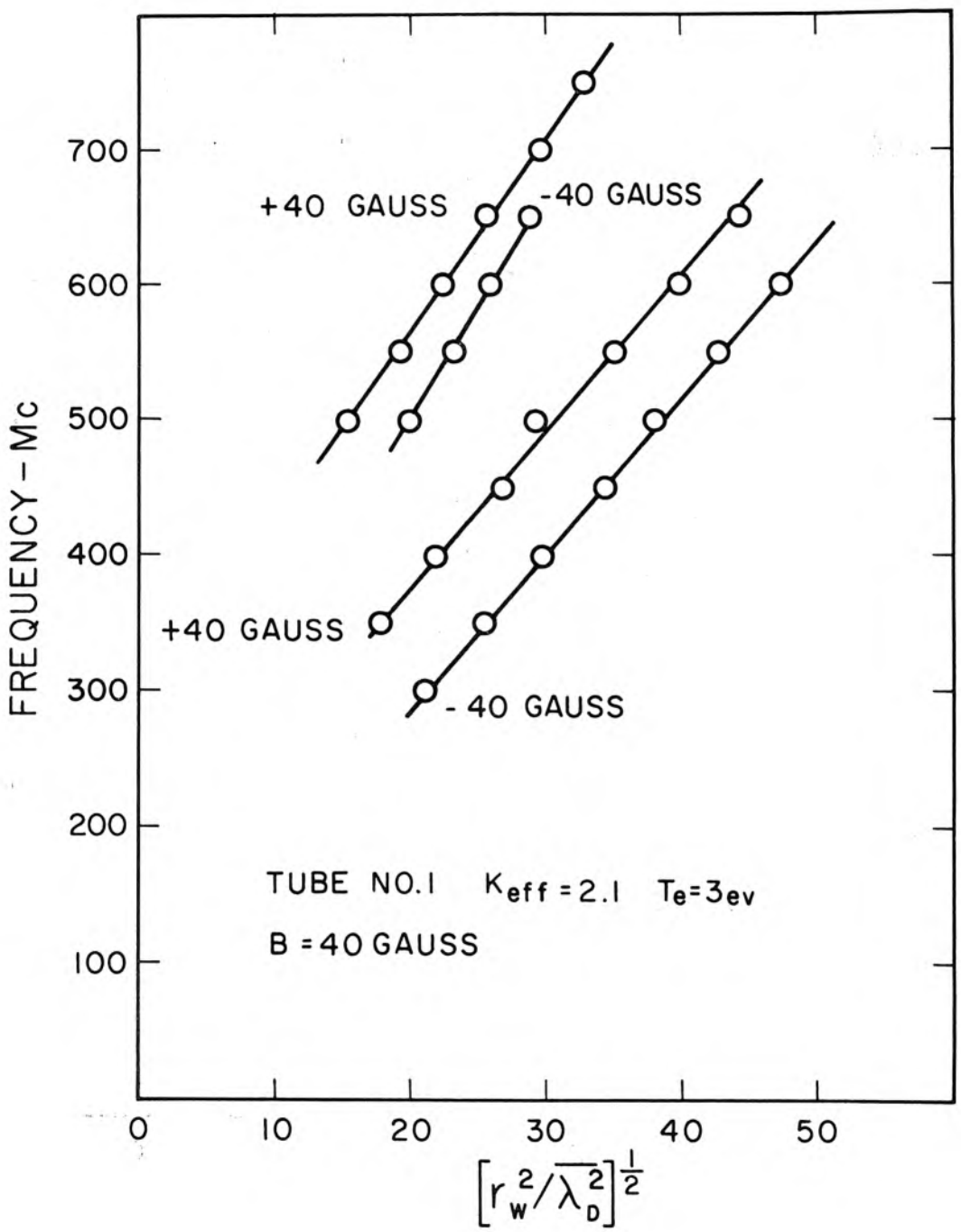

Figure 5.6 Dipole Resonance Spectrum for B_o = 40 Gauss

of Section 5.1 where the value of ω_o^2 predicted by the hot plasma model instead of $\omega_o^2 = \overline{\omega_p^2}/1 + K_{eff}$ has been used in equations 5.14 and 5.16.

The cold plasma theory (equations 5.15 and 5.17) states that for a given $r_w^2/\overline{\lambda_D^2}$ the main resonance should be split by ω_g with the application of B_o. It is interesting to see how much both the main and first resonances split compared with ω_g. Figures 5.5 and 5.6 present the same data given in Figures 5.3 and 5.4. Here, however, we plot the actual resonant frequency f as a function of $\left[r_w^2/\overline{\lambda_D^2}\right]^{1/2}$. For the 20 Gauss case (Figure 5.5) $f_g = \omega_g/2\pi$ is 56 mc, while for the 40 Gauss case $f_g = 112$ mc. We note that for both values of magnetic field the main resonance is split by slightly less than ω_g. The split in the first plasma wave resonance, however, is significantly less than ω_c. For the data presented we have

$$\Delta f_{main}/f_g \equiv \frac{f_+ - f_-}{f_g} = 0.8 \pm 0.1 \quad \text{and} \quad \Delta f_1/f_g = .5 \pm .2 \ .$$

More data is needed to determine the actual dependence of $\Delta f/f_g$ upon B_o and $r_w^2/\overline{\lambda_D^2}$.

It is interesting to note that in order to observe the splitting of the higher order resonances, the axis of the column must be aligned quite carefully parallel to the magnetic field. In our first attempts to observe the splitting of the resonances, a Helmholtz type coil was used as a source of magnetic field. In this arrangement the magnetic field was not totally parallel to the axis of the tube over

the length of the resonance detecting device. It was observed that the main resonance split as predicted but the first resonance simply broadened and disappeared. It is also found in the solenoid that if the column is oriented even at a small angle with respect to the magnetic field, the first resonance broadens and disappears. Thus one might conclude that the behavior of at least the higher order resonances is sensitive to a perpendicular component of B_o.

VI. SUMMARY AND CONCLUSIONS

6.1 Comparison of Theory and Experiment

The generally good agreement between theory and experiment in the zero magnetic field case is indicative of the validity of both the electron density profiles and the moment equation approach used by Parker (24) and discussed in Chapter II. The resonance phenomena arise from standing radial plasma waves associated with the hot plasma model. We have seen that the resonant frequency spectrum $\omega^2/\overline{\omega_p^2}$ depends upon the parameters $r_w^2/\overline{\lambda_D^2}$ and K_{eff} where K_{eff} measures the influence of material exterior to the plasma column. For a given K_{eff} and r_w, changing $\overline{\lambda_D}$ (by varying the current in the column) has two effects. The first effect is to change the propagating wavelength everywhere in the propagating region, while the second effect is to change the shape of the electron density profile (which changes the effective propagating region; see Section 1.3). To properly take these effects into account, one must call upon the moment equations and density profiles used by Parker. It should be noted that the cold plasma theory not only fails to predict the higher order resonances, but for $r_w^2/\overline{\lambda_D^2} \leq 3000$ fails to accurately predict the main resonance.

It must be kept in mind, however, that we have not performed a "closed" set of experiments in checking the theory. For example, we have not directly measured the density profiles $n(r)$ as a function of $r_w^2/\overline{\lambda_D^2}$. As mentioned in Chapter III, such a measurement was attempted by trying to measure the third radial moment of the density profile using the TM_{110} mode of a circular cavity, but the frequency

shifts were so small that the measurement was not feasible. Furthermore, no direct measurement of the electron temperature T_e has been made. The electron temperatures quoted in Chapter IV are best fit temperatures. As mentioned in Chapter IV, however, measurements made by Klarfeld (29) and measurements that we have made on similar tubes indicate that the best fit temperatures of ~ 3 ev are quite reasonable. The fact that in any given tube, a single temperature yields good agreement between theory and experiment over such a large range of $r_w^2/\overline{\lambda_D^2}$ $(10^2 - 10^4)$ is indicative of the validity of the theory.

It is perhaps fortuitous that the theory and experiment agree so well in the two magnetic field cases discussed in Chapter V. It is recalled that in making the magnetic field resonance calculations Parker used the zero magnetic field density profiles (24). Since for our cases the electron cyclotron radius is of the order of the column radius, we are probably pushing the validity of the electron density profiles. There are several conclusions that can be drawn from this preliminary study of the effect of an axial magnetic field on the resonances. The first is that the first plasma wave resonance as well as the main resonance splits into two resonances upon the application of the magnetic field. To our knowledge the splitting of the first plasma wave resonance has not been reported. It should be remarked that there is no reason to suspect that the higher order resonances (second, third, etc) would not be split also. The second conclusion is that the hot plasma model and consequently the plasma wave picture is valid and will adequately describe the results. Clearly, much work remains to be done on the magnetic field case to

determine when the zero magnetic field density profiles prove inadequate. One would then need to calculate adequate profiles and incorporate them into the hot plasma model in order to predict the resonances. Finally, one can conclude that for a given value of $r_w^2/\overline{\lambda_D^2}$, the actual frequency splitting of the first plasma resonance is considerably less than the splitting of the main resonance. For our data $\Delta f_{main}/f_g = 0.8 \pm .1$ while $\Delta f_{first}/f_g = 0.5 \pm .2$. Again, more work needs to be done in order to determine the dependence of the splitting on the plasma parameters.

6.2 Plasma Wave Resonances as a Diagnostic Tool

The plasma wave resonances appear to be quite a useful diagnostic tool for determining the properties of the low density positive column. For example, consider a plasma column operating at some current I, with no static magnetic field, and suppose we wish to determine its parameters (density profile, temperature, etc.). If we know the radius of the column and K_{eff} then, in principle, we need to measure the frequencies of only two plasma wave resonances to determine these parameters. We would use the first and second plasma wave resonances since they are relatively insensitive to K_{eff}. Suppose we measure ω_1 and ω_2, the frequencies of the first and second plasma wave resonances, respectively. Then the theory tells us that

$$\frac{\omega_1^2}{\overline{\omega_p^2}} = f_1\left(\frac{r_w^2}{\overline{\lambda_D^2}}\right) \qquad (6.1)$$

$$\frac{\omega_2^2}{\overline{\omega_p^2}} = f_2\left(\frac{r_w^2}{\overline{\lambda_D^2}}\right) \tag{6.2}$$

or

$$\frac{\omega_2^2}{\omega_1^2} = \frac{f_2\left(\frac{r_w^2}{\overline{\lambda_D^2}}\right)}{f_1\left(\frac{r_w^2}{\overline{\lambda_D^2}}\right)} \quad . \tag{6.3}$$

Knowing K_{eff} we can plot a theoretical curve of f_2/f_1 as a function of $r_w^2/\overline{\lambda_D^2}$. We can now determine the value of $r_w^2/\overline{\lambda_D^2}$ which satisfies equation 6.3. Once $r_w^2/\overline{\lambda_D^2}$ has been determined, both f_1 and f_2 can be determined. Then from $\overline{\omega_p^2} = \omega_1^2/f_1 = \omega_2^2/f_2$, $\bar{n}$ can be determined. Finally, since we know r_w^2, $\bar{n}$ and $r_w^2/\overline{\lambda_D^2}$, T_e can be determined. Such a method has several difficulties. First, it is difficult to measure the resonant frequencies at fixed current. Second, and more important, the ratio ω_2^2/ω_1^2 (shown in Figure 6.1 for $K_{eff} = 2.1$) is only a weak function of $r_w^2/\overline{\lambda_D^2}$. For example, for $K_{eff} = 2.1$ ω_2^2/ω_1^2 varies only from about 1.69 to 1.5 in the range of $r_w^2/\overline{\lambda_D^2} = 70$ to $r_w^2/\overline{\lambda_D^2} = 5000$. Thus small errors in the measurement of ω_2^2/ω_1^2 lead to large errors in $r_w^2/\overline{\lambda_D^2}$. A more useful diagnostic technique would be to use a cavity and make measurements over a wide current range just as described in Chapter III. By comparing these measurements with theory an accurate determination of the temperature could be made. Then if we wished the density profile at any particular current, we could make a measurement of the average density at that current; knowing

Figure 6.1 ω_2^2/ω_1^2 as a Function of $r_w^2/\overline{\lambda_D^2}$

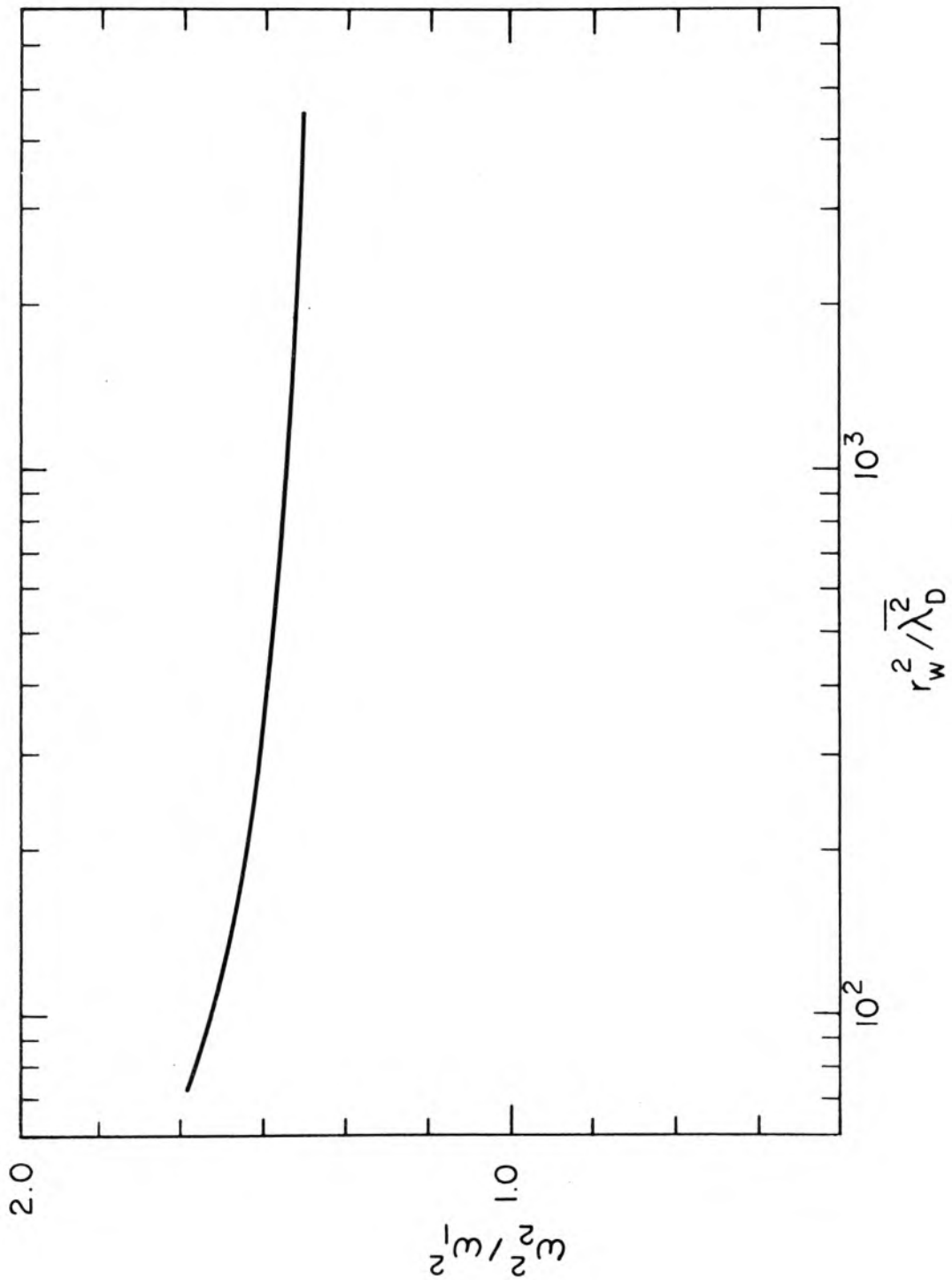

r_w^2, $\bar{n}$ and T_e, we could determine $r_w^2/\overline{\lambda_D^2}$ and hence the profile (assuming the theory to be correct, of course).

6.3 Proposed Problems

There are several problems which remain unsolved and which seem worthy of further study. One of the most interesting problems is the direct measurement of the logarithmic derivative L_n as a function $\omega^2/\overline{\omega_p^2}$ and $r_w^2/\overline{\lambda_D^2}$. In the theory presented in Chapter II, no damping was taken into account and the theoretical values of L_n were entirely real. In the real problem, however, there would be damping (collisional and perhaps Landau damping) and L_n would be complex. By actually measuring L_n as a function of $\omega^2/\overline{\omega_p^2}$ and $r_w^2/\overline{\lambda_D^2}$, one would obtain a further check on the theory and perhaps an experimental determination of the damping. One scheme for measuring L_n is presented in Appendix D. There we consider a split cylinder dipole device with $c \geq 3r_w$ (Figure 2a) so that only the dipole mode is appreciably excited. If Y is the input admittance to the device with the plasma on, and if Y_o is the input admittance with the plasma off, we find

$$Y - Y_o \approx i\omega A_1 \frac{r_w L_1 - 1}{r_w L_1 + K_{eff}} \tag{6.4}$$

where A_1 is a constant defined in Appendix D. Thus by measuring the input admittance to the device as a function of $\omega^2/\overline{\omega_p^2}$ and $r_w^2/\overline{\lambda_D^2}$, one could obtain L_1. The same information could be obtained by carrying out free space or waveguide scattering experiments. The waveguide scattering experiment might be complicated by the necessary

variation of applied fields along the axis of the column.

Another interesting problem would be the investigation of the plasma wave resonance spectrum in gases having different ion masses. Although the plasma wave phenomenon itself is strictly an electron gas phenomenon, the density profiles and hence the spectra are influenced by the ion mass. Equations 2.38 and 2.45 show that while the equation for the potential itself depends on $r_w^2/\overline{\lambda_D^2}$ (or β^2), the equation determining the wall depends on the ion mass m_i.

Finally, another problem would be the investigation of propagation effects along the axis of the column. The theory we have used is z independent, and the devices used have been constructed so as to make the applied fields as z independent as possible. Several authors (30,39) studying the main resonance have shown that if these restrictions are relaxed, multipolar waves can be propagated along the axis of the column. Thus if we think in terms of an ω-β diagram (β corresponding to an $e^{i\beta z}$ dependence), we could say that our experiments have been done in the $\beta = 0$ limit. The propagation effects of the higher order resonances have never been systematically studied.

APPENDIX A

A.1 Introduction

The first part of Appendix A will be devoted to sketching the derivation of the moment equations from the correlationless Boltzmann equation. In the second part we shall discuss the adiabatic approximation and attempt to justify the choice of $\gamma = 3$ in equation 2.18 by considering one-dimensional waves propagating in a rectangular coordinate system.

A.2 The Moment Equations

In a quite general way we can describe the electron gas by the distribution function $f(\underset{\sim}{r},\underset{\sim}{w},t)$ where

$$dN = f(\underset{\sim}{r},\underset{\sim}{w},t)d^3\underset{\sim}{r}\, d^3\underset{\sim}{w} \tag{A.1}$$

is equal to the number of electrons in the volume $d^3\underset{\sim}{r}$ at position $\underset{\sim}{r}$ with velocities between $\underset{\sim}{w}$ and $\underset{\sim}{w} + d\underset{\sim}{w}$ at time t. We assume that $f(\underset{\sim}{r},\underset{\sim}{w},t)$ satisfies the correlationless Boltzmann equation (23)

$$\frac{\partial f}{\partial t} + \underset{\sim}{w} \cdot \nabla_{\underset{\sim}{r}} f - \frac{e}{m}\left[\underset{\sim}{E} + \underset{\sim}{w} \times \underset{\sim}{B}\right] \cdot \nabla_{\underset{\sim}{w}} f = 0 \tag{A.2}$$

where

$$\nabla_{\underset{\sim}{r}} = \underset{\sim}{I}_x \frac{\partial}{\partial x} + \underset{\sim}{I}_y \frac{\partial}{\partial y} + \underset{\sim}{I}_z \frac{\partial}{\partial z} \tag{A.3}$$

$$\nabla_{\underset{\sim}{w}} = \underset{\sim}{I}_x \frac{\partial}{\partial w_x} + \underset{\sim}{I}_y \frac{\partial}{\partial w_y} + \underset{\sim}{I}_z \frac{\partial}{\partial w_z} \quad . \tag{A.4}$$

If we take moments of equation A.2 with respect to various functions of the velocity $\underset{\sim}{w}$, we generate an infinite set of equations in terms of macroscopic quantities such as the density $n(\underset{\sim}{r},t)$, the average velocity $\underset{\sim}{v}(\underset{\sim}{r},t)$, the pressure tensor $\underset{\approx}{P}(\underset{\sim}{r},t)$, etc.

From the definition of $f(\underset{\sim}{r},\underset{\sim}{w},t)$ given in equation A.1, we can write for the average density $n(r,t)$ at the point $\underset{\sim}{r}$ at time t

$$n(\underset{\sim}{r},t) = \int_{-\infty}^{+\infty} f(\underset{\sim}{r},\underset{\sim}{w},t)d^3\underset{\sim}{w} \quad . \tag{A.5}$$

The average velocity of the electron gas at $\underset{\sim}{r}$ and t is

$$\underset{\sim}{v}(\underset{\sim}{r},t) = <\underset{\sim}{w}> = \frac{1}{n}\int_{-\infty}^{+\infty} \underset{\sim}{w}\, f(\underset{\sim}{r},\underset{\sim}{w},t)\, d^3\underset{\sim}{w} \quad . \tag{A.6}$$

In general the velocity average of any scalar quantity $Q(\underset{\sim}{r},\underset{\sim}{w},t)$ is given by

$$< Q(\underset{\sim}{r},\underset{\sim}{w},t) > = \frac{1}{n}\int_{-\infty}^{+\infty} Q(\underset{\sim}{r},\underset{\sim}{w},t)f(\underset{\sim}{r},\underset{\sim}{w},t)\, d^3\underset{\sim}{w} \quad . \tag{A.7}$$

If we now multiply equation A.2 by $Q(\underset{\sim}{r},\underset{\sim}{w},t)$ and integrate over the velocity space, we obtain

$$\frac{\partial}{\partial t}\, n<Q> - n<\frac{\partial Q}{\partial t}> + \nabla_{\underset{\sim}{r}} \cdot n < Q\underset{\sim}{w} > - n < \nabla_{\underset{\sim}{r}} Q \cdot \underset{\sim}{w} > \tag{A.8}$$

$$+ \frac{en}{m} < (\underset{\sim}{E} + \underset{\sim}{w} \times \underset{\sim}{B}) \cdot \nabla_{\underset{\sim}{w}} Q > = 0 \quad .$$

The various moment equations are generated by choosing suitable functions $Q(\underset{\sim}{r},\underset{\sim}{w},t)$.

If we set $Q = 1$ in equation A.8 we obtain the equation of continuity:

$$\frac{\partial n}{\partial t} + \nabla \cdot n\underset{\sim}{v} = 0 \quad . \tag{A.9}$$

By setting $Q(\underset{\sim}{w},\underset{\sim}{r},t) = w_x, w_y$ and w_z , respectively, and adding the results to form a vector equation, we obtain the momentum transfer equation:

$$\frac{\partial \underset{\sim}{v}}{\partial t} + (\underset{\sim}{v} \cdot \nabla)\underset{\sim}{v} = -\frac{e}{m}\left[\underset{\sim}{E} + \underset{\sim}{v} \times \underset{\sim}{B}\right] - \frac{1}{mn}\nabla_T \cdot \underset{\sim\sim}{P} \tag{A.10}$$

where $\underset{\sim\sim}{P}$ is the kinetic stress tensor defined by

$$P_{ij} = m \int_{-\infty}^{+\infty} u_i u_j \, f(\underset{\sim}{r},\underset{\sim}{w},t) \, d^3\underset{\sim}{w} \tag{A.11}$$

and $\underset{\sim}{u}$ is the peculiar velocity defined by

$$\underset{\sim}{u} = \underset{\sim}{w} - \underset{\sim}{v} \quad . \tag{A.12}$$

The tensor divergence $\nabla_T \cdot \underset{\sim\sim}{P}$ is defined by

$$\nabla_T \cdot \underset{\sim\sim}{P} = \left[\frac{\partial}{\partial x} P_{xx} + \frac{\partial}{\partial y} P_{xy} + \frac{\partial}{\partial z} P_{xz}\right]\underset{\sim}{I}_x + \cdots \quad . \tag{A.13}$$

By setting $Q(\underset{\sim}{w},\underset{\sim}{r},t) = u_x u_x$, $u_x u_y$, $u_x u_z$, etc. and combining the results, we obtain an equation for the kinetic stress tensor:

$$\left(\frac{\partial}{\partial t} + \underset{\sim}{v} \cdot \nabla + \nabla \cdot \underset{\sim}{v}\right)\underset{\approx}{P} + \nabla\underset{\sim}{v} \cdot \underset{\approx}{P} + (\nabla\underset{\sim}{v} \cdot \underset{\approx}{P})^{T}$$

$$+ \nabla \cdot \underset{\approx}{Q} = \underset{\approx}{H} \qquad \text{(A.14)}$$

where

$$Q_{ijk} = m \int_{-\infty}^{+\infty} u_i u_j u_k \, f(\underset{\sim}{r},\underset{\sim}{w},t) d^3\underset{\sim}{w} \qquad \text{(A.15)}$$

is the heat flux tensor and

$$H_{xy} = -\frac{e}{m}\left[(\underset{\sim}{B} \times \underset{\sim}{I}_x) \cdot (\underset{\sim}{I}_y \cdot \underset{\approx}{P}) + (\underset{\sim}{B} \times \underset{\sim}{I}_y) \cdot (\underset{\sim}{I}_x \cdot \underset{\approx}{P})\right] \qquad \text{(A.16)}$$

$\nabla\underset{\sim}{v} \cdot \underset{\approx}{P}$ is the scalar product of the two tensors $\nabla\underset{\sim}{v}$ and $\underset{\approx}{P}$ where

$$\nabla\underset{\sim}{v} = \begin{pmatrix} \frac{\partial v_x}{\partial x} & \frac{\partial v_x}{\partial y} & \frac{\partial v_x}{\partial z} \\ \frac{\partial v_y}{\partial x} & \frac{\partial v_y}{\partial y} & \frac{\partial v_y}{\partial z} \\ \frac{\partial v_z}{\partial x} & \frac{\partial v_z}{\partial y} & \frac{\partial v_z}{\partial z} \end{pmatrix} \qquad \text{(A.17)}$$

The above procedure can be carried out ad infinitum, yielding an infinite set of moment equations like equations A.9, A.10 and A.14. One characteristic of this set of equations is that each successive equation contains a new unknown quantity. For example the equation for n (equation A.9) contains the new quantity $\underset{\sim}{v}$ while the equation for $\underset{\sim}{v}$ (equation A.10) contains a new quantity $\underset{\approx}{P}$. Similarly, the equation

for $\underset{\approx}{P}$ (equation A.14) contains a new quantity $\underset{\approx}{Q}$, and so on. To obtain a finite closed set of equations, the moment equations must be terminated at some point. For the theory presented in Chapter II, the moment equations have been terminated by neglecting $\nabla \cdot \underset{\approx}{Q}$ in equation A.14. This is the so-called adiabatic approximation. By setting $\nabla \cdot \underset{\approx}{Q} = 0$, one can determine the behavior of the pressure tensor $\underset{\approx}{P}$ by using equation A.14.

A.3 Example of the Adiabatic Approximation

As an example of the adiabatic approximation, and as an attempt to justify the choice of $\gamma = 3$ in equation 2.18, let us consider the propagation of acoustic waves along the z direction in the plasma. We shall assume that in the absence of any disturbances the electron velocity distribution is isotropic. Then the off diagonal terms of the pressure tensor vanish and we have, for example:

$$P_{xx} = m \int_{-\infty}^{+\infty} u_x^2 f \, d^3w = nm \langle u_x^2 \rangle = \frac{1}{3} nm(u^2) \tag{A.17}$$

where

$$\langle u^2 \rangle = (u_x^2) + (u_x^2) + (u_z^2) \quad . \tag{A.18}$$

If we assume the electron gas to be Maxwellian, we can write

$$P_{xx} = \frac{1}{3} nm(u^2) = nkT = P_o \tag{A.19}$$

where P_o is the electron gas pressure. Similarly we have

$P_{xx} = P_{yy} = P_{zz} = P_o$. Thus in the absence of any disturbances, the pressure tensor becomes

$$\underset{\approx}{P} = \begin{pmatrix} P_o & 0 & 0 \\ 0 & P_o & 0 \\ 0 & 0 & P_o \end{pmatrix} . \tag{A.20}$$

If we now consider wave propagation in the z direction ($e^{-i\omega t}$ time dependence), the pressure tensor will become weakly anisotropic:

$$\underset{\approx}{P} = \begin{pmatrix} P_o + \tilde{P}_{xx}(z)e^{-i\omega t} & \tilde{P}_{xy}(z)e^{-i\omega t} & \tilde{P}_{xz}(z)e^{-i\omega t} \\ \tilde{P}_{yx}(z)e^{-i\omega t} & P_o + \tilde{P}_{yy}(z)e^{-i\omega t} & \tilde{P}_{yz}(z)e^{-i\omega t} \\ \tilde{P}_{zx}(x)e^{-i\omega t} & \tilde{P}_{zy}(z)e^{-i\omega t} & P_o + \tilde{P}_{zz}(z)e^{-i\omega t} \end{pmatrix} \tag{A.21}$$

where we assume that the perturbed quantities are much smaller than P_o . If we write

$$n = n_o + \tilde{n}\, e^{-i\omega t} \tag{A.22}$$

$$\underset{\sim}{v} = v_z\, e^{-i\omega t}\, \underset{\sim}{I}_z \quad , \tag{A.23}$$

linearize equation A.14 using A.21, and invoke the continuity equation we find that

$$\tilde{P}_{xx}(z) = \tilde{P}_{yy}(z) = kT\,\tilde{n} \tag{A.24}$$

$$\tilde{P}_{zz}(z) = 3kT\,\tilde{n} \quad , \tag{A.25}$$

$$\tilde{P}_{ij} = 0 \quad , \quad i \neq j \quad . \tag{A.26}$$

Now only $\tilde{P}_{zz}(z)$ is important in the momentum transfer equation, since

$$\nabla_T \cdot \underset{\sim}{\tilde{P}} = \frac{\partial \tilde{P}_{zz}}{\partial z} \underset{\sim}{I}_z \tag{A.27}$$

and does not involve $\tilde{P}_{xx}$ or $\tilde{P}_{yy}$. Thus if we were to describe this problem using a scalar pressure $P = P_o + \tilde{P}(z)e^{-i\omega t}$, it would be appropriate to choose

$$P_o = nkT \tag{A.28}$$

$$\tilde{P} = 3nkT \tag{A.29}$$

which is analogous to equations 2.17 and 2.18. There we are, however, considering waves traveling in the single r direction rather than the z direction.

It is interesting to note that retaining higher and higher order terms in the moment expansion is equivalent to expanding ω^2/ω_p^2 in powers of $(\frac{\text{thermal speed}}{\text{wave speed}})^2$ or in powers of $(\frac{kv_e}{\omega})^2$ where $v_e^2 = \frac{2kT_e}{m}$ (35). Except for Landau damping, this expansion agrees with that obtained by directly integrating the Boltzmann equation and expanding the resulting plasma dispersion function (36).

APPENDIX B

The purpose of this section is to derive the resonance conditions used in Chapter III for the split cylinder and wire multipole devices. The devices considered and the nomenclature used is shown in Figure B.1a,b,c,d. Since the dimensions of the devices are small compared to a free space wavelength, the quasi-static approximation will be used throughout.

For all of the devices considered we can write:

Region I $(r \leq r_w)$

$$\phi^I(r,\theta,\frac{r_w^2}{\lambda_D^2},\frac{\omega^2}{\omega_p^2}) = \sum_n \phi_n^I(r,\frac{r_w^2}{\lambda_D^2},\frac{\omega^2}{\omega_p^2})\sin(n\theta + \psi) \qquad (B.1)$$

Region II $(r_w \leq r \leq b)$

$$\phi^{II}(r,\theta) = \sum_n \left[B_n(\frac{r}{b})^n + F_n(\frac{r}{b})^{-n} \right] \sin(n\theta + \psi) \qquad (B.2)$$

Region III $(b \leq r \leq c)$

$$\phi^{III}(r,\theta) = \sum_n \left[D_n(\frac{r}{b})^n + S_n(\frac{r}{b})^{-n} \right] \sin(n\theta + \psi) \quad . \qquad (B.3)$$

Resonance will occur when the fields in the plasma become large or when S_n has a pole. This agrees with the resonance condition discussed in Section 1.2, since S_n is analogous to the scattering amplitude.

Figure B.1 Multipole Device Geometry

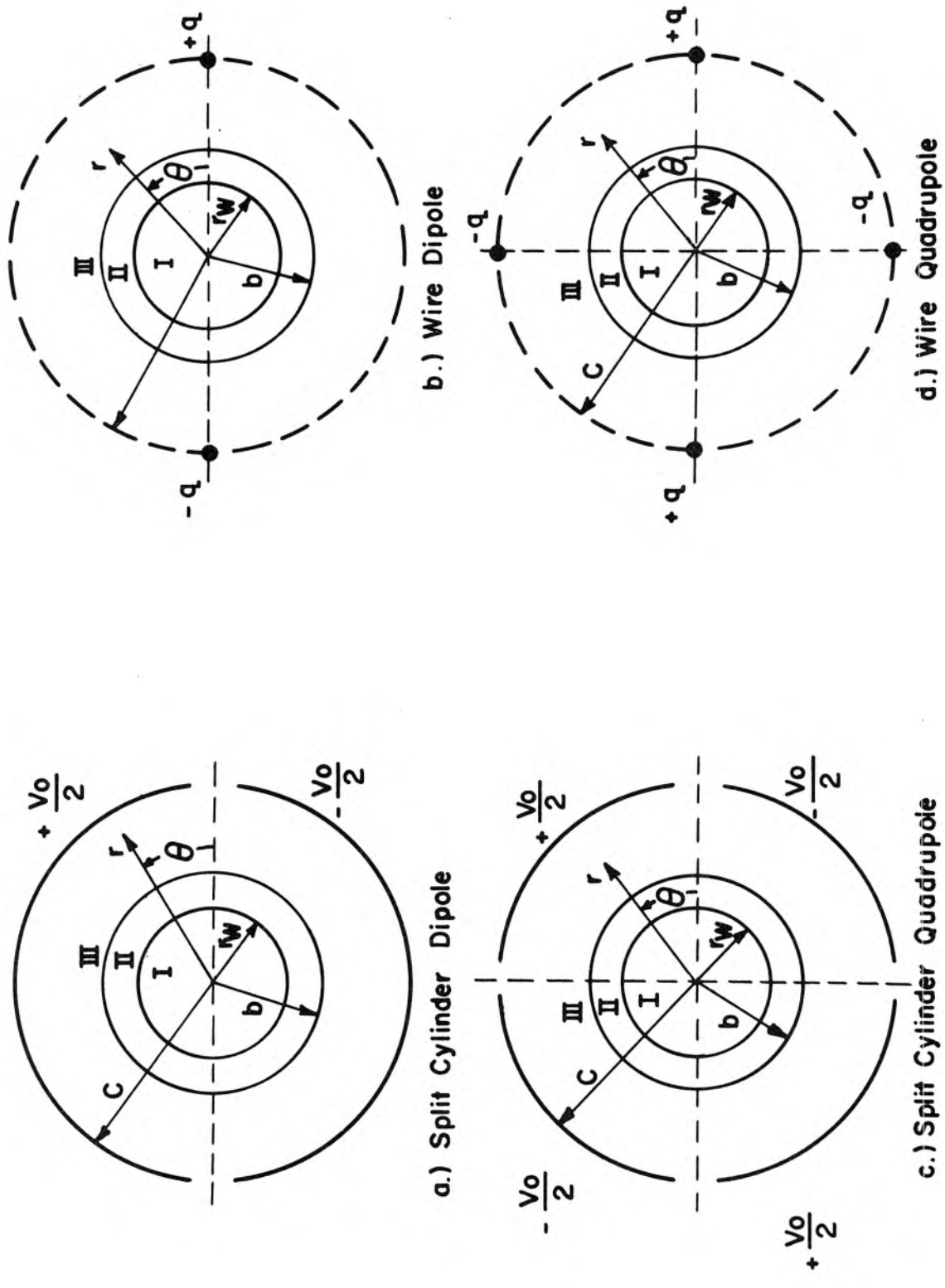

Now at $r = r_w$ and $r = b$ the potentials and normal displacements must be continuous, or

$$\phi_n^I\left(r_w, \frac{r_w^2}{\lambda_D^2}, \frac{\omega^2}{\omega_p^2}\right) = B_n\left(\frac{r_w}{b}\right)^n + F_n\left(\frac{r_w}{b}\right)^n \tag{B.4}$$

$$K_p \frac{d\phi_n^I}{dr}\left(r, \frac{r_w^2}{\lambda_D^2}, \frac{\omega^2}{\omega_p^2}\right)\Bigg|_{r=r_w} = \frac{Kn}{b}\left[B_n\left(\frac{r_w}{b}\right)^{n-1} - F_n\left(\frac{r_w}{b}\right)^{-n-1}\right] \tag{B.5}$$

$$B_n + F_n = D_n + S_n \tag{B.6}$$

$$K(B_n - F_n) = D_n - S_n \tag{B.7}$$

where K_p and K are the relative dielectric constants of the plasma region and glass regions respectively. If we define the logarithmic derivative L_n (as in Chapter I) as

$$L_n \equiv \left[\frac{K_p}{\phi_n^I}\frac{d\phi_n^I}{dr}\right]_{r=r_w} \tag{B.8}$$

we can write D_n in terms of L_n and S_n as

$$D_n = p_n S_n \tag{B.9}$$

where

$$p_n = \frac{\frac{r_w L_n}{nK}\left[(K+1)(\frac{b}{r_w})^n + (K-1)(\frac{r_w}{b})^n\right] + \left[(K+1)(\frac{b}{r_w})^n - (K-1)(\frac{r_w}{b})^n\right]}{(K+1)(\frac{r_w}{b})^n - (K-1)(\frac{b}{r_w})^n - \frac{r_w L_n}{nK}\left[(K+1)(\frac{r_w}{b})^n + (K-1)(\frac{b}{r_w})^n\right]} . \quad (B.10)$$

Thus in Region III we can write

$$\phi^{III}(r,\theta) = \sum_n \left\{p_n(\frac{r}{b})^n + (\frac{r}{b})^{-n}\right\} S_n \sin(n\theta + \psi) \quad (B.11)$$

To determine S_n we must investigate the conditions at $r = c$.

Case A. Split Cylinder Devices. For the split cylinder devices (Figure B.1a,c), the potential is specified on the cylinder $r = c$. Let us choose $\psi = 0$ so that the angular dependence in the above equations goes as $\sin n\theta$. Then by evaluating equation B.11 at $r = c$, multiplying both sides by $\sin m\theta\, d\theta$, and integrating from $\theta = 0$ to $\theta = 2\pi$, we obtain

$$S_n = \frac{1}{\pi\left\{p_n(\frac{c}{b})^n + (\frac{c}{b})^{-n}\right\}} \int_0^{2\pi} \phi^{III}(c,\theta)\sin n\theta\, d\theta \quad (B.12)$$

where $\phi^{III}(c,\theta)$ is the value of the potential on the cylinder $r = c$. For the dipole case

$$S_n = \frac{2v_o}{n\pi\left\{p_n(\frac{c}{b})^n + (\frac{c}{b})^{-n}\right\}} \qquad n = 1,3,5,\cdots \quad (B.13)$$

while for the quadrupole case,

$$S_n = \frac{4v_o}{n\pi \left\{ p_n \left(\frac{c}{b}\right)^n + \left(\frac{c}{b}\right)^{-n} \right\}} \qquad n = 2,6,10,\cdots \quad . \tag{B.14}$$

We see that for the dipole and quadrupole devices (as well as for higher order devices) the poles in S_n occur when

$$p_n \left(\frac{c}{b}\right)^n + \left(\frac{c}{b}\right)^{-n} = 0 \quad . \tag{B.15}$$

Equation B.15 thus determines the resonance condition for the split cylinder devices. If this equation is solved for L_n we obtain

$$L_n = -\frac{n}{r_w} K \frac{\left(\frac{b}{r_w}\right)^n (K+g) - \left(\frac{r_w}{b}\right)^n (K-g)}{\left(\frac{b}{r_w}\right)^n (K+g) + \left(\frac{r_w}{b}\right)^n (K-g)} = -\frac{n}{r_w} K_{eff}(r_w,b,c,K) \tag{B.16}$$

where

$$g = \frac{1 + (b/c)^{2n}}{1 - (b/c)^{2n}} \tag{B.17}$$

and

$$K_{eff}(K,r_w,b,c) = K \frac{\left(\frac{b}{r_w}\right)^n (K+g) - \left(\frac{r_w}{b}\right)^n (K-g)}{\left(\frac{b}{r_w}\right)^n (K+g) + \left(\frac{r_w}{b}\right)^n (K-g)} \quad . \tag{B.18}$$

Case B. Wire Multipole Devices. To handle the wire multipole devices oriented as shown in Figure B.1b,d, we assume $\psi = \pi/2$ in

equation B.11 and introduce a potential in Region IV of

$$\phi^{IV}(r,\theta) = \sum_n Q_n \left(\frac{r}{b}\right)^{-n} \cos n\theta \qquad (B.19)$$

We further assume that the wires carry a charge per unit length q (arranged as in Figure B.1b,d with an $e^{-i\omega t}$ time dependence). At $r = c$ we must have

$$\phi^{III}(c,\theta) = \phi^{IV}(c,\theta) \qquad (B.20)$$

$$E_r^{IV}(c,\theta) - E_r^{III}(c,\theta) = \frac{\sigma(c,\theta)}{\epsilon_o} \qquad (B.21)$$

where $\sigma(c,\theta)$ is the charge density on the cylinder $r = c$. With equations B.19 and B.11 (with $\psi = \pi/2$) these boundary conditions reduce to

$$\sum_n \frac{2n}{c} p_n \left(\frac{c}{b}\right)^n S_n \cos n\theta = \frac{\sigma(c,\theta)}{\epsilon_o} \quad . \qquad (B.22)$$

Again we determine S_n by multiplying equation B.22 by $\cos m\theta \, d\theta$, and integrating from $\theta = 0$ to $\theta = 2\pi$ which gives:

$$S_n = \frac{c}{2n\pi \, p_n \epsilon_o} \left(\frac{b}{c}\right)^n \int_0^{2\pi} \sigma(c,\theta) \cos n\theta \, d\theta \quad . \qquad (B.23)$$

For the dipole device we can write

$$\sigma(c,\theta) = \frac{q}{c} \left[\delta(\theta) - \delta(\theta - \pi) \right] \qquad (B.24)$$

which yields

$$S_n = \frac{q}{n\pi\epsilon_o}\left(\frac{b}{c}\right)^n \frac{1}{p_n} \qquad n = 1,3,5,\cdots \quad . \tag{B.25}$$

For the quadrupole device we have

$$\sigma(c,\theta) = \frac{q}{c}\left[\delta(\theta) - \delta(\theta - \frac{\pi}{2}) + \delta(\theta - \pi) - \delta(\theta - \frac{3\pi}{2})\right] \tag{B.26}$$

which gives

$$S_n = \frac{2q}{n\pi\epsilon_o}\left(\frac{b}{c}\right)^n \frac{1}{p_n} \qquad n = 2,6,10,\cdots \tag{B.27}$$

We see that for the wire multipole devices the poles in S_n occur when

$$p_n = 0 \quad . \tag{B.28}$$

Using equation B.10 we see that equation B.28 holds when

$$L_n = -\frac{n}{r_w} K \frac{(K+1)\left(\frac{b}{r_w}\right)^n - (K-1)\left(\frac{r_w}{b}\right)^n}{(K+1)\left(\frac{b}{r_w}\right)^n + (K-1)\left(\frac{r_w}{b}\right)^n} = -\frac{n}{r_w} K_{eff}(K, r_w, b, c = \infty) \quad . \tag{B.29}$$

Equations B.16 and B.29 are just the resonance conditions used in Chapter III.

APPENDIX C

C.1 Introduction

Let us consider an empty cavity having a resonant frequency ω_{oo} and field distributions given by $\underset{\sim}{E}_o(\underset{\sim}{r})$ and $\underset{\sim}{B}_o(\underset{\sim}{r})$. Let us now introduce a piece of dielectric of dielectric constant ϵ into the cavity. The resonant frequency will now be ω and the field distributions will be given by $\underset{\sim}{E}(\underset{\sim}{r})$ and $\underset{\sim}{B}(\underset{\sim}{r})$. It can be shown (31) that the exact frequency shift of the cavity is given by

$$\frac{\omega - \omega_{oo}}{\omega} = - \frac{\int_{v_o} \Delta\epsilon \, \underset{\sim}{E}_o^* \cdot \underset{\sim}{E} dv}{\int_{v_o} \left\{ \epsilon_o \underset{\sim}{E}_o^* \cdot \underset{\sim}{E} + \frac{\underset{\sim}{B}_o^* \cdot \underset{\sim}{B}}{\mu_o} \right\} dv} \qquad (C.1)$$

where

$$\Delta\epsilon = \epsilon - \epsilon_o \qquad (C.2)$$

and v_o is the volume of the cavity. Let us write $\Delta\epsilon$ in C.1 as $\lambda\Delta\epsilon$ where λ is an expansion parameter with $0 \leq \lambda \leq 1$. We see that if $\lambda = 0$, $\omega = \omega_{oo}$ which effectively removes the dielectric from the cavity, and if $\lambda = 1$ we have the problem which we are trying to solve.

Let us expand the perturbed quantities $\underset{\sim}{E}$, $\underset{\sim}{B}$ and ω in a power series in λ.

$$\underset{\sim}{E} = \underset{\sim}{E}_o + \lambda \underset{\sim}{E}_1 + \lambda^2 \underset{\sim}{E}_2 + \cdots \tag{C.3}$$

$$\underset{\sim}{B} = \underset{\sim}{B}_o + \lambda \underset{\sim}{B}_1 + \lambda^2 \underset{\sim}{B}_2 + \cdots \tag{C.4}$$

$$\omega = \omega_{oo} + \lambda \omega_1 + \lambda^2 \omega_2 + \cdots \quad . \tag{C.5}$$

If we substitute the above expressions into equation C.1, we obtain to first order (neglecting all terms of $O(\lambda^2)$):

$$\frac{\omega - \omega_{oo}}{\omega_{oo}} = - \frac{\int_{V_o} \Delta\epsilon \, \underset{\sim}{E}_o \cdot \underset{\sim}{E}_o^* dv}{\int_{V_o} \left[\epsilon_o \underset{\sim}{E}_o^* \cdot \underset{\sim}{E}_o + \frac{\underset{\sim}{B}_o^* \cdot \underset{\sim}{B}_o}{\mu_o} \right] dv} = - \frac{\int \Delta\epsilon \, \underset{\sim}{E}_o^* \cdot \underset{\sim}{E}_o dv}{8 \overline{w}_e} = - \frac{\Delta v}{8 \overline{w}_e} \tag{C.6}$$

where

$$\overline{w}_e = \frac{1}{4} \epsilon_o \int_{V_o} \underset{\sim}{E}_o^* \cdot \underset{\sim}{E}_o dv = \overline{w}_B = \frac{1}{4\mu_o} \int_{V_o} \underset{\sim}{B}_o^* \cdot \underset{\sim}{B}_o dv \tag{C.7}$$

is the average stored electric field energy in the empty cavity ($\overline{w}_e = \overline{w}_B$ at resonance).

C.2 Determination of the Average Electron Density $\bar{n}$ in a Plasma Column Using the TM_{010} Mode of a Cylindrical Cavity

Let us now consider the specific case of a plasma column along the axis of a right circular cylindrical cavity operating in the TM_{010} mode which is illustrated in Figure C.1. We assume that the electron density $n(r)$ in the plasma region has a radial gradient. The plasma will then be described by the dielectric constant

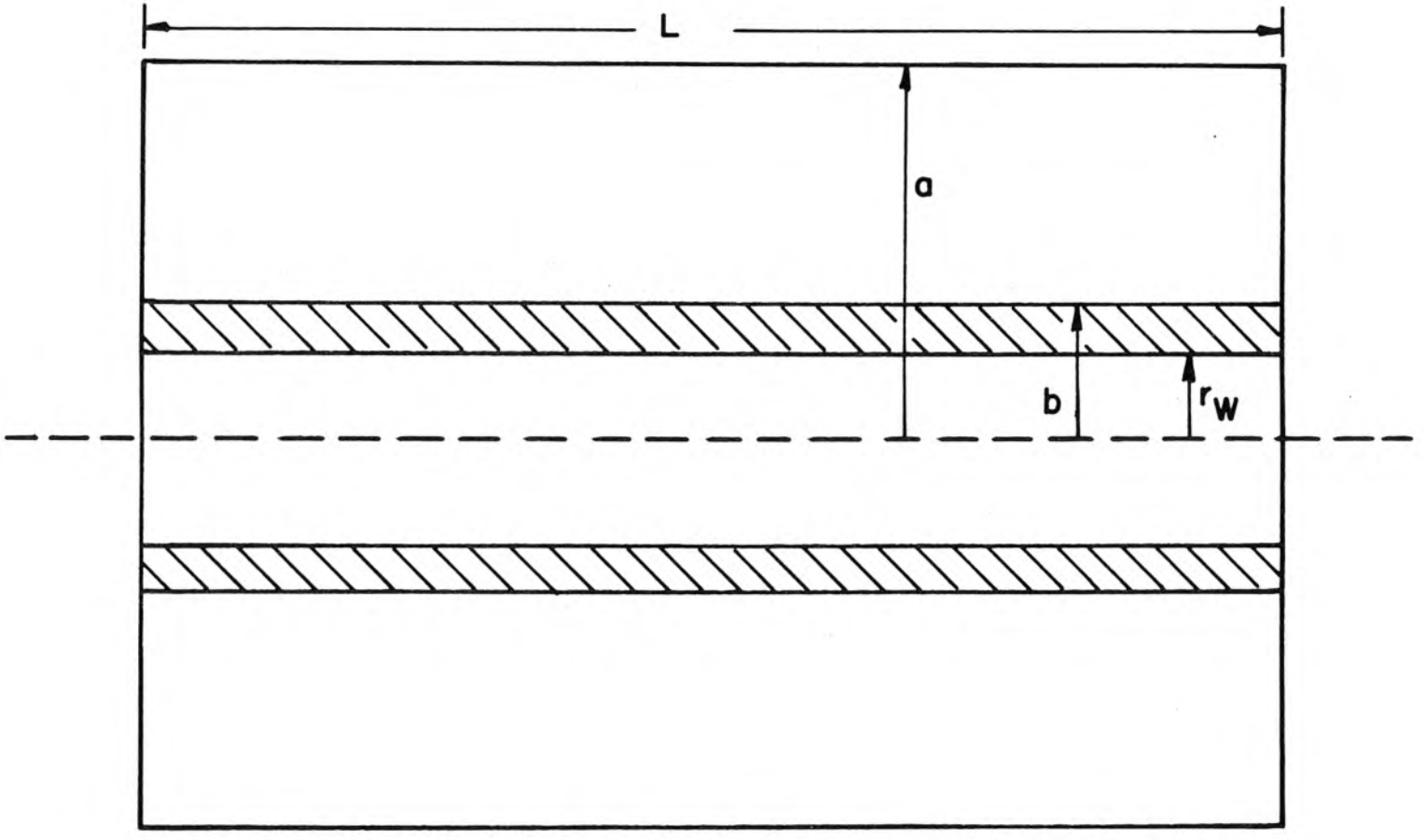

Figure C.1 Cavity Geometry

$$\epsilon_p(r) = \epsilon_o\left[1 - \frac{\omega_p^2(r)}{\omega^2}\right] = \epsilon_o\left[1 - \frac{e^2}{\omega^2 m\,\epsilon_o} n(r)\right] \quad . \quad (C.8)$$

Thus in the plasma region

$$(\Delta\epsilon)_p = \epsilon_p - \epsilon_o = -\frac{\epsilon_o e^2}{m\epsilon_o\omega^2} n(r) \quad . \quad (C.9)$$

In the glass region

$$(\Delta\epsilon)_{glass} = \epsilon - \epsilon_o = \epsilon_o(K-1) \quad (C.10)$$

where K is the relative dielectric constant of the glass. For the TM_{010} mode we can write (32)

$$E_o = E_z(r)\,\underset{\sim}{I}_z = A\,J_o\left(\frac{\beta_{01} r}{a}\right)\underset{\sim}{I}_z \quad (C.11)$$

where β_{01} is the first root of $J_o(x)$ and a is the radius of the cavity. This yields for the average stored electric energy

$$\overline{w}_e = \frac{\epsilon_o \pi L a^2}{4} A^2 J_1^2(\beta_{01}) \quad (C.12)$$

where L is the length of the cavity.

We can now use equations C.9, C.10, C.11 and C.12 in equation C.6 to determine the frequency shift of the cavity. In evaluating the numerator of equation C.6, we take the small argument approximation of $J_o\left(\frac{\beta_{01} r}{a}\right)$ or assume that $E_z \approx A$. Thus we assume that over the glass and plasma regions the electric field is approximately

uniform. If we observe that the average value of $n(r)$ is given by

$$\bar{n} = \frac{2}{r_w^2} \int_0^{r_w} n(r)dr \tag{C.13}$$

we find that

$$\frac{\omega - \omega_{oo}}{\omega_o} \approx \frac{1}{2J_1^2(\beta_{01})} \left\{ \frac{1}{\omega^2} \left(\frac{e^2}{m\epsilon_o}\right) \frac{r_w^2}{a^2} \bar{n} - (K-1)\frac{b^2 - r_w^2}{a^2} \right\} \tag{C.14}$$

where r_w and b are respectively the inner and outer radii of the glass tube.

Now let ω_{oo} be the resonant frequency of the empty cavity, ω_o be the resonant frequency of the cavity with the glass tube but no plasma, and ω be the resonant frequency of the cavity with the glass and the plasma. Then

$$\frac{\omega - \omega_{oo}}{\omega_{oo}} = \frac{1}{2J_1^2(\beta_{01})} \left\{ \frac{1}{\omega^2} \left(\frac{e^2}{m\epsilon_o}\right) \frac{r_w^2}{a^2} \bar{n} - (K-1)\left(\frac{c^2 - r_w^2}{a^2}\right) \right\} \tag{C.15}$$

$$\frac{\omega_o - \omega_{oo}}{\omega_{oo}} = -\frac{1}{2J_1^2(\beta_{01})} (K-1)\left(\frac{c^2 - r_w^2}{a^2}\right) . \tag{C.16}$$

Subtracting C.16 from C.15 we have

$$\frac{\omega - \omega_o}{\omega_{oo}} = \frac{1}{2J_1^2(\beta_{01})} \left\{ \frac{1}{\omega^2} \left(\frac{e^2}{m\epsilon_o}\right) \frac{r_w^2}{a^2} \bar{n} \right\} . \tag{C.17}$$

If we remember that $\omega = \omega_{oo} + \lambda\omega_1 + \cdots$ and $\omega_o = \omega_{oo} + \lambda\omega_{o1} + \cdots$, we can write

$$\frac{\omega - \omega_o}{\omega_{oo}} = \frac{\lambda(\omega_1 - \omega_{o1})}{\omega_{oo}} = \frac{\lambda(\omega_1 - \omega_{o1})}{\omega_o}\left(\frac{\omega_o}{\omega_{oo}}\right)$$

$$= \frac{\lambda(\omega_1 - \omega_{o1})}{\omega_o}\left[1 + \lambda\frac{\omega_{o1}}{\omega_{oo}}\right] = \lambda\frac{\omega_1 - \omega_{o1}}{\omega_o} + \lambda^2\frac{\omega_1 - \omega_{o1}}{\omega_o\,\omega_{oo}}\omega_{o1} \quad .$$

Thus to the order that we have been keeping, we can write

$$\frac{\omega - \omega_o}{\omega_{oo}} = \frac{\omega - \omega_o}{\omega_o} \quad . \tag{C.18}$$

Using the right hand side of equation C.18 in equation C.17 (which we have seen in Section 3.4 is appropriate for dielectric measurements), we can write

$$\omega_o(\omega - \omega_o) = \frac{1}{2J_1^2(\beta_{o1})}\frac{e^2}{m\epsilon_o}\frac{r_w^2}{a^2}\,\bar{n} \tag{C.19}$$

or

$$\bar{n} = \frac{2J_1^2(\beta_{o1})}{e^2/4\pi^2 m\epsilon_o}\frac{a^2}{r_w^2}\,f_o\Delta f \tag{C.20}$$

or

$$\bar{n} = 6.686 \times 10^{-3}\frac{a^2}{r_w^2}\,f_o\,\Delta f \tag{C.21}$$

where

$$\Delta f = f - f_o \quad . \tag{C.22}$$

Equation C.20 is the relation which was discussed in Section 3.4 and which was used to relate the cavity shifts to the average electron densities.

C.3 Determination of the Dielectric Constant of a Dielectric Rod Using the TM_{010} Mode of a Cylindrical Cavity

Let us consider a dielectric rod of relative dielectric constant K_L and radius r_w which is surrounded by a glass tube of relative dielectric constant K and with inner and outer radii r_w and b respectively. The calculation of the frequency shift produced by this arrangement is done exactly the same as in Section C.2 with one exception. In the region $r = r_w$ we no longer have plasma but a real dielectric. Thus in this region

$$(\Delta\epsilon)_{dielectric} = \epsilon - \epsilon_o = \epsilon_o(K_L - 1) \quad . \tag{C.23}$$

Again

$$(\Delta\epsilon)_{glass} = \epsilon - \epsilon_o = \epsilon_o(K - 1) \quad . \tag{C.24}$$

If we again make the approximation that $E_z \approx A$ for $r < b$ and use equation C.6, we find that

$$\frac{\omega - \omega_{oo}}{\omega_{oo}} \approx \frac{1}{2J_1^2(\beta_{01})} \left\{ - (K_L - 1) \frac{r_w^2}{a^2} - (K - 1) \frac{b^2 - r_w^2}{a^2} \right\} . \tag{C.25}$$

For a dielectric rod alone (without the glass mantle), we can set $b = r_w$ and obtain

$$\frac{\omega - \omega_{oo}}{\omega_{oo}} = \frac{-1}{2J_1^2(\beta_{01})} (K_L - 1) \frac{r_w^2}{a^2} \qquad (C.26)$$

where ω_o is the resonant frequency of the cavity with only the dielectric rod.

C.4 Determination of the Third Moment of the Electron Density Distribution $I_3 = \int_0^{r_w} n(r) r^3 dr$ Using the TM_{110} Mode of a Right Circular Cavity

Again the method is similar to that used in Section C.2. We employ equation C.6 to calculate the frequency shift of the cavity. For the TM_{110} mode we can write (32)

$$E_z = A J_1(\frac{\beta_{11} r}{a}) \cos \theta \qquad (C.27)$$

$$E_r = E_\theta = 0 \quad . \qquad (C.28)$$

This yields for the average stored electric energy:

$$\bar{w}_e = \frac{1}{4}\epsilon_o \quad E^* \cdot Edv = \frac{\pi\epsilon_o La^2A^2}{8} J_2^2(\beta_{11}) \tag{C.29}$$

where β_{11} is the first root of $J_1(x)$. As in equation C.9, we take for $\Delta\epsilon$ in the plasma region

$$(\Delta\epsilon)_p = -\frac{e^2}{m\omega^2} n(r) \tag{C.30}$$

and in the glass region

$$(\Delta\epsilon)_g = \epsilon_o(K - 1) \ . \tag{C.31}$$

Using equations C.26, C.28, C.29 and C.30 we can now evaluate equation C.6 for the frequency shift of the cavity. In evaluating the numerator of equation C.6 we make the small argument approximation to $J_1(\frac{\beta_{11}r}{a})$ or we assume that

$$E_z \approx \frac{A\beta_{11}r}{2a} \cos\theta \quad \text{for} \quad r < b \ . \tag{C.32}$$

Then if we remember that

$$I_3 = \int_0^{r_w} n(r) r^3 dv \quad , \tag{C.33}$$

equation C.6 yields

$$\frac{\omega - \omega_{oo}}{\omega_{oo}} \approx \frac{1}{4}\frac{e^2}{m\epsilon_o}\frac{\beta_{11}^2}{a^4}\frac{1}{\omega^2}\frac{I_3}{J_2^2(\beta_{11})} - (K-1)\frac{\beta_{11}^2}{16J_2^2(\beta_{11})}\frac{b^4 - r_w^4}{a^4} \ . \tag{C.34}$$

Again if we let ω_o be the resonant frequency of the cavity with the

glass present but the plasma off, we have

$$\frac{\omega_o - \omega_{oo}}{\omega_{oo}} \approx - (K - 1) \frac{\beta_{11}^2}{16 J_2^2(\beta_{11})} \frac{b^4 - r_w^4}{a^4} \quad . \tag{C.35}$$

Subtracting equation C.35 from C.36 we have

$$\frac{\omega - \omega_o}{\omega_{oo}} \approx \frac{\omega - \omega_o}{\omega_o} \approx \frac{1}{4}\left(\frac{e^2}{m\epsilon_o}\right)\left(\frac{\beta_{11}^4}{a^4}\right) \frac{1}{\omega_o^2} \frac{I_3}{J_2^2(\beta_{11})} \tag{C.36}$$

or

$$I_3 = \frac{16\pi^2 m\epsilon_o J_2^2(\beta_{11})}{\beta_{11}^2 e^2} a^4 f_o \Delta f \tag{C.37}$$

where f_o is the resonant frequency of the cavity with the glass present but the plasma off, $\Delta f = f - f_o$ and f is the resonant frequency of the cavity in the presence of the glass. Equation C.37 is the relation discussed in Section 3.5.

APPENDIX D

D.1 Introduction

In this section we shall investigate a method of directly measuring the logarithmic derivative L_n as a function of the plasma parameters by making admittance measurements on the split cylinder arrangement. In the first section we shall relate the logarithmic derivative to possible admittance measurements, while in the second section we shall investigate some equivalent circuits of the plasma-split cylinder system.

D.2 Admittance of the Split Cylinder Capacitor

We shall consider the split cylinder dipole device shown in Figure B.1a. It was shown in Appendix B that the potential in Region III ($b \leq r \leq c$) is given by

$$\phi^{III}(r,\theta) = \sum_{n=1,3,5\cdots} \frac{2v_o}{n\pi} \frac{p_n(\frac{r}{b})^n + (\frac{r}{b})^{-n}}{p_n(\frac{c}{b})^n + (\frac{c}{b})^{-n}} \sin n\theta \qquad (D.1)$$

where p_n is defined by equation B.10.

We can write for the input admittance Y of this device

$$Y = \frac{I}{v_o} \qquad (D.2)$$

where

$$I = i\omega q \qquad (D.3)$$

and q is the charge on one of the plates. We first calculate q in the following manner. The charge density on the upper plate, for

instance, is given by

$$\sigma(\theta) = -\epsilon_o E_r(c,\theta) = \epsilon_o \left.\frac{\partial \phi^{III}}{\partial r}\right|_{r=c} . \qquad (D.4)$$

The total charge on the upper plate is then

$$q = \int_0^\pi \sigma(\theta)\, L c d\theta = \frac{2v_o L \epsilon_o}{\pi} \sum_{n=1,3,5} \frac{p_n(\frac{c}{b})^n - (\frac{c}{b})^{-n}}{p_n(\frac{c}{b})^n + (\frac{c}{b})^{-n}} \int_0^\pi \sin n\theta\, d\theta$$

$$= \frac{4v_o L \epsilon_o}{\pi} \sum_{n=1,3,5} \frac{1}{n} \frac{p_n - (\frac{b}{c})^{2n}}{p_n + (\frac{b}{c})^{2n}} \qquad (D.5)$$

where L is the length of the capacitor (neglecting end effects).

Thus:

$$Y = \frac{i\omega q}{v_o} = i\omega \epsilon_o \frac{4L}{\pi} \sum_{n=1,3,5} \frac{1}{n} \frac{p_n - (\frac{b}{c})^{2n}}{p_n + (\frac{b}{c})^{2n}} . \qquad (D.6)$$

We can write

$$Y = \sum_{n=1,3,5} Y_n \qquad (D.7)$$

where

$$Y_n = i\omega\epsilon_o \frac{4L}{\pi n} \frac{p_n - (\frac{b}{c})^{2n}}{p_n + (\frac{b}{c})^{2n}} . \qquad (D.8)$$

Let us introduce the dimensionless parameters

$$\alpha_n = 1 - \left(\frac{r_w}{b}\right)^{2n} \tag{D.9}$$

$$\beta_n = 1 + \left(\frac{r_w}{b}\right)^{2n} \tag{D.10}$$

$$X_n = \frac{K\beta_n g + \alpha_n}{K\beta_n + \alpha_n g} \tag{D.11}$$

and

$$F_n = \frac{K\alpha_n g + \beta_n}{K\beta_n g + \alpha_n} \tag{D.12}$$

where once again K is the dielectric constant of the surrounding glass and

$$g = \frac{1 + \left(\frac{b}{c}\right)^{2n}}{1 - \left(\frac{b}{c}\right)^{2n}} \quad . \tag{D.13}$$

We can then rewrite equation D.8 for Y_n as

$$Y_n = i\omega\epsilon_o \frac{4LX_n}{n\pi} \frac{r_w L_n + nKF_n}{r_w L_n + nK_{eff}} \tag{D.14}$$

where K_{eff} is the effective dielectric constant defined by equation B.18.

Now if there is no plasma the logarithmic derivative at $r = r_w$ becomes

$$L_n = \frac{n}{r_w} \tag{D.15}$$

so that we can write

$$Y_{on} = i\omega\epsilon_o \frac{4LX_n}{n\pi}\left[\frac{1+KF_n}{1+K_{eff}}\right] \tag{D.16}$$

Let us now form the difference $Y_n - Y_{on}$:

$$Y_n - Y_{on} = \Delta Y_n = i\omega\epsilon_o \frac{4LX_n}{n\pi}\left[\frac{r_w L_n + nKF_n}{r_w L_n + nK_{eff}} - \frac{1+KF_n}{1+K_{eff}}\right] \tag{D.17}$$

$$= i\omega\epsilon_o \frac{16K^2L(g+1)^2}{n\pi(K\beta_n + \alpha_n g)^2}\left(\frac{a}{c}\right)^{2n}\left(\frac{1}{1+K_{eff}}\right)\left(\frac{r_w L_n - n}{r_w L_n + n K_{eff}}\right).$$

In the following discussion we shall write

$$Y_n - Y_{on} = \Delta Y_n = i\omega A_n\left(\frac{r_w L_n - n}{r_w L_n + nK_{eff}}\right) \tag{D.18}$$

where

$$A_n = \frac{16K^2L\epsilon_o(g+1)^2}{n\pi(K\beta_n + \alpha_n f)^2}\left(\frac{r_w}{c}\right)^{2n}\left(\frac{1}{1+K_{eff}}\right). \tag{D.19}$$

Since $Y_n = Y_{on} + \Delta Y_n$, we can write

$$Y = \sum_{n=1,3,5} Y_n = \sum_n Y_{on} + \sum_n \Delta Y_n = Y_o + \sum_n \Delta Y_n \tag{D.20}$$

or

$$Y - Y_o = \sum_{n=1,3,5} \Delta Y_n . \tag{D.21}$$

We see from equation D.21 that we can experimentally measure $\sum_n \Delta Y_n$ by measuring the difference in the input impedance with the

plasma on and off respectively. The coefficients A_n in the expression for ΔY_n decrease very rapidly with increasing n. For example, if we consider tube No. 1 in the split cylinder dipole device discussed in Chapter III (r_w = .506 cm, b = .616 cm, c = 1.905 cm, L = 7.64 cm, and K = 4.74), then $A_1 = 1.28 \times 10^{-13}$ and $A_3 = 1.85 \times 10^{-16}$. Thus if we are working near a dipole resonance ($n = 1$), ΔY_1 will be the only important term in $\sum \Delta Y_n$. Since for the dipole devices used we apparently cannot see the $n = 3$ resonance, ΔY_1 may be the only important term throughout the range of plasma parameters observed.

D.3 Equivalent Circuits

We have seen that the input admittance to the split cylinder dipole device can be written as

$$Y = Y_o + \sum_n \Delta Y_n \quad . \tag{D.22}$$

In the ideal case (neglecting radiation), Y_o will be the admittance of a capacitor and the input admittance can be represented by the equivalent circuit of Figure D.1.

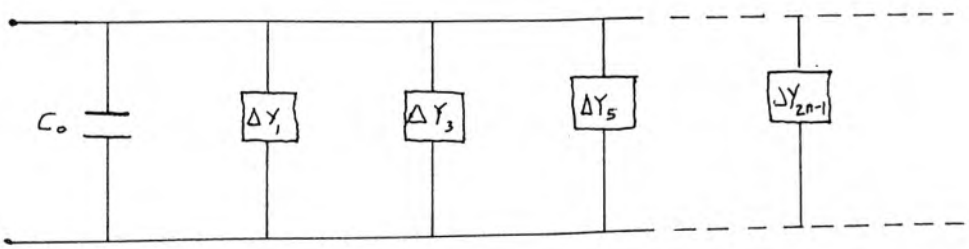

Figure D.1

If we assume that we are near a dipole resonance so that ΔY_1 is the dominant term, then we have the circuit shown in Figure D.2.

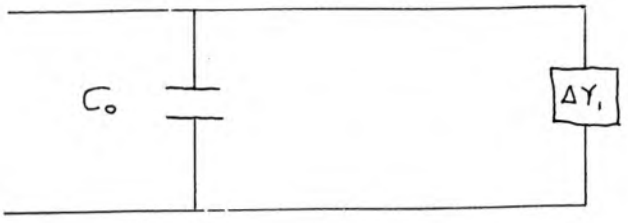

Figure D.2

A certain amount of insight can be gained by examining the case in which the plasma is assumed to be described by a lossy dielectric constant:

$$K_p = \frac{\epsilon_p}{\epsilon_o} = 1 - \frac{\omega_p^2}{\omega^2} - i\,\frac{\nu\omega_p^2}{\omega^3} \quad , \tag{D.23}$$

where ν is the collision frequency. Here we assume the plasma to be uniform and that $\frac{\nu^2}{\omega^2} \ll 1$. The logarithmic derivative will then be

$$L_1 = \frac{K_p}{r_w} = \frac{1}{r_w}\left[1 - \frac{\omega_p^2}{\omega^2} - i\,\frac{\nu\omega_p^2}{\omega^3}\right] \quad . \tag{D.24}$$

From equation D.18 we have

$$\Delta Y_1 = \frac{- i\omega A_1 \left(\frac{\omega_p^2}{\omega^2} + i \frac{\nu \omega_p^2}{\omega^3} \right)}{\left(1 + K_{eff} - \frac{\omega_p^2}{\omega^2}\right) - i \frac{\nu \omega_p^2}{\omega^3}} \tag{D.25}$$

and

$$\Delta Z_1 = \frac{1}{\Delta Y_1} = i \frac{\left(1 + K_{eff} - \frac{\omega_p^2}{\omega^2}\right) - i \frac{\omega_p^2}{\omega^3}}{\omega A_1 \left(\frac{\omega_p^2}{\omega^2} + i \frac{\nu \omega_p^2}{\omega^3} \right)} . \tag{D.26}$$

If we rationalize equation D.26 and again neglect ν^2/ω^2 with respect to 1, we can write

$$\Delta Z_1 = i\omega \frac{1 + K_{eff}}{A_1 \omega_p^2} + \frac{1}{i\omega A_1} + \frac{\nu(1 + K_{eff})}{A_1 \omega_p^2} . \tag{D.27}$$

The impedance function ΔZ_1 looks like the impedance function of a series LRC circuit where

$$L_p = \frac{1 + K_{eff}}{A_1 \omega_p^2} \tag{D.28}$$

$$C_p = A_1 \tag{D.29}$$

$$R = \nu \left(\frac{1 + K_{eff}}{A_1 \omega_p^2} \right) = \nu L_p . \tag{D.30}$$

Thus for this case the equivalent circuit of the plasma device arrangement looks like that shown in Figure D.3.

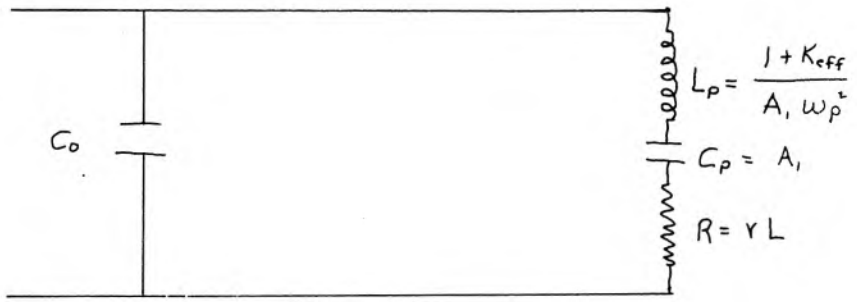

Figure D.3

BIBLIOGRAPHY

1. D. Romell, Nature 167, 243 (1951).
2. F. Boley, Nature 182, 790 (1958).
3. A. Dattner, Ericsson Technics 2, 309 (1957).
4. L. Tonks, Phys. Rev. 37, 1458 (1931).
   L. Tonks, Phys. Rev. 38, 1219 (1931).
5. A. Dattner, Proc. Vth Int. Conference on Ionization Phenomena in Gases, Munich (August 1961), North Holland Publishing Company, Amsterdam 2, 1477.
6. A. Dattner, Phys. Rev. Letters 10, 205 (1963).
7. A. Dattner, Ericsson Technics 1, 1 (1963).
8. A. M. Messiaen and P. E. Vandenplas, Physica 28, 537 (1962).
9. F. W. Crawford, G. S. Kino, S. Self, J. Spalter, J. Appl. Phys. 34, 2186 (1963).
10. G. H. Bryant, N.R. Franklin, Proc. Phys. Soc. 81, 531,790 (1963).
11. J. H. Battocletti and W. D. Hershberger, J. Appl. Phys. 33, 2618 (1962).
12. W. D. Hershberger, Phys. Fluids 4, 740 (1961).
13. F. W. Crawford, Phys. Letters 5, 244 (1963).
14. W. D. Hershberger, J. Appl. Phys. 31, 417 (1960).
15. F. I. Boley, J. Appl. Phys. 31, 1692 (1960).
16. T. Kaiser, R. Closs, Phil. Mag. 43, 1 (1952).
17. G. Keitel, Proc. IRE 43, 1481 (1955).
18. E. Astrom, Arkiv för Fysik 19, 163 (1961).
19. N. Herlofsen, Arkiv för Fysik 3, 247 (1951).
20. R. W. Gould, Proc. Linde Conference on Plasma Oscillations, Indianapolis, June 1959.
21. R. W. Gould, CIT Report No. 1, Contract DA36-039 SC-85317, April 1960.
22. J. V. Parker, Phys. Fluids 6, 1657 (1963).
23. J. L. Delcroix, Introduction to the Theory of Ionized Gases, (Interscience Publishers Inc., New York 1960).
24. J. V. Parker, PhD Thesis, California Institute of Technology 1964.
25. F. W. Crawford, G. S. Kino, Phys. Letters 4, 240 (1963).
26. A. M. Messiaen and P. E. Vandenplas, Phys. Letters 2, 193 (1962).
27. F. W. Crawford, G. S. Kino, A. B. Cannara, J. Appl. Phys. 34, 3168 (1963).

28. D. Rose, M. Clark, Plasmas and Controlled Fusion, J. Wiley and Sons, New York, 1961.

29. B. Klarfeld, Acad. of Sci. of USSR, Jour. of Phys. 5, 155 (1941).

30. A. Trivelpiece and R. W. Gould, J. Appl. Phys. 30, 1784 (1959).

31. R. F. Harrington, Time Harmonic Electromagnetic Fields, McGraw-Hill Book Co., New York, 1961, pp. 317.

32. W. R. Smythe, Static and Dynamic Electricity, McGraw-Hill Book Co., New York, 1950, 2nd Ed.

33. L. Tonks, I. Langmuir, Phys. Rev. 34 (1929).

34. S. Dushman, Vacuum Technique, J. Wiley and Sons, New York, 1949.

35. R. W. Gould, Plasma Physics Lecture Notes, California Institute of Technology, 1963.

36. B. D. Fried, S. Conte, The Plasma Dispersion Function, Academic Press, New York, 1961.

37. American Institute of Physics Handbook, McGraw-Hill Book Co., New York, 1957.

38. R. W. Gould, CIT Report No. 7, Contract DA36-039 SC-85317, July 1961.

39. Yasuo Akao, Yoshio I da, J. Appl. Phys. 34, 2119 (1963).

DISTRIBUTION LIST

Chief of Naval Research 2
Navy Department - CODE 427
Washington 25, D. C.

Director, Naval Research Lab.
Washington 25, D. C.
Attn: CODE 5240 1
CODE 7130 1
CODE 2000 6
CODE 5430 1

Commanding Officer 1
ONR Branch Office
1000 Geary Street
San Francisco, California

Scientific Liaison Officer 25
ONR, London
c/o Navy 100, Box 39, FPO
New York, New York

Commanding Officer 1
ONR Branch Office
1030 E. Green Street
Pasadena, California

Commanding Officer 1
ONR Branch Office
The John Crerar Library Bldg.
86 E. Randolph Street
Chicago 1, Illinois

Commanding Officer 1
ONR Branch Office
346 Broadway
New York 13, New York

Officer-in-Charge 3
Office of Naval Research
Navy 100, FPO
New York, New York

Chief, Bureau Aeronautics EL4 1
Navy Department EL43 1
Washington 25, D. C. EL45 1

Chief, Bureau of Ordnance
Navy Department Re 4 1
Washington 25, D. C. Re 9 1

Chief of Naval Operations Op20X 1
Navy Department Op421 1
Washington 25, D. C. Op 55 1

Director, Naval Ordnance Lab. 1
White Oak, Maryland

Director, Naval Electronics Lab 1
San Diego 52, California

Professor Norman L. Oleson 1
Department of Physics
U.S. Naval Postgraduate School
Monterey, California

Commander CODE 366 1
Naval Air Missile Test Center
Point Mugu, California

U.S. Naval Proving Ground 1
Attn: W. H. Benson
Dahlgren, Virginia

Commander 1
U.S.Naval Air Development Center
Johnsville, Pennsylvania

Thermionics Branch 5
Signal Corps Eng. Labs.
Evans Signal Lab, Bldg.42
Belmar, New Jersey

Defense Documentation Center 20
Cameron Station, Bldg. 5
5010 Duke Street
Alexandria, Virginia 22314

Ballistics Research Labs 2
Aberdeen Proving Ground
Maryland
Attn: D.W.H. Delsasso

Chief, Ordnance Develop. Div. 2
Natl.Bureau of Standards
Connecticut Av, Van Ness St.NW
Washington 25, D. C.

Naval Research Laboratory 6
Washington 25, D. C.

Committee on Electronics 1
Research and Development Board
Department of Defense
Washington 25, D. C.

Director, Natl.Bureau of Stds. 1
Washington 25, D. C.
Attn: Div.14.0 CRPL, Librarian

Commanding Officer 1
Engineering Res. and Dev. Lab
Fort Belvoir, Virginia

Commanding Officer 1
Frankford Arsenal
Bridesburg, Philadelphia, Pa.

Eitel-McCullough, Inc. 1
301 Industrial Way
San Carlos, California
ATTN: Research Library

Commanding General WCLC 1
Wright Air Devel.Center WCLRC 1
Wright-Patterson AF Base, Ohio

Commanding General, CRRE 1
A.F. Cambridge Research Center
230 Albany Street
Cambridge 39, Massachusetts

Commanding General RCRW 1
Rome Air Development Center
Griffiss Air Force Base
Rome, New York

Chief, West Coast Office 1
Signal Corps Eng. Labs
75 So. Grand Avenue
Pasadena 2, California

Signal Corps Resident Engineer 1
Electronic Defense Laboratory
P.O. Box 205
Mountain View, California

Chief, Bureau of Ships 816 1
Department of the Navy 820 1
Washington, D. C. 340 1

Material Lab. Library 912B 1
New York Naval Shipyard
Brooklyn 1, New York

Office of Technical Services 1
Department of Commerce
Washington 25, D. C.

Director CR4582 1
Air University Library
Maxwell A.F. Base, Alabama

Chief, Western Division 1
Office of Aerospace Research
Office of Scientific Research
P.O.Box 2035, Pasadena, Calif.

Technical Library 1
Research and Development Board
Pentagon Building
Washington 25, D. C.

Advisory Group on Electron Tubes 1
346 Broadway (8th Floor)
New York 13, New York

Dr. G. E. Barlow 1
Australian Joint Service Staff
Box 4837
Washington 8, D. C.

Microwave Library 1
W. W. Hansen Labs. of Physics
Stanford University
Stanford, California

Engineering Library 1
Stanford University
Stanford, California

Electronics Lab. Library 1
Stanford University
Stanford, California

Technical Library 1
General Electric Microwave Lab.
601 California Avenue
Palo Alto, California

General Electric Company 1
Electronic Components Div.
Power Tube Department
Microwave Lab at Stanford
Palo Alto, California

Dr. E. D. McArthur 1
Electron Tube Laboratory
General Electric Company
Schenectady, New York

University of Michigan 1
Electron Tube Laboratory
Ann Arbor, Michigan
Attn: J. Rowe

Johns Hopkins University 1
Radiation Laboratory
1315 St. Paul Street
Baltimore 2, Maryland
Attn: M.Poole, Librarian

Research Lab. of Electronics 1
Massachusetts Inst. of Tech.
Cambridge 39, Massachusetts

Sloane Physics Laboratory 1
Yale University
New Haven, Connecticut
Attn: R. Beringer

Mr. H. J. Reich 1
Department of Electrical Eng.
Yale University
New Haven, Connecticut

Laboratory for Insulation Res. 1
Massachusetts Inst. of Tech.
Cambridge 39, Massachusetts
Attn: A. von Hippel

Lincoln Laboratory 1
Massachusetts Inst. of Tech.
Cambridge 39, Massachusetts

Dr. J. M. Lafferty, Manager 1
Physical Studies
General Electric Company
P.O. Box 1088
Schenectady, New York

General Electric Company 1
One River Road
Schenectady 5, New York
Attn: Miss W. Crain, Librarian

Technical Report Collection 1
303A Pierce Hall
Harvard University
Cambridge 38, Massachusetts

Electron Tube Section 1
Electrical Engineering Dept.
University of Illinois
Champaign, Illinois

Chairman, Div.of Elec. Eng. 1
University of California
Berkeley 4, California

Radiation Laboratory 1
Tech. Information Division
University of California
Berkeley 4, California

Dr. A. W. Trivelpiece 1
Department of Elec. Eng.
University of California
Berkeley 4, California

Periodicals Librarian 1
General Library
California Inst. of Technology
Pasadena, California

Dr. Z. Kaprielian 1
Electrical Engineering Dept.
University of Southern Calif.
Los Angeles 7, California

Supervisor of Research Lab. 1
Electrical Engineering Bldg.
Purdue University
Lafayette, Indiana

Georgia Institute of Techn. 1
Atlanta, Georgia
ATTN: Librarian

W. E. Lear 1
University of Florida
Department of Electrical Eng.
Gainesville, Florida

Director Electronics Defense 1
Engineering Research Inst.
University of Michigan
Ann Arbor, Michigan

Cornell Aeronautical Lab 1
Cornell Research Foundation
Buffalo 21, New York

Director, Microwave Res.Inst. 1
Polytechnic Inst.of Brooklyn
55 Johnson Street
Brooklyn 1, New York

University of Washington
Department of Elec. Eng.
Seattle, Washington
ATTN: E. A. Harrison 1
A. V. Eastman 1

University of Colorado 1
Department of Elec. Eng.
Boulder, Colorado

University of Colorado 1
Engineering Experiment Sta.
Boulder, Colorado
ATTN: W. G. Worcester

Electrical Engineering Dept. 1
Princeton University
Princeton, New Jersey

Professor W. P. Dyke 1
Linfield College
McMinnville, Oregon

Research Lab.of Electronics 1
Chalmers Institute of Tech.
Gothenburg, Sweden
ATTN: Librarian

Columbia Radiation Lab. 1
538 W. 120th Street
New York 27, New York

Cascade Research 1
5245 San Fernando Road
Los Angeles 39, California

Fred D. Wilimek 1
Varian Associates
611 Hansen Way
Palo Alto, California

John Dyer 1
Airborne Instrument Lab
Mineola, New York

Bell Telephone Laboratories 1
Murray Hill, New Jersey
ATTN: J. R. Pierce

Hughes Aircraft Company 1
Culver City, California
ATTN: Mr. Milek, Librarian

Hughes Aircraft Company 1
Microwave Laboratory
Culver City, California
ATTN: Dr. A. D. Berk

Bell Telephone Laboratories 1
Technical Information Library
463 W. Street
New York 14, New York

RCA Laboratories 1
Princeton, New Jersey
ATTN: Dr. W. M. Webster

Federal Telecommunic. Labs 1
500 Washington Avenue
Nutley, New Jersey
ATTN: W. Derrick
K. Wing 1

Countermeasures Laboratory 1
Gilfillan Brothers, Inc.
1815 Venice Boulevard
Los Angeles, California

The Rand Corporation 1
1700 Main Street
Santa Monica, California
ATTN: Librarian

Motorola Riverside Res. Lab. 1
8330 Indiana Avenue
Riverside, California
ATTN: Mr. John Byrne

Ramo-Wooldridge Corporation 1
Control Systems Division
P.O. Box 900B
Hawthorne, California
ATTN: Librarian

Dr. James E. Shepherd 1
General Manager
Sperry Rand Research Center
P.O. Box 400
Sudbury, Massachusetts

W. L. Maxson Corporation 1
460 West 34th Street
New York 1, New York
ATTN: M. Simpson

Bertram G. Ryland, Manager 1
Spencer Laboratory
Raytheon Manufacturing Co.
Burlington, Massachusetts

Westinghouse Electric Corp. 1
Electronic Tube Division
Elmira, New York
ATTN: Mr. S.S.King, Librarian

Mr. Gilbert Kelton 1
Security Officer
Philips Laboratories
Irvington-on-Hudson, New York

R. E. McGuire, Librarian 1
Boeing Airplane Company
P.O. Box 3707
Seattle 24, Washington

A. Simon 1
General Atomic
P. O. Box 608
San Diego, California

Image Instruments, Inc. 1
2300 Washington Street
Newton Lower Falls 62, Mass.

Sylvania Electric Prod. Inc. 1
Waltham, Massachusetts
ATTN: Charles A. Thornhill

Research Division Library 1
Raytheon Company
28 Seyon Street
Waltham 54, Massachusetts

ITT Laboratories 1
15151 Bledsoe Street
San Fernando, California

Technical Research Group Inc. 1
2 Aerial Way
Syosset, New York

Advanced Techniques Branch 1
Electronics Technology Lab.
Aeronautical Systems Division
Wright-Patterson AFB, Ohio

Microwave Physics Laboratory 1
Sylvania Electric Products
P.O. Box 1296
Mountain View, California

U. S. Atomic Energy Commission 1
Tech. Information Service Ext.
P.O. Box 62
Oak Ridge, Tennessee

Electromagnetic Research Corp
5001 College Avenue 1
College Park, Maryland 20740
ATTN: R. E. Skinner

Bomac Laboratories, Inc. 1
Salem Road
Beverly, Massachusetts
ATTN: Arthur McCoubrey

Aerospace Corporation 1
Post Office Box 95085
Los Angeles 45, California
Attn: F. L. Vernon, Jr.

Space-General Corp 1
9200 E. Flair Drive
El Monte, California
ATTN: Bruce Ferrell, Lib.

Northern Electric Co. Ltd. 1
Research and Devel. Labs.
Library, Dept. 8421
P.O. Box 3511, Station C
Ottawa, Ontario, Canada

Dalmo Victor Company 1
Division of Textron, Inc.
Belmont, California
ATTN: Librarian

Dr. W. E. Drummond 1
General Atomic
P. O. Box 608
San Diego 12, California

Dr. M. Gottlieb 1
Princeton University
Plasma Physics Laboratory
Princeton, New Jersey

Dr. R. F. Post 1
Radiation Laboratory
Livermore, California

Dr. W. Kunkel 1
U.C. Radiation Laboratory
Berkeley, California

Dr. R. J. Mackin 1
Jet Propulsion Laboratory
Pasadena, California

Dr. M. Allen 1
Microwave Associates
Burlington, Massachusetts

Dr. Irving Kaufman 1
Space Technology Laboratories
1 Space Park
Redondo Beach, Calif.

Prof. J. Van Bladel 1
Technicum der Rijksuniversiteit
Sint-Pietersnieuwstraat
Gent, Belgium

Prof. C. C. Johnson 1
Electrical Engineering Dept.
University of Utah
Salt Lake City 12, Utah